REPROGRAMMING OF CELLULAR DIFFERENTIATION BY THE ONCOGENE SYT-SSX2

By

Christina Valerie Boma Garcia

Dissertation

Submitted to the Faculty of the

Graduate School of Vanderbilt University

in partial fulfillment of requirements

for the degree of

DOCTOR OF PHILOSOPHY

in

Cancer Biology

December, 2011

Nashville, Tennessee

Approved:

Dr. Barbara Fingleton

Dr. Stephen Brandt

Dr. P. Anthony Weil

Dr. Josiane Eid

AMDG

ACKNOWLEDGEMENTS

I want to thank the Sarcoma Foundation of America and Alex's Lemonade Stand Foundation for providing the financial resources to be able to perform this research. I would also like to thank the Department of Cancer Biology for their support and assistance throughout this process.

I would like to acknowledge those who provided me with scientific assistance for this project. I thank my dissertation committee members Dr. Barbara Fingleton, Dr. Steve Brandt, and Dr. Tony Weil. I truly value the advice and guidance they offered as well as the reagents they provided to advance the project. I would also especially like to thank Christian Shaffer whose help was invaluable in performing the ChIPSeq and microarray analyses and without whom I would still be staring at millions of ChIPSeq tags.

I would like to thank my adviser, Dr. Josiane Eid, for being a great mentor and friend. I will be forever grateful for her concern for my success as a student, and without her, I would not have been able to achieve everything that I have done. I will always remember the unspoken lessons in compassion and determination given by her example, and I hope that my career will be a credit to all that I have learned from her.

Lastly, I thank my friends and family for being my support. I thank them for their encouragement and their perspective, for their patience and their understanding. I am truly blessed to have them in my life.

TABLE OF CONTENTS

Page

LIST OF TABLES

Page

LIST OF FIGURES

Page

LIST OF PUBLICATIONS

Garcia CB, Shaffer CM, Alfaro MP, Smith AL, Sun J, Zhao Z, Young PP, VanSaun M, Eid JE. (2011). “Reprogramming of mesenchymal stem cells by the synovial sarcoma-associated oncogene SYT-SSX2.” *Oncogene* (in press).

Barco R, Garcia CB, Eid JE. (2009). “The synovial sarcoma-associated SYTSSX2 oncogene antagonizes the Polycomb complex protein Bmi1.” *PLoS One* **4:** e5060 **doi:** 10.1371/journal.pone.0005060.

Eid J, Garcia C, Frump A . (2008). ”SSX2 (Synovial Sarcoma, X breakpoint 2).” *Atlas Genet Cytogenet Oncol Haematol.* **URL :** http://AtlasGeneticsOncology.org/Genes/SSX2ID42406chXp11.html

Barco R, Hunt LB, Frump AL, Garcia CB, Benesh A, Caldwell RL, Eid JE. (2007). “The synovial sarcoma SYT-SSX2 oncogene remodels the cytoskeleton through activation of the ephrin pathway.” *Mol Biol Cell* **18:** 4003-12.

LIST OF ABBREVIATIONS

Acetylated histone H3 lysine 9 ..... H3K9Ac

Acetylated histone H3 lysine 14 ..... H3K14Ac

Acetylated histone H3 lysine 18 ..... H3K18Ac

Acetylated histone H4 lysine 12 ..... H4K12Ac

B lymphoma Mo-MLV insertion region 1 ..... Bmi1

Bone morphogenetic protein ..... BMP

Brahma-related gene 1 ..... Brg1

Brahma homolog ..... Brm

Chromatin immunoprecipitation ..... ChIP

ChIP sequencing ..... ChIPSeq

Dimethylated histone H3 lysine 4 ..... H3K4me2

Delta-like 1 ..... Dll1

DNA methylation ..... DNA me

Extracellular signal-regulated kinase ..... ERK

Fibroblast growth factor ..... FGF

Fibroblast growth factor receptor ..... FGFR

Histone deacetylase ..... HDAC

(Human) mesenchymal stem cell ..... (h)MSC

Insulin-like growth factor 2 ..... Igf2

Mammalian Switch/Sucrose Nonfermentable complex homolog ..... (m)SWI/SNF

Monomethylated histone H3 lysine 4 ..... H3K4me1

Myogenic differentiation 1 ..... MyoD

Myogenic factor 5 ..... Myf5

Nerve growth factor receptor ..... Ngfr

Neurofilament ..... NEF

Polycomb group ..... PcG

Polycomb Repressive Complex 1 ..... PRC1

Polycomb Repressive Complex 2 ..... PRC2

RNA polymerase II ..... PolII

Synovial sarcoma ..... SS

Synovial sarcoma translocation ..... SYT

Synovial sarcoma X chromosome breakpoint ..... SSX

SSX repressor domain ..... SSXRD

SYT N-terminal homology ..... SNH

Transforming growth factor β ..... TGFβ

Trimethylated histone H3 lysine 4 ..... H3K4me3

Trimethylated histone H3 lysine 27 ..... H3K27me3

Trimethylated histone H3 lysine 36 ..... H3K36me3

Trithorax group ..... TrxG

Ubiquitylated histone H2A lysine 119 ..... H2AUb

Ubiquitylated histone H2B lysine 123 ..... H2BUb

Wingless-type MMTV integration site family ..... Wnt

CHAPTER I

INTRODUCTION

Synovial sarcoma

Clinical features and treatment

Synovial sarcoma (SS) is an aggressive malignancy with few specific therapies (Haldar et al., 2008). It is a rare disease, comprising between 7 and 10 percent of all sarcoma cases and is diagnosed primarily in adolescents and young adults. Tumors are typically found near the joints but can arise in many locations throughout the body (Ladanyi, 2001; dos Santos et al., 2001). SS displays a high degree of metastasis, particularly to the lungs as well as the bone marrow and lymph nodes (dos Santos et al., 2001). The primary treatment involves tumor resection and may include the addition of radiation or chemotherapy (Haldar et al., 2008). Even with these interventions, the survival rates of SS remain low and can range from 25-60% 5-year survival and a 10-year survival between 10 and 30% (Ladanyi, 2001; dos Santos et al., 2001).

In spite of its name, synovial sarcoma is not actually derived from synovial tissue and is believed to arise from the transformation of some type of stem cell with the capacity to differentiate into epithelial and mesenchymal lineages (dos Santos et al., 2001). This is based on tumor histology which also allows for the classification of SS into three clinical subtypes: monophasic, biphasic, and poorly

differentiated. Monophasic tumors have spindle shaped cells that are small with little cytoplasm (Haldar et al., 2008). Biphasic tumors have compartments displaying glandular structures in addition to the spindle cell compartment, and the cells in poorly differentiated tumors have a morphology intermediate between the spindle and epithelial cells. Interestingly, all subtypes of SS display markers of epithelial differentiation making them unique among sarcomas. Another feature of SS is the presence of a recurrent chromosomal translocation t(X;18)(p11.2;q11.2) which can be detected in over 90% of all SS tumors (dos Santos et al., 2001). This genetic abnormality provides a characteristic feature which can be exploited to understand the molecular biology of synovial sarcoma tumors and lead to the development of more specific therapies in the future.

Molecular features of synovial sarcoma

Because of its specific association with SS as well as its presence in all compartments of the tumor and persistence throughout tumor growth, the product of the t(X;18) translocation is thought to drive SS tumor formation (dos Santos et al., 2001; Ladanyi, 2001). This mutation results in the aberrant fusion of the *SYT* gene (for “synovial sarcoma translocation,” also known as *SS18)* on chromosome 18 with one of the *SSX* (“synovial sarcoma X chromosome breakpoint”) family members located on the X chromosome (Clark et al., 1994; Crew et al., 1995; Skytting et al., 1999). The fusion gene is transcribed and encodes a functional protein in which the C-terminal 78 amino acids of SSX replace the last 8 amino acids of SYT (Figure 1; Clark et al., 1994). Most

translocations involve the same breakpoints in *SYT* and either *SSX1* or *SSX2,* but variations in the fusion are seen involving different breakpoints and alternate family members like *SYT-like* (*SYTL*) and *SSX4* (Crew et al., 1995; Skytting et al., 1999; Brodin et al, 2001; Storlazzi et al., 2003). SYT-SSX proteins localize in the nucleus where they may dictate tumorigenesis through the modulation of gene transcription (Thaete et al., 1999; Brett et al., 1997; dos Santos et al.,1999).

Both wild-type SYT and SSX proteins are nuclear co-regulators of transcription, and the subversion of their normal activities could contribute to cellular transformation. SYT is a ubiquitously expressed protein that is essential for development. Knock-out animals display embryonic lethality due to placental and cardiac defects (de Bruijn et al., 1996; de Bruijn et al., 2006b; Kimura et al., 2009). SYT resides predominantly in the nucleus where it displays a distinct speckled pattern (Thaete et al., 1999; Brett et al., 1997; dos Santos et al., 1999). It colocalizes with Brg1 and Brm in these nuclear foci, and this association is dependent on the N-terminus of SYT (Thaete et al., 1999; Ishida et al., 2004). This interacting region is evolutionarily conserved and is called the SYT N-terminal Homology (SNH) domain (Thaete et al., 1999). The SNH domain also mediates interactions with other proteins including the transcription factor AF10 and the histone modifiers p300 and mSin3a (Figure 1; de Bruijn et al., 2001; Eid et al., 2000; Ito et al., 2004). SYT contains an additional function domain at its C-terminus that has transactivation activity. It is referred to as the QPGY domain because of the abundance of glutamine, proline, glycine, and tyrosine residues (Figure 1; Thaete et al., 1999; Brett et al., 1997). This bears similarity to the

activation domain found in EWS/FUS/TLS proteins and is a domain that is also seen in the p250 and p250R proteins that are components of the mammalian SWI/SNF (mSWI/SNF) complex (Thaete et al., 1999; Kato et al., 2002). Interaction with the nuclear receptor Co-activator Activator (CoAA) protein occurs through the QPGY domain, and SYT may homo-dimerize through this module as well (Iwasaki et al., 2005; Perani et al., 2005; Perani et al., 2003). Notably, SYT lacks a DNA binding domain (Clark et al., 1994), and together these data indicate that SYT may mediate its function through protein-protein interactions that regulate transcription.

Early studies on the function of SYT reveal a role in transcriptional activation; however, the mechanism of its activity is still not understood. Previous work indicates that SYT plays a role in general transcription, and fusion of SYT to the Gal4 DNA binding domain results in reporter gene activation (Iwasaki et al., 2005; Ishida et al., 2004). This can be enhanced by deletion of the N-terminus and may be due to the association of mSin3a with the SNH domain (Ishida et al., 2004; Ito et al. 2004). Some evidence suggests that negative regulation of SYT activity also occurs through its interaction with Brg1/Brm; however, this is not corroborated by other reports (Ishida et al., 2004; Iwasaki et al., 2005). In addition, SYT can activate hormone-responsive promoters in a ligand-dependent manner with its binding partner, CoAA, requiring either Brm or Brg1 and the QPGY domain (Perani et al., 2005; Iwasaki et al., 2005). In summary, SYT involvement in transcriptional activation requires its interaction with other proteins suggesting that it may function as a recruitment factor for multiple complexes.

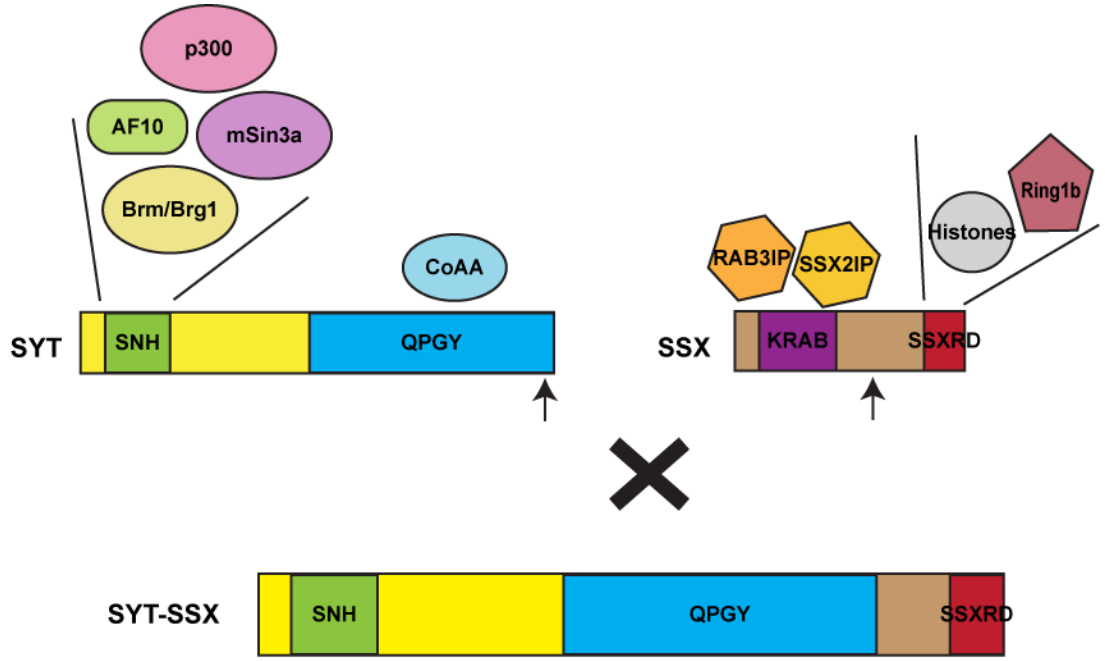

Figure 1. Schematic representations of SYT, SSX, and the translocation SYT-SSX.
Top left depicts the domain structure and interacting proteins of wild-type SYT. Green rectangle (SNH) represents the SYT N-terminal Homology domain spanning amino acids 20-73. Blue rectangle (QPGY) symbolizes the QPGY domain (residues 187-387) named for the abundance of glutamine, proline, glycine, and tyrosine residues in this region. Top right depicts the domain structure and interacting proteins of wild-type SSX proteins. Purple rectangle (KRAB) represents the Krüppel-associated box located between amino acid residues 20-83. Red rectangle (SSXRD, amino acids 155-188) depicts the SSX Repressor Domain. Proteins that are known to bind to SYT or SSX are shown above the domain with which they interact. Arrows mark the location of the breakpoint in each wild-type protein. Bottom diagram is a schematic of SYT-SSX translocation which retains the SNH and QPGY domains of SYT and the SSXRD of SSX.

Downstream of transcription, SYT appears to play a role in the regulation of adhesion. Association with p300 occurs specifically in the context of adherent cells (Eid et al., 2000). Moreover, adhesion to fibronectin is inhibited in the presence of a C-terminal mutant of SYT lacking the last 8 amino acids (mimicking the portion of the protein involved in the SYT-SSX translocation) (Eid et al., 2000). Additional studies have revealed a role for SYT in the formation of epithelial cysts in 3D culture as well as migration, further highlighting the importance of SYT in adhesion (Chittezhath et al., 2008; Kimura et al., 2009). Overall, SYT mediates transcriptional activation through interactions with multiple proteins and may integrate signals from a variety of pathways including hormones and extracellular matrix adhesion.

In contrast, the *SSX* genes encode transcriptional co-repressors whose physiological function remains unclear. These proteins are typically 188 amino acids in length, and their genes are found in 2 clusters on the X chromosome that are approximately 3Mb away from one another (Güre et al., 2002). There are 9 family members in all, and they are characterized by the presence of 2 domains involved in transcriptional repression: an N-terminal Krüppel-associated box (KRAB) domain and a C-terminal SSX Repressor Domain (SSXRD) (Figure 1; Crew et al., 1995; Lim et al., 1998). The primary functional domain of SSX proteins is the SSXRD, a region that is highly conserved among all family members (Güre et al., 2002). This domain is responsible for SSX nuclear localization as well as the bulk of its repressor activity (dos Santos et al., 2000; Thaete et al., 1999). The KRAB domain is found in a large sub-family of

transcriptional repressors, but in SSX proteins, it appears to play a supplementary role by augmenting repression mediated by the SSXRD (Crew et al., 1995; Lim et al., 1998; Thaete et al., 1999). Notably, like SYT, SSX proteins lack a DNA binding domain; therefore, they may also exert their function via protein-protein interactions (Crew et al., 1995).

Very few interacting partners of SSX proteins have been identified to date. Early studies reveal nuclear localization of SSX1 and SSX2, and it was later determined that SSX2 associated with Polycomb proteins (Brett et al., 1997; dos Santos et al., 1999; dos Santos et al., 2000). The Polycomb proteins are important regulators of differentiation and development that maintain silencing of lineage-specific genes through the modulation of chromatin structure (see below). The interaction between Polycomb proteins and SSX is dependent on the SSXRD, further highlighting the functional importance of this domain (dos Santos et al., 2000). In addition, SSX can co-precipitate histone oligomers and oligo-nucleosomes suggesting that SSX proteins may also be targeted through direct interactions with chromatin (Kim et al., 2009). Nevertheless, SSX1 binds to the transcription factor LHX4, and this association leads to the decreased expression of an LHX4-responsive reporter gene (de Bruijn et al., 2008). Other studies have identified additional interacting proteins; however, the functional consequences of SSX binding with these partners has not been elucidated (de Bruijn et al., 2002).

SSX proteins are also of general interest because of their potential role in many different cancers. The SSX family belongs to a class of proteins known as cancer-testis (CT) antigens because of their normal tissue distribution and

expression in malignancies (Smith and McNeel, 2010). CT antigens are nearly exclusively expressed in the testis; however, their aberrant expression in a variety of tumors derived from multiple tissues can produce an immune response in patients. This opens the possibility of using SSX peptides in vaccines for tumor immunotherapy for several cancers in addition to synovial sarcoma (Smith and McNeel, 2010). Thus, SSX as well as SYT are important proteins outside of their association with SS, and understanding their wild-type functions will expand our knowledge of both development and cancer.

Cellular Reprogramming and Cancer

Recently, it has been hypothesized that tumors are maintained by a small population of cancer stem cells (CSCs) that, when isolated, are able to repopulate the entire tumor with all of its various phenotypes (Lobo et al., 2006). The mechanism of how CSCs arise is not known; however, there are parallels between tumorigenesis and the process of cellular reprogramming by which normal, terminally differentiated somatic cells can be induced to behave like pluripotent stem cells (Abollo-Jiménez et al., 2010; Castellanos et al., 2010). Both require the gain of stem cell characteristics as well as the active repression of a cell's endogenous differentiation program (Lobo et al., 2006; Gurdon and Melton, 2008; Abollo-Jiménez et al., 2010). These alterations, in turn, depend on changes in gene transcription through the action of lineage-specific transcription factors, epigenetic regulators, and signaling molecules (Abollo-Jiménez et al.,

2010; Castellanos et al., 2010). SYT-SSX expression is associated with the activation of multiple signaling pathways, and it can interact with a number of proteins that control transcription through genetic and epigenetic mechanisms. These data suggest that SYT-SSX mediates transformation through aberrant cellular reprogramming.

Activation of signaling pathways by SYT-SSX

Many molecules involved in extracellular signaling pathways are activated in SS tumors and cell lines. A number of studies have reported the upregulation of various receptor tyrosine kinase pathway components including Igf2, HGF and c-Met, ephrin ligands and Eph receptors, FGF ligands and receptors, EGFR, and PDGFR (de Bruijn et al., 2006a; Watanabe et al., 2006; Barco et al., 2007; Ishibe et al., 2005; Bozzi et al., 2008). Several of these pathways converge on MAPK signaling leading to changes in cell proliferation, migration, and anchorage-independent growth and thus contribute to cellular transformation (Fukukawa et al., 2009; Watanabe et al., 2009; Watanabe et al., 2006). Moreover, the expression of ligands and their cognate receptors, as in the case of HGF and c-Met, ephrin and Eph receptors, and FGF signaling molecules, indicates that SYT-SSX mediates the formation of autocrine signaling loops. This may help to establish and maintain the transformed program in SS.

The non-canonical Wnt pathway is also active in some SS cell lines (Fukukawa et al., 2009). Signaling through this pathway affects anchorage-independent growth through Rac1 and JNK activation (Fukukawa et al., 2009).

Similarly, in the absence of canonical signaling events, β-catenin localizes in the nucleus and forms a complex with SYT-SSX2. This complex can activate a reporter gene, but the endogenous targets of this complex are not known (Pretto et al., 2006). This is evidence that not only does SYT-SSX activate different signaling pathways that contribute to the transformed phenotype, but it also has the capacity to change transcriptional programs directly.

Transcriptional deregulation by SYT-SSX

Based on their wild-type activities, the fusion of SYT to SSX generates a protein with an enigmatic function as it has the potential to mediate opposing behaviors. In the translocation, the SNH and QPGY domains of SYT are retained and fused to the C-terminal end of SSX with the SSXRD remaining intact (Figure 1, Pretto et al., 2006). Because these domains mediate protein-protein interactions with activators and repressors of transcription, it can be conjectured that SYT-SSX functions through both aberrant silencing and activation of target genes that contribute to tumorigenesis.

One mechanism by which SYT-SSX may induce and maintain tumor formation is through downregulation of tumor suppressor genes. SYT-SSX1 was shown to associate with wild-type SYT, and both proteins are bound to the COM1 tumor suppressor promoter region (Ishida et al., 2007). Expression of SYT-SSX1 led to the downregulation of COM1 which could be abrogated by exogenous expression of wild-type SYT. This suggests that SYT-SSX acts in a dominant negative manner to inhibit the normal function of SYT (Ishida et al.,

2007). Similarly, SYT-SSX2 directly repressed the activity of *EGR1*, a putative tumor suppressor and SYT target gene (Lubieniecka et al., 2008). Wild-type SYT and SYT-SSX2 associate with the *EGR1* promoter; however, SYT-SSX2 uniquely recruits Polycomb proteins to this locus. Altogether, these studies indicate that silencing of SYT target genes is one method of transcriptional deregulation mediated by SYT-SSX.

The activation of gene transcription by the fusion protein also contributes to tumor formation. As mentioned above, the IGF pathway is implicated in SS formation by a number of studies and correlates with increased cell proliferation and metastasis (Xie et al., 1999; Allander et al., 2002; de Bruijn et al., 2006a; Sun et al., 2006; Törnkvist et al., 2008). Furthermore, IGF2 neutralizing antibodies are able to increase apoptosis in SS cell lines (Sun et al., 2006). SYT-SSX proteins may directly affect expression of the *IGF2* gene through deregulation of its imprinting (de Bruijn et al., 2006a; Sun et al., 2006; Cironi et al., 2009). The exact mechanism of how this occurs is unclear, but altered methylation of the imprinting control region appears to play a role in this process (Sun et al., 2006; Cironi et al., 2009).

We have already discussed how Polycomb proteins may be aberrantly targeted to SYT target genes, and previous work in our lab reveals that the reverse may also occur. SYT-SSX2 expression in U2OS human osteosarcoma cells leads to a reduction in total protein levels of Bmi1 through enhanced degradation (Barco et al., 2009). This results in reduced association between Bmi1 and its functional partner, Ring1b, a global decrease in histone H2A

ubiquitylation, the enzymatic activity catalyzed by Ring1b and facilitated by Bmi1, and the increased expression of Polycomb target genes (Barco et al., 2009). Together, these data demonstrate that SYT-SSX alters the gene expression profile of the cell by epigenetic mechanisms.

Additionally, SYT-SSX interacts with sequence-specific transcription factors to mediate transcriptional activation. SYT-SSX induces the expression of E-cadherin. E-cadherin protein is found in biphasic SS which displays glandular differentiation of its epithelioid compartment. Both SYT-SSX1 and SYT-SSX2 activate the E-cadherin promoter through interaction with the repressors Snail and Slug (Saito et al., 2006). SYT-SSX also binds to LHX4 resulting in the activation of an LHX4 reporter gene (de Bruijn et al., 2008). LHX4 is involved in pituitary development and is linked to human disorders related to aberrant pituitary function (Machinis et al., 2001). Thus SYT-SSX can mediate transcriptional activation through association with lineage-specific transcription factors. In summary, the studies described above indicate that SYT-SSX regulates transcription via both genetic and epigenetic means.

Tumorigenesis depends on cell-intrinsic and extrinsic factors

The process of reprogramming is inefficient and depends on the level of differentiation in the original cell (Gurdon and Melton, 2008) suggesting that tumor formation by this mechanism will display similar characteristics. The potential of SYT-SSX to cause widespread transcriptional deregulation implies that its expression will always result in transformation; however, this is not the

case. SYT-SSX1 induces anchorage-independent growth and tumor formation in nude mice when expressed in rat 3Y1 fibroblasts (Nagai et al., 2001), yet additional reports on SYT-SSX-mediated transformation provide conflicting results. Human MSCs expressing SYT-SSX1 are unable to form tumors in immune deficient mice (Cironi et al., 2009), and previous work in our lab reveals that SYT-SSX2 is unable to transform NIH3T3 fibroblasts *in vitro* (Barco et al., 2007). This may be due to the ability of SYT-SSX to activate expression of p21, a direct target of the fusion in some cell types, including NIH3T3 cells (Tsuda et al., 2005). Interestingly, it is postulated that tumor suppressor pathways function as barriers to reprogramming (Abollo-Jiménez et al., 2010; Castellanos et al., 2010). Taken together, these data suggest that transformation by SYT-SSX proteins only occurs under conditions (intrinsic and extrinsic to the cell) that are permissive for reprogramming.

In vivo experiments indicate that tumorigenesis also relies on the cell differentiation status and the surrounding microenvironment. Mouse modeling of SS revealed that SYT-SSX2 alone could drive tumorigenesis, however, its effect was limited to transgenic animals in which the oncogene was expressed in Myf5-positive myoblasts (Haldar et al., 2007). Induction of SYT-SSX2 in less differentiated myogenic progenitor populations or in more differentiated myocytes did not result in tumor formation. Moreover, even in Myf5-positive cells, SYT-SSX2 caused apoptosis *in vivo* except in populations growing adjacent to the future cartilage of the rib. Thus, the target cell must meet certain requirements of

cell fate commitment and location in order to become transformed by SYT-SSX (Haldar et al., 2007; Haldar et al., 2009).

Overall, it appears that the fusion protein functions through the recruitment of regulators that can override the normal transcriptional status at a given locus. Moreover, contributions from both components of the fusion protein are required for its molecular activity; therefore, transformation by SYT-SSX depends on its ability to alter gene expression. This causes the activation of multiple signaling pathways, silencing of tumor suppressors, and the expression of other genes resulting in the acquisition of SS-associated phenotypes. In addition, the nature of the initiating cell is also important, and its properties can determine whether tumors form. These attributes parallel features of cellular reprogramming and leads to the hypothesis that SYT-SSX directs tumorigenesis by this process. Elucidating the characteristics of the aberrant program initiated by SYT-SSX, therefore, is essential to understanding the biology of SS.

Epigenetic Regulation of Development

Epigenetics refer to inherited changes in gene expression that occur independently of alterations in the DNA primary structure (Jones and Baylin, 2007). Stem cells employ epigenetic mechanisms to control the expression of developmental regulators either to maintain multipotency or to carry out cellular differentiation. Modulation of chromatin structure is one aspect of epigenetic regulation and is mediated by the action of many proteins the best characterized

being the Polycomb group (PcG) proteins and the SWI/SNF complex (Lessard and Crabtree, 2010).

PcG proteins are an evolutionarily conserved family of proteins that make up 2 classes of complexes in mammals: Polycomb Repressive Complex 1 (PRC1) and PRC2 (Kerppola, 2009; Schuettengruber et al., 2007). Each complex has a unique set of core components, some with multiple homologs, as well as associated activities that characterize it (Kerppola, 2009). The core PRC1 proteins are Bmi1, Cbx, Phc, and Ring1, which catalyzes the ubiquitylation of histone H2A on lysine 119 (H2AUb) (Kerppola, 2009; Schuettengruber et al., 2007). In addition, PRC1 can associate with methylated histone tails via the chromodomain of Cbx proteins (Kerppola, 2009). Through the activity of the Ezh1 and Ezh2 proteins, PRC2 is able to trimethylate histone H3 on lysine 27 (H3K27me3) (Schuettengruber et al., 2007). The other core proteins of PRC2 are Eed and Suz12 and are required for the methyltransferase activity of the Ezh proteins (Kerppola, 2009; Simon and Kingston, 2009; Schuettengruber et al., 2007). Additional factors may associate with both PRCs increasing the variability of these complexes, and the function of PRC1 and PRC2 may be modulated by the presence of these proteins (Kerppola, 2009; Simon and Kingston, 2009).

PcG proteins were discovered in *Drosophila* through mutations resulting in aberrant development (Simon and Kingston, 2009; Schuettengruber et al., 2007). It has since been determined that Polycomb proteins function in stem cells to prevent inappropriate differentiation through the repression of target genes (Kerppola, 2009). Indeed, many targets of Polycomb are lineage-specific and

become activated during development (Lessard and Crabtree, 2010). The mechanisms of how Polycomb complexes mediate gene silencing are not well-understood, however, it may occur through chromatin compaction, cooperation with DNA methylation, or blockade of transcriptional elongation (Kerppola, 2009; Simon and Kingston, 2009; Schuettengruber et al., 2007).

The activity of Polycomb complexes is antagonized by another class of proteins known as the Trithorax group (TrxG) (Schuettengruber et al., 2007). TrxG proteins also function in complexes that fall into 2 categories: histone methyltransferases and nucleosome remodelers (Schuettengruber et al., 2007). The mammalian SWI/SNF complex (SWI/SNF, also known as the BAF complex) is an ATP-dependent chromatin remodeler comprised of 12 proteins and homologous to a yeast complex bearing the same name (Lessard and Crabtree, 2010). Like Polycomb complexes, SWI/SNF complexes containing alternate components mediate different functions. For example, Brg1 is required for embryonic development and mediates the activation of the zygotic genome while Brm does not appear to be essential for this process (Lessard and Crabtree, 2010). The mechanism of how SWI/SNF complexes abrogate Polycomb silencing is not clear; however, it may involve the decompaction of chromatin as well as the activity of other TrxG members.

The PcG and TrxG proteins function to maintain the expression status of genes when the initiating signal for either repression or activation is gone (Kerppola, 2009). This indicates that these proteins are responsible for the persistence of a particular program that was established by another factor.

Interestingly, SYT-SSX proteins interact with both PcG proteins and the SWI/SNF ATPases (Thaete et al., 1999; Nagai et al., 2001; dos Santos et al., 2000; Barco et al., 2009). The capacity to bring together these opposing functions implies not only the deregulation of the targets of these complexes but also the persistence of the altered program in the resulting tumor.

SYT-SSX directly mediates both transcriptional activation and repression through regulating the activity of PcG complexes (Lubieniecka et al., 2008; Barco et al., 2009). These data provide a mechanistic basis for epigenetic changes that may result in cellular reprogramming. Controlling transcription is central to tumorigenesis by SYT-SSX, thus further defining how the fusion accomplishes alterations in gene expression is essential to the development of specific therapies for the treatment of SS.

Purpose of this study

Players that are central to the maintenance of nuclear programs interact with SYT-SSX proteins. This enables SYT-SSX to dictate its own agenda within a target cell and propagate that program to daughter cells. Investigating the nature of the oncogenic program of SYT-SSX is necessary for the generation of more effective therapeutic interventions. The goal of this study is to define that program and the mechanism by which it is established.

Chapter 3 discusses the nature of the program activated by SYT-SSX2 in mesenchymal stem and progenitor cells. SS is a tumor believed to be derived

from mesenchymal tissues, and previous studies have suggested that it originates in stem cells. Upon its expression, SYT-SSX2 induces the expression of developmental and tissue-specific differentiation regulators. Moreover, a predominant activation of genes involved in neural lineages (neuronal and glial) occurs. This is associated with the formation of long projections and the expression of neurofilament protein. Genome-wide binding studies on SYT-SSX2 reveal that it is targeted to many of the neural-associated genes indicating their direct regulation by the fusion protein. In addition, SYT-SSX2 is recruited to the *Fgfr2* gene, and its association with *Fgfr2* correlates with expression. FGF signaling mediates the neural phenotype displayed by SYT-SSX2-expressing cells, and the inhibition of this signaling pathway results in decreased neurofilament expression in hMSCs transduced with the oncogene and SS tumor cell lines.

In Chapter 4, the genome-wide binding of SYT-SSX2 is studied in more depth in order to identify potential mechanisms of recruitment to target loci. SS likely originates from more than 1 progenitor cell population, and because it interacts with epigenetic regulators, its exact targets may differ depending on the initiating cell; however, the mode by which it is recruited will be similar across cell types. SYT-SSX2 association with the genome is non-random, and it localizes to distinct regions. Comparison with publicly available datasets defining regions enriched in specific histone modifications reveals a predominant association with H3K27me3, the modification characteristic of Polycomb-silenced genes. In fact, SYT-SSX2 occupies H3K27me3-labeled regions within or near over 70% of

positively-regulated and 40% of negatively-regulated genes in oncogene-expressing cells. These data support a role for SYT-SSX2 in the re-activation of Polycomb-silenced genes and suggest that Polycomb complexes serve as a recruitment module for the fusion protein. An additional subset of downregulated SYT-SSX2 target genes are characterized by association of the protein with histone modifications that correlate with transcriptional activation. Taken together, there are at least 2 mechanisms of SYT-SSX2 recruitment to target genes, one dependent on PcG proteins, and the other Polycomb-independent.

Chapter 5 covers the molecular mechanism of SYT-SSX2-mediated Polycomb derepression. Previous work shows that SYT-SSX2 abrogates silencing by PRC1 resulting in transcriptional activation due to enhanced degradation by Bmi1. A variety of cellular stresses in myoblasts, including SYT-SSX2 expression, results in alterations of Bmi1 mobility by SDS-PAGE. This is due to increased phosphorylation. SYT-SSX2 expression also leads to the loss of Bmi1 from a PRC1 target gene, *Ngfr*. This change was accompanied by alterations in histone modifications (from silent to active) and expression of *Ngfr* transcripts. *Ngfr* expression depends on the presence of the N-terminus of SYT, known to interact with Brg1 and p300. Studies with purified PRC1 components Ring1b and Bmi1 reveal that the ubiquitin E3-ligase activity of Ring1b is inhibited in the presence of SYT-SSX2-purified complexes. These data provide the foundation for additional mechanistic studies and indicate that SYT-SSX2 deregulates PRC1 function by inhibition of Ring1b activity. This may occur directly or by the recruitment of deubiquitylase activity. In summary, these data

support the hypothesis that SYT-SSX2 causes oncogenic transformation by cellular reprogramming.

CHAPTER II

MATERIALS AND METHODS

Molecular and cellular biology

Cell culture

U2OS human osteosarcoma cells, C2C12 mouse myoblasts (ATCC), and HeLa cells were maintained in DMEM supplemented with 10% FBS. The human synovial sarcoma SYO-1 cells (Kawai et al., 2004) were provided by T. Ito and M. Ladanyi and grown in collagen-coated (20 µg/ml) dishes with DMEM and 10% FBS. Human multipotent bone marrow mesenchymal stem cells (hMSCs) were acquired from Darwin Prockop's laboratory at the Texas A&M Health Science Center College of Medicine (TAMHSCCOM) Institute for Regenerative Medicine at Scott and White Hospital and maintained in their recommended growth medium. These were used in the experiments described throughout Chapter 3 and Appendix B Figure B3 and were early passage. They were isolated according to protocols established by the Prockop group (Colter et al., 2001; Sekiya et al., 2002) for the identification of multipotent MSCs. The hMSCs shown in Appendix B Figure B4 were provided by P. Young and M. Alfaro (Vanderbilt University, IRB#101438).

Antibodies and reagents

Mouse anti-Flag antibody, (Sigma, St. Louis, MO), mouse anti-H3K27me3, mouse anti-H3K4me3, mouse control IgG MOPC-173, (Abcam, Cambridge, MA), mouse anti-H3K18Ac (Cell Signaling, Danvers, MA), mouse anti-Ring1b (MBL, Woburn, MA), mouse anti-Bmi1, mouse anti H3K14Ac, mouse anti- H2AUb (Millipore, Billerica, MA), were used in chromatin immunoprecipitation (ChIP) assays and Western blotting. Rabbit polyclonal anti-HA (Sigma), mouse anti-NEF (light, medium, and heavy neurofilaments; Abcam), mouse anti-alpha-tubulin (Sigma), rabbit anti-FGFR2 (N-Term, Abgent, San Diego, CA), rabbit polyclonal anti-SSX2 B56 (Pretto et al., 2006), and mouse monoclonal anti-SYT SV11 (Pretto et al., 2006) antibodies were used for immunofluorescence staining and Western blotting. Mouse anti-Glu-Glu (2PY, Covance, Princeton, NJ) and mouse monoclonal anti-HA 12CA5 were used for immunoprecipitation (IP) and Western blotting. Rabbit anti-Brg1 (Millipore) was used for Western blotting. PD173074 was purchased from Cayman Chemical Company (Ann Arbor, MI). MG132 was obtained from Calbiochem (San Diego, CA). Sodium orthovanadate was obtained from Sigma.

Retroviral Infection of C2C12 cells

The double-tagged pOZ-HA-Flag parental vector and pOZ-SYT-SSX2-HA-Flag, and retroviral production and infection were described previously (Pretto et al., 2006). The LZRS-2PY-Bmi1 vector was provided by M. van Lohuizen. Construction of the SXdel3 mutant was described in Barco et al., 2009.

mRNA Isolation and Microarray

C2C12 myoblasts infected with retroviral pOZ vector and pOZ-SYT-SSX2 with greater than 90% efficiency were used as source of RNA. Human MSCs expressing pOZ and pOZ-SYT-SSX2 were selected as described (Nakatani and Ogryzko, 2003), prior to RNA isolation**.** Total cellular RNA was isolated 2 days and 4 days post-infection from SYT-SSX2- or control vector-expressing C2C12 and hMSCs cells, respectively**,** using the RNeasy Mini Kit (Qiagen, Valencia, CA) according to the manufacturer's protocol. RNA obtained from 2 independent experiments with each cell line was submitted to the Vanderbilt Functional Genomics Shared Resource. cDNA was produced from RNA samples using the Ambion WT Expression Kit (Applied Biosystems, Foster, CA) then fragmented and labeled according to the WT Terminal Labeling and Hybridization protocol (Affymetrix, Santa Clara, CA) prior to hybridization to the Affymetrix Mouse (C2C12) or Human (MSCs) Gene 1.0 ST array. Signal intensities were normalized by RMA, and fold enrichment was determined by calculating the ratio of the linearized signal intensities of the experimental versus control samples (or the negative reciprocal of the linearized signal ratio for values < 1). Genes with fold enrichments either greater than 1.6 or less than -1.6 (in C2C12) and greater than 2.0 or less than -2.0 (in hMSCs) were considered significant. Significant genes with known functions were manually annotated based on descriptions given in the GeneCards database (Safran et al., 2010; available at http://www.genecards.org) and Entrez Gene (Maglott et al., 2006; available at http://ncbi.nlm.nih.gov/gene).

Chromatin Immunoprecipitation

Chromatin immunoprecipitation was carried out as reported (Boyer et al., 2005) with some modifications. All lysis steps were carried out at 4˚C with rotation. Nuclei were sonicated (Misonix XL-2000) by performing 8 rounds of 3 x 5s pulses with at least 20s rest between pulses and 2 min rest between rounds. After sonication, lysis with 1% Triton-X was extended to 10 minutes at 4˚C with rotation prior to centrifugation. The supernatant was collected and precleared with 1µg control IgG bound to protein G Dynabeads (Invitrogen, Carlsbad, CA) for 1 hour at 4˚C. The precleared lysate was added to 5µg Flag or control mouse IgG antibody bound to protein G Dynabeads and incubated overnight at 4˚C with rotation. Washes, elution, and DNA purification were performed as noted. DNA was precipitated with ethanol (200 mM NaCl with 8 µg glycogen added to facilitate precipitation) and stored at –80˚C overnight. DNA was pelleted by centrifugation (13k rpm, 30 minutes), washed 2x with 70% ethanol, and allowed to dry before resuspension in 10mM Tris pH 8.0.

Analysis of ChIP DNA by Next-Generation Sequencing

250ng of ChIP DNA samples were sequenced by the Illumina Genome Analyzer II in the Vanderbilt Genome Technology Core. Sample DNA size and concentration were measured by Pico Chip and NanoDrop, respectively, followed by further sonication to generate DNA sizes between 150-200bp (Bioruptor, Diagenode, Denville, NJ; 5 min, low, 30s on and 30s off). Samples were further prepared by following the Illumina ChIP preparation protocol, then DNA ranging

from 150-275bp was gel purified, amplified by PCR, and diluted to 10nM for cluster generation.

RT-PCR

For RT-PCR analysis, total cellular RNA was isolated as described above, and 1 µg RNA was used to generate cDNA using the Superscript II Reverse Transcriptase kit (Invitrogen) according to the manufacturer's protocol. PCR conditions for RT-PCR were as follows: 94˚C for 1 min; 33 cycles of 94˚C for 1 min, 54˚C (or 56˚C for Ngfr, Dll1, Igf2, Tle4, Fgfr2, Kdm4b, Dkk3, Rarg, and Pdgfra) for 1 min, and 72˚C for 1 min 30 sec; 72˚C for 10 min. All PCR reactions were carried out using Platinum PCR Supermix (Invitrogen) according to the manufacturer's protocol. RT-PCR primer sequences are as follows:
Fgfr2 - Forward 5'-TGGTCACCATGGCAACCTTGTC-3', Reverse 5'-TAGCCTCCAATGCGATGCTCCT-3'; Fgfr3 - Forward 5'-CCCTCCATCTCC-TGGCTGAAG-3', Reverse 5'-CACCAGCCACGCAGAGTGATG-3'; Dll1 - Forward 5'-GCCAGGTACCTTCTCTCTGATC-3', Reverse 5'-TGGTGAGTACA-GTAGTTCAGGTC-'3; Gli2 - Forward 5'-GGACAGGGATGACTGTAAGCAG-3', Reverse 5'-CTCTTGGTGCAGCCTGGGATCT-3'; Hoxb5 - Forward 5'-CGCCAA-TTTCACCGAAATAGACG-3', Reverse 5'-CAAGATAACCAGTCCAGGAGAGA-3'; Wnt4 - Forward 5'-CAGGTGTGGCCTTTGCAGTGAC-3', Reverse 5'-CACTG-CCGGCACTTGACGAAG-3'; Wnt11 - Forward 5'-GGCCAAGTTTTCCGATGCT-CCT-3', Reverse 5'-CCCACCTTCTCATTC-TTCATGCA-3'; Id2 - Forward 5'-CGACTGCTACTCCAAGCTCAAG-3', Reverse 5'-CCTTCTGGTATTCACGCTC-

CAC-3’; Pth1r - Forward 5’-TGCACTGCACGCGCAACTACAT-3’, Reverse 5’-CCCTGGAAGGAGTTGAAGAGCA-3’; Sox9 - Forward 5’-CCCTTCATGAAGA-TGACCGACG-3’, Reverse 5’-CCGTTCTTCACCGACTTCCTCC-3’; Tle3 - Forward 5’-CGGTGAAGGATGAGAAGAACCAC-3’, Reverse 5’-GTTGGTGTGT-TGGACTTGAGCC-3’; Tle4 - Forward 5’-TCCTGTGATCGGATTAAGGAAGAG-3’, Reverse 5’-GGAGTCTCTGTCTCTTTGGTGAT-3’; Ngfr - Forward 5’-CAGGACTCGTGTTCTCCTGCC-3’, Reverse 5’-CCACAAGGCCCACAACCA-CAG-3’; Igf2 - Forward 5’-GGAAGTCGATGTTGGTGCTTCT-3’, Reverse 5’-CTGAACTCTTTGAGCTCTTTGGC-3’; Myogenin - Forward 5’-GCCCAGTGAAT-GCAACTCCCACA-3’, Reverse 5’-CTCTGGACTCCATCTTTCTCTCCT-3’; Tnnt1 - Forward 5’-GGCAGAAGATGAGGAAGCGGTG-3’, Reverse 5’-CCACGCTTCT-GTTCTGCCTTGAC-3’; Kdm4b - Forward 5’-GGGACTTCAACAGATATGTGG-CGT-3’, Reverse 5’-GCCAGGCAAACGTGGTCTTCCA-3’; Rarg - Forward 5’-CCCGACAGCTATGAACTGAGTCC-3’, Reverse 5’-AGGCAGATAGCACTAAGT-AGCCCA-3’; Pdgfra - Forward 5’-GGAGAAACGATCGTGGTGACCTG-3’, Reverse 5’-CCTGACTCTTCTGTACATCAGTGG-3’; Dkk3 - Forward 5’-CCTCC-CAACTATCACAATGAGACC-3’, Reverse 5’-GGTGATGAGATCCAGCAGCTGG-3’; Gapdh - Forward 5’-CCTTCATTGACCTCAACTAC-3’, Reverse 5’-GGAAGGCCATGCCAGTGAGC-3’.

ChIP-PCR Analysis

For ChIP-PCR experiments, ChIP DNA was isolated as described above. Whole cell extract DNA was taken from precleared lysates prior to addition of antibody-

bound beads. PCR conditions for ChIP-PCR were as follows: 94˚C for 5 min; 33 cycles of 94˚C for 1 min, 56˚C for 1 min, and 72˚C for 3 min; 72˚C for 10 min. PCR reactions were carried out using AmpliTaq Gold 360 DNA Polymerase (Applied Biosystems) according to the manufacturer's protocol. Fgfr2 ChIP primers are as follows: Forward 5'-GCGGACTCTCATCTCAACACTG-3', Reverse 5'-CCTGCCAGC-GATCATCATAAGC-3'.

Immunofluorescence

Immunofluorescent C2C12 and mesenchymal stem cell staining was generally performed 2 days post-retroviral (pOZ vectors) or lentiviral infections (shRNA), following standard protocols. Cells plated on gelatin (C2C12 and hMSCs)- or collagen (SYO-1)- coated cover slips were fixed in 3% para-formaldehyde, blocked with 3% goat serum and incubated with the designated primary antibodies for 2 hours at room temperatures and 30 minutes with the appropriate secondary antibodies (Alexa-Fluor, Invitrogen).1x PBS solution was used for all washes. The Zeiss Axioplan2 fluorescent microscope was used for imaging.

Human bone marrow-derived mesenchymal stem cells and differentiation assays

Adipogenic and osteogenic differentiation assays in the hMSCs were conducted according to the Protocol for Expansion of Human MSCs provided by the Institute for Regenerative Medicine at Scott and White Hospital (TAMHSCCOM). Oil-Red-O staining was performed as previously described in (Feldman and Dapson, 1974). The Alkaline Phosphatase kit from Sigma was used for osteogenic

staining. Alizarin Red method was provided by the Institute for Regenerative Medicine at Scott and White Hospital (TAMHSCCOM).

Growth inhibition sulforhodamine B (SRB) assay

Two days after lentiviral FGFR2-shRNA infection, SYO-1 cells were seeded in 96-well plates at $2x10^4$/well and allowed to grow for two additional days. Or, one day after seeding the SYO-1 cells as described above, PD173074 was added for a 48 hour-duration. After the indicated times in both experiments, the cells were fixed with 10%TCA and stained with SRB to measure protein density at 488 nm excitation and 585 nm emission wavelengths following established protocols (Vichai and Kirtikara, 2006).

SYT-SSX2 SiRNA

For SYT-SSX2 depletion in SYO-1 cells, one control (INV) and two SSX2-specific (Si-SSX2A and Si-SSX2B) RNA duplexes were used. Successful depletion with INV, Si-SSX2A (Pretto et al., 2006), and Si-SSX2B (Lubieniecka et al., 2008) was previously reported. siLentFect reagent (BioRAD, Hercules, CA) was used for transfections performed according to company protocols. Protein levels in cellular lysates and NEF-positivity were quantitated 3 days after siRNA addition.

FGFR2 ShRNA

Lentiviral human FGFR2-specific ShRNA bacterial stocks were purchased from Sigma (NM_000141). The vector that failed to target FGFR2 (2910) was used as

a negative control. It contained the following oliogomer: 5'-CCGGGCCAACCT-CTCGAACAGTATTCTCGAGAATACTGTTCGAGAGGTTGGCTTTTT-3'. Two lentiviral vectors allowed FGFR2 depletion (clones 833 and 703). They contained the following targeting sequences: ShRNA 833: 5'-CCGGCCCAACAATAGGAC-AGTGCTTCTCGAGAAGCACTGTCCTATTGTTGGGTTTTT-3' and ShRNA 703: 5'-CCGGGCCACCAACCAAATACCAAATCTCGAGATTTGGTATTTGGTTGG-TGGCTTTTT-3'. The ShRNA lentiviruses were produced in 293T cells as previously described (Brown et al., 2009). 20 µg of lentiviral DNA were used to transfect one 100mm plate of 293T cells. 48 hours post-transfection, the viruses were harvested and used to infect hMSCs and SYO-1 cells for a 6-hour duration with added polybrene. The hMSCs were routinely infected with the FGFR2-shRNA vectors 24 hours after prior transduction with the pOZ and pOZ-SYT-SSX2 retroviral vectors. Effects of shRNAs on FGFR2 levels and NEF expression in hMSCs and SYO-1 cells were measured 2 days and 3 days post-lentiviral infection, respectively.

Generation of bacterial expression plasmids

The bacterial expression plasmids pLM302 and pLM302-yTAF12 were kind gifts from P.A. Weil. Human Ring1b, mouse Bmi1, and human SYT-SSX2 were PCR amplified with the following primers:

Ring1b-forward 5'-GCGCGGATCCTCTCAGGCTGTGCAGACAAAC-3', Ring1b-reverse 5'-GCGCCTCGAGTCATTTGTGCTCCTTTGTAGGTG; Bmi1-forward 5'-GCGCGGATCCCATCGAACAACCAGAATCAAGATC-3', Bmi1-reverse 5'-

GCGCCTCGAGCTAACCAGATGCCGTTGCTGATGACC-3'; SYTSSX2-forward 5'-GCGCGAATTCGTCTGTGGCTTTCGCGGCCCC-3', SYTSSX2-reverse 5'-GCGCCTCGAGTTACTCGTCATCTTCCTCAGGGTCGC-3'. Amplified fragments were digested with BamH1 and Xho1 (Ring1b and Bmi1) or EcoR1 and Xho1 (SYT-SSX2), gel purified, and ligated into pLM302. Ligation products were transformed into *E.coli* DH5α and plated on kanamycin-containing (50 µg/mL) selection plates. Colonies were screened for the presence of the appropriate insert and then sequenced.

2PY-Bmi1 immunoprecipitation and λ-phosphatase assay

MG132- or DMSO-treated C2C12 cells expressing 2PY-Bmi1 were lysed in 20 mM Tris pH 8.0, 150 mM NaCl, 0.5% NP-40, plus protease and phosphatase inhibitors for 30 minutes at 4˚C with rotation. Cellular debris was pelleted by centrifugation (13k rpm, 4˚C, 15 minutes), and the supernatant was collected. 1 µL Glu-Glu antibody was added to each supernatant and rotated for 2h at 4˚C, and antibody-bound proteins were captured with rabbit antiserum to mouse IgG (whole molecule, Cappel) for 0.5h at 4˚C then protein A sepharose (GE Healthcare Bio-sciences, Piscataway, NJ) for 0.5h at 4˚C. Beads were washed twice with lysis buffer lacking inhibitors then once with lysis buffer plus protease inhibitors. Wash buffer was aspirated and the samples were stored on ice during λ-phosphatase preparation. Reaction buffer was prepared in separate tubes according to the manufacturer's protocol (NEB, Ipswich, MA) plus 10 µL/mL aprotinin and 10 µL/mL leupeptin with and without 5 mM NaF and 10 mM NaOV.

500 U λ–phosphatase were added to each tube containing reaction buffer and activated by incubation at 30˚C for 2 minutes. Enzyme-reaction mixture was added to the immunoprecipitated material and incubated at 30˚C for 2h with intermittent mixing. Reactions were quenched by the addition of 2x sample buffer and stored at -20˚C. Samples were analyzed by SDS-PAGE without boiling to prevent the dissociation of the antibody chains.

Purification of bacterially-expressed Ring1b, Bmi1, and SYT-SSX2

Expression vectors were transformed into Rosetta 2(DE3)pLysS competent *E.coli* (Novagen, Rockland, MA) according to the manufacturer's protocol and grown on kanamycin/chloramphenicol (50 ug/mL kanamycin, 34 ug/mL chloramphenicol) selection plates. All subsequent growth and induction steps were performed at 25˚C. Single colonies were inoculated in LB containing antibiotics and grown overnight. For Bmi1 and Ring1b, overnight cultures were diluted 1:20 into fresh LB, grown for 2 hours then induced with 0.5 mM IPTG for 4 hours. For SYT-SSX2, 1:20 dilution of overnight cultures was grown for 4h then induced with 0.1 mM IPTG overnight. After induction, bacteria were pelleted and resuspended in buffer (20 mM Tris 7.5, 150 mM NaCl or 300 mM NaCl for Bmi1). Bacteria were treated with lysozyme (0.75 mg/mL) for 20 minutes on ice, subjected to 2 freeze/thaw cycles, then centrifuged for 1 hour at 12k rpm at 4˚C. Glycerol was added to the supernatants to a final concentration of 10% (v/v), and the crude extracts were snap frozen in a dry ice/ethanol bath and stored at -80˚C. Amylose resin (NEB) was washed with bacterial resuspension buffer, and crude

extracts were added to pre-washed resin. Proteins were allowed to bind for 30 minutes at 4˚C with rotation and eluted using 10 mM maltose added to resuspension buffer. An aliquot of eluate was reserved to measure protein concentration before the addition of glycerol (10% v/v final concentration), snap freezing, and storage at -80˚C.

Nucleosome isolation

Nucleosomes were prepared as described by Hernández-Muñoz et al, 2005. C2C12 or HeLa cells were washed 3 times with 1x PBS then harvested and pelleted at 2k rpm, 4˚C for 10 minutes. Cells were resuspended in 2 packed cell volumes of buffer containing 10 mM HEPES pH 7.9, 1.5 mM $MgCl_2$, 10 mM KCl, 0.5 mM DTT and incubated on ice for 10 minutes. Cell suspensions were transferred to a Dounce homogenizer and lysed with 10 strokes using a loose pestle. The cell lysates were then centrifuged for 5 minutes at 2.8k rpm (750 x g), 4˚C. Pellets were resuspended in buffer containing 50 mM Tris pH 7.5, 0.34 M sucrose, 3 mM $CaCl_2$, 60 mM KCl, 0.5 mM PMSF, 0.4 mM benzamidine, 10 µM leupeptin, and 1 µg/mL aprotinin. The DNA was digested using micrococcal nuclease (NEB; 325 U/mL lysate) at 37˚C for 10 minutes, and the reaction was quenched by adding EGTA to a final concentration of 0.05 mM. The extracts were further lysed by Dounce homogenization (100 strokes, tight pestle) followed by the addition of 500 mM NaCl (final concentration). Cellular debris was pelleted (12.1k rpm [14k x g], 4˚C, 20 minutes), and the supernatant was dialyzed overnight against 20 mM HEPES pH 7.5, 2 mM EDTA, 2 mM EGTA, 650 mM

NaCl, 1 mM β-mercaptoethanol, 0.5 mM PMSF, 2 mM benzamidine, and 16 mM β-glycerophosphate. 2x sample buffer was added to an aliquot of nucleosome extract and analyzed by western blotting for the presence of H2A, H2B, H3, and H4. To check DNA digestion, nucleosome extracts were diluted to 150 mM NaCl, 20 mM HEPES pH 7.5, 2 mM EDTA, and 2 mM EGTA. 20µg proteinase K was added, and the extracts were incubated overnight at 55˚C. The next day, the DNA was purified by phenol:chloroform extraction and precipitated overnight with ethanol (200 mM NaCl and 1µg glycogen were added to facilitate precipitation) at -80˚C. The DNA was pelleted, washed with 70% ethanol, and air dried before resuspension in TE and analysis by gel electrophoresis.

Preparation of nuclear extracts

Naïve, pOZ-, or SYT-SSX2-expressing C2C12 cells were washed 3 times with and harvested in 1x PBS (48 hours post-infection for pOZ and SYT-SSX2 samples). Cells were collected by pulse-spinning and washed once with hypotonic buffer (10 mM HEPES pH 7.9, 1.5 mM $MgCl_2$, 10 mM KCl, 0.5 mM DTT). The cells were then incubated in 2 packed cell volumes of hypotonic buffer for 10 minutes on ice. Cells were lysed by the addition of 2 µL 5% NP-40 and gentle mixing 5 times by pipet. Nuclei were pelleted by pulse-spinning then lysed in buffer containing 2 0mM Tris pH 8.0, 300 mM NaCl, 0.5% NP-40, 10% glycerol, and protease/phosphatase inhibitors for 20 minutes at 4˚C with rotation. Nuclear debris was pelleted by centrifugation (13k rpm, 15 minutes, 4˚C), and supernatants were flash frozen and stored at -80˚C.

In vitro ubiquitylation assay

Ubiquitylation assays were performed as described previously (Cao et al., 2005) with some modification. Bacterially purified Ring1b and Bmi1 were added individually or in complex (equimolar amounts of Ring1b and Bmi1 were incubated together on ice for 10-15 minutes) to an ubiquitylation reaction mixture containing 50 mM Tris pH 7.9, 5 mM $MgCl_2$, 2 mM NaF, 0.6 mM DTT, 2 mM ATP, 10 µM okadaic acid, 0.1 µg recombinant human ubiquitin-activating enzyme (E1, Calbiochem, La Jolla, CA), 0.6 µg recombinant human UbcH5c (E2, Calbiochem), and 1 µg FLAG-ubiquitin (Sigma, St. Louis, MO). Bacterially purified SYT-SSX2, pOZ- or SYT-SSX2-expressing cell nuclear extracts, and/or 5 µg of HeLa nucleosomes were added as indicated. Reactions were incubated for 1 hour at 37˚C and stopped by the addition of 2x sample buffer.

Computer analyses

Data accessibility

All microarray and ChIPSeq data are available at the Gene Expression Omnibus (available at www.ncbi.nlm.nih.gov/geo/; Edgar et al., 2002) accessions GSE26562 (C2C12 microarray), GSE26563 (hMSC microarray, GSE26564 (SYT-SSX2 ChIPSeq), and GSE26565 (accession for all datasets).

Analysis of SYT-SSX2 ChIPSeq

The Illumina Analysis Pipeline was used for image analysis and base calling. Sequence reads from the control IgG ChIP and SYT-SSX2 ChIP were aligned to the mouse genome using Bowtie (Langmead et al., 2009) utilizing the "--best" option to generate SAM files for each condition. The output SAM files were used as the input for the Model-based Analysis of ChIPSeq (MACS) program (Zhang et al., 2008) to determine peak regions in SYT-SSX2-expressing cells using default parameters except "--mfold" was 16. For each peak, the distance to the nearest gene was calculated based on the position of the 5' end of the peak and transcription start sites annotated in the UCSC Genome Browser (July 2007, build mm9) (Kent et al., 2002; Fujita et al., 2010).

Cross-validation of C2C12 Microarray with ChIPSeq

Distances to the nearest upstream and downstream peaks were determined for each significantly upregulated gene of the C2C12 microarray. Distances were determined by calculating the average distance between the transcription start site annotated for the given RefSeq accession (Pruitt et al., 2007) and the nearest peak summit.

Motif Analysis

ChIPSeq peaks within 10kb upstream of transcription start sites of upregulated genes were utilized for motif analysis. Repeat elements were masked using the DUST program (Morgulis et al., 2006) prior to motif search analysis using MEME

using default parameters (Bailey and Elkan, 1994). The position-specific probability matrix derived from MEME was used as input for the TOMTOM program (used with default parameters) to determine potential transcription factor binding sites within the motifs (Gupta et al., 2007).

Overlap of SYT-SSX2 with histone modifications, DNA methylation, and PolII in C2C12 cells

Previously published ChIPSeq datasets for ubiquitylated histone H2B (H2BUb); mono-, di-, and trimethylated histone H3 lysine 4 (H3K4me1/2/3); acetylated histone H3 lysine 9 (H3K9Ac), lysine 18 (H3K18Ac), and histone H4 lysine 12 (H4K12Ac); trimethylated histone H3 lysine 27 (H3K27me3) and lysine 36 (H3K36me3); and RNA polymerase II (PolII) were downloaded from the Gene Expression Omnibus (GEO) accession GSE25308 (Asp et al., 2011). MeDIP-ChIP data were obtained from GEO accession GSE22077 (Hupkes et al., 2011). Overlapping regions between individual datasets and SYT-SSX2 were determined using the Coverage and Intersect tools from the Galaxy program (available at http://main.g2.bx.psu.edu/) (Giardine et al., 2005; Goecks et al., 2010; Blankenberg et al., 2010).

Association of SYT-SSX2 ChIPSeq peaks with gene expression

SYT-SSX2 peaks were annotated to the nearest downstream gene on both strands by measuring the distance from the 5’ end of the peak to the gene

transcription start site (TSS). Peaks associated with differentially expressed genes were identified.

Hierarchical clustering

Differentially regulated genes containing overlapping sites between SYT-SSX2 and specific epigenetic markers within the gene and up to 50kb upstream of the TSS were used in the clustering analysis. For each gene, coverage ratios (the number of bases covered by overlapping regions divided by the total number of bases in a given window) for the gene body and for 5kb bins upstream of the TSS (up to 50kb) were calculated for each epigenetic marker. These coverage ratios served as the input data for the clustering analysis. Hierarchical clustering was performed separately for up- and downregulated genes using Cluster 3.0 (de Hoon et al., 2004) with gene and array clustering. The similarity metric used was Spearman Rank Correlation, and the clustering method used was centroid linkage. The output file was uploaded to Java Treeview (Saldanha, 2004) for visualization. Heat map images were downloaded from Java Treeview.

CHAPTER III

REPROGRAMMING OF MESENCHYMAL STEM CELLS BY SYT-SSX2

Introduction

SS tumors display a wide spectrum of phenotypes including characteristics of neural, mesenchymal, and epithelial differentiation (Ladanyi, 2001; Ishibe et al., 2008; Naka et al., 2010). SS tumor cell lines exhibit limited differentiation potential implying a stem cell origin for this malignancy (Ishibe et al., 2008; Naka et al., 2010). One study revealed that SYT-SSX silencing in SS cells permits their differentiation into multiple mesenchymal lineages, while another group was able to show neuronal differentiation after treatment with FGF2 or ATRA (all-trans retinoic acid), supporting the hypothesis that SS arises in human multipotent stem cells (Naka et al., 2010, Ishibe et al., 2008). Deregulation of normal differentiation driven by SYT-SSX is therefore believed to be the basis for transformation that leads to cancer development (Naka et al., 2010). However, it remains to be determined how SYT-SSX expression affects the differentiation of normal somatic stem cells. Another interesting facet to this issue is the question of whether SYT-SSX itself confers plasticity on its target cell or if the plasticity of the tumor cells is solely a reflection of multipotency in the cell-of-origin. Elucidating the nuances of this topic will be crucial in developing effective therapies for SS with minimal repercussions to normal tissues.

Recent efforts have focused on determining the cell-of-origin for SS since it is still unclear what cell type is involved the formation of SS tumors. Distinguishing these target cells is of particular interest since knowledge of their identity may lead to the development of more effective therapies. It is generally believed that SS arises from a mesenchymal stem or progenitor cell (Mackall et al., 2004); however, investigations into the ability of SS tumor cells to differentiate into multiple lineages have confounded this issue (Naka et al., 2010; Ishibe et al., 2008). Tumors display increased expression of genes associated with neural functions like axon growth and signaling suggesting that SS is derived from neural crest cells. The disparate sites of tumor growth also imply that the originating cell may be of neural crest lineage. Treatment of cell lines with ATRA or FGF2 leads to neuronal differentiation adding additional support to this hypothesis (Ishibe et al., 2008). In contrast, tumor cell lines express osteogenic, chondrogenic, adipocytic, and hematopoietic markers, and knock-down of the oncogene causes the expression of additional mesenchymal and hematopoietic markers and the adoption of a morphology resembling that of MSCs. Moreover, these cells could also be induced to differentiate into mesenchymal lineages and macrophage-like cells with the efficiency of differentiation increasing after knock-down of SYT-SSX1. These results implicate the transformation of a multipotent stem cell with both mesenchymal and hematopoietic potential (Naka et al., 2010). While tissue-specific stem cells with this spectrum of differentiated lineages have not been discovered, neural crest-derived stem cells have the capacity to differentiate into mesenchymal lineages, and MSCs can be induced to form

neurons indicating that these cell populations are capable of forming cell-types outside of their normal lineages (Shakhova and Sommer, 2010; Chen et al., 2006).

Results

SYT-SSX2 expression deregulates developmental programs and differentiation in myoblasts

SYT-SSX expression is sufficient to drive tumorigenesis (Nagai et al., 2001; Haldar et al., 2007) and previous studies show that SYT-SSX fusions might alter the differentiation potential of synovial sarcoma cells (Naka et al., 2010; Ishibe et al., 2008). What has been lacking, however, is a thorough analysis of the initial changes that occur in the mesenchymal precursor cell when SYT-SSX is expressed. We chose to conduct such analysis in C2C12 myoblasts because they are a well-characterized, untransformed system of mesenchymal lineage capable of differentiation into multiple cell types (Odelberg et al., 2000). Additionally, in a transgenic synovial sarcoma model, SYT-SSX2 expression in muscle progenitors formed tumors that recapitulated the human disease (Haldar et al., 2007), further indicating that myoblasts are a relevant model system.

After confirming their myogenic identity with a marker profile and myotube formation (Appendix B Figure B1), we transduced C2C12 myoblasts with HA-Flag-SYT-SSX2 or vector control to define their genetic programs. The microarray analysis generated 700 upregulated and over 800 downregulated genes. Comparison of this data to a microarray of 8 human synovial sarcomas (Nielsen et al., 2002) identified nearly 100 upregulated genes shared between SYT-SSX2-myoblasts and human tumors (Appendix B Table B1). Strikingly, many of these shared genes were lineage determinants (Pth1r, Ngfr, Hoxb5, and

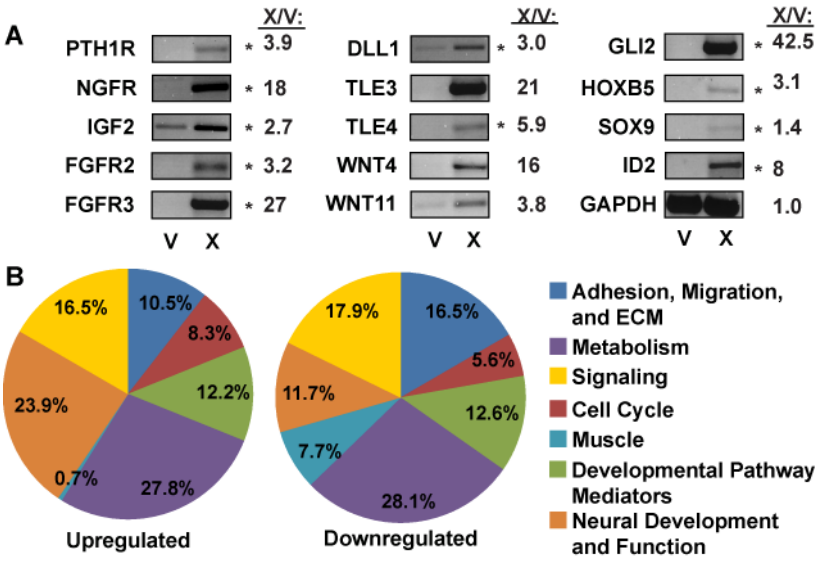

Figure 2. Alterations in cellular programs in myoblasts by SYT-SSX2.
A) RT-PCR in myoblasts expressing SYT-SSX2 (X) or vector control (V). Of 17 genes tested, 14 showed upregulated expression in SYT-SSX2 cells. Asterisks (*) denote genes shared by SYT-SSX2-myoblasts and human SS tumors (Nielsen, et al., 2002). GAPDH served as loading control. X/V ratios represent fold increase in gene transcription, as measured by the Fluorchem 8900 densitometer with the AlphaEase FC program. B) Functional categorization of significantly (1.6-fold change) regulated genes in SYT-SSX2-positive cells. Of the total upregulated and downregulated genes, 695 upregulated (left) and 677 downregulated (right) genes had known functions and are represented in the pie charts.

Sox9) and mediators of developmental pathways such as FGF (Fgfr2 and Fgfr3), Notch (Dll1), Hedgehog (Gli2), and Wnt (Tle4) (Figure 2A). Their expression was validated by RT-PCR (Figure 2A, asterisks). Furthermore, upregulation of various Wnt ligands, (Figure 2A, Wnt4 and Wnt11; Nielsen et al., 2002) in both SYT-SSX2-myoblasts and human SS tumors reflected a sustained activation of this pathway.

An overall functional categorization of the upregulated genes revealed 85 (12.2%) to be involved in development (Figure 2B), the majority of which function in lineage specification (Appendix B Table B2). Similarly, 85 (12.6%) of the downregulated genes are involved in differentiation and development (Figure 2B). Most striking, however, was the upregulation of 166 genes (23.9%) normally involved in neural differentiation and function (Figure 2B and Appendix B Table B3). Notably, we observed a simultaneous downregulation of 52 (7.7%) myogenic genes (Figure 2B), including terminal differentiation markers (troponin and muscle-specific myosins) as well as transcriptional controllers of myogenesis (Myf5, MyoD, and myogenin; Appendix B Table B4 and Figure B2A). These data suggested a block of myogenic differentiation that was confirmed when SYT-SSX2-expressing myoblasts failed to form multinucleated myotubes and continued to grow as mononucleated cells (Appendix B Figure B1). Altogether, SYT-SSX2 expression in myoblasts led to the abrogation of myogenesis with an apparent concomitant reprogramming towards neural lineages.

Targeting of SYT-SSX2 to chromatin is required for occupancy of neural genes and induction of the neural phenotype

To identify the specific subset of genes to which the SYT-SSX2 complex is recruited, we conducted ChIP-Sequencing (ChIPSeq) analysis and determined the genome-wide occupancy of SYT-SSX2. We used myoblasts transduced with HA-Flag-SYT-SSX2 due to lack of an appropriate antibody that efficiently recognizes native SYT-SSX2 epitopes in ChIP experiments. ChIPSeq for SYT-SSX2 yielded over 19 million unique tags compared with over 16 million unique tags in the control. Putative SYT-SSX2 target sites were determined by the Model-based Analysis of ChIPSeq (MACS) program. This analysis validates true peaks by calculating the significance of each candidate peak relative to the control using a significance threshold (Zhang et al., 2008). In our study, this method generated approximately 53,000 peaks with a maximum false discovery rate of 2.8%. The ChIP peaks were categorized by their distance upstream of transcription start sites (TSS, +1) and the results are shown in Table 1. On the whole, the majority of peaks (approximately 60%) are located at distances greater than 50kb from TSS. Closer to known genes, 20% of the peaks are located within 20kb upstream of TSS, with over 6000 sites (11.5% of the total peaks) between 0-10kb (Table 1). 3440 sites are located within 5kb upstream of TSS corresponding to 1352 genes (Table 1). As an extension of this data, we also found that SYT-SSX2 bound within a total of 3,290 genes and exclusively within the body of 821 genes. Given that SYT-SSX2 associates with transcription regulators, we decided to analyze more closely the genes with SYT-SSX2

occupancy near their TSS. As a starting point, we selected the genes with SYT-SSX2 peaks situated up to 10kb upstream of their TSS, in the event the oncogene, like other known transcription regulators, binds beyond the traditional promoter region (Farnham, 2009). Moreover, by nature of their function, the Polycomb and SWI/SNF chromatin modifying complexes SYT-SSX2 associates with, may direct its docking at sites farther from the traditional 5 kb proximal regulatory region (Mateos-Langerak and Cavalli, 2008).

Table 1. Distribution of SYT-SSX2 ChIP peaks relative to gene transcription start sites and corresponding genes.

Distance	Number of peaks	Percentage of total peaks	Total number of genes
0-5kb	3440	6.5	1352
5-10kb	2654	5.0	1076
10-15kb	2400	4.5	1016
15-20kb	2287	4.3	933
20-50kb	10230	19.3	2026
50-100kb	10312	19.5	1693
100-150kb	6035	11.4	973
150-200kb	3956	7.5	659
>200kb	11678	22.0	984

Focusing on the window 10kb upstream of gene TSS, cross-validation of the microarray with the ChIPSeq data revealed that SYT-SSX2 was physically recruited to approximately 200 of the upregulated genes and to only 51 of the downregulated genes. Functionally, the downregulated 51 genes followed the general distribution of genes in the overall microarray (Appendix B Figure B2B). Strikingly, genes associated with neural development and function, were quite prevalent (42.8%; 68 genes) among the 200 upregulated genes bound by the SYT-SSX2 complex (Figure 3A). These genes are active in different aspects of

neural differentiation including patterning, axon guidance, signaling, and growth (Table 2). This is remarkable as C2C12 cells are mesenchymal progenitors and do not naturally differentiate into neural lineages.

Table 2. Selected list of upregulated genes bound by the SYT-SSX2 complex involved in neural development and function.

Symbol	Gene Description	Symbol	Gene Description
Development and Differentiation			
Bhlhe23	basic helix-loop-helix, e23	Fezf2	Fez family zinc finger
L1cam	cell adhesion molecule	Olig2	oligodendrocyte lineage factor
Prox1	prospero homeobox	Ptpru	protein tyrosine phosphatase
Zcchc12	zinc finger with CCHC domain	Zic2	Zinc finger protein of cerebellum
Patterning and Axon Guidance			
Crmp1	collapsin response mediator	Dpysl5	dihydropyrimidinase-like 5
Epha8	Eph receptor A8	Efnb1	ephrin B1
Ephb1	Eph receptor B1	Slit3	slit homolog 3
Unc5a	Netrin receptor		
Neurotransmitter Signaling and Metabolism			
Abat	aminotransferase	Adra2c	adrenergic receptor
Cacna1h	calcium channel	Cacng5	calcium channel
Chrna4	cholinergic receptor	Grm4	glutamate receptor
Kcnip3	Kv channel interacting protein 3	Nptx1	neuronal pentraxin 1
Slc6a1	GABA transporter	Th	tyrosine hydroxylase
Neuropeptide, Lipid, and Hormone Signaling			
Cck	cholecystokinin	Faah	fatty acid amide hydrolase
Gpr50	G protein-coupled receptor 50	Gal	galanin
Mgll	monoglyceride lipase	Ntsr1	neurotensin receptor 1
Pdyn	prodynorphin	Sst	somatostatin
Adhesion, Growth, and Survival			
Amigo2	adhesion molecule	Bai1	brain angiogenesis inhibitor 1
Bai2	brain angiogenesis inhibitor 2	Cdh23	cadherin 23
Gjb2	gap junction protein	Ngfr	nerve growth factor receptor

Further analysis of the ChIPSeq peaks located upstream of the 200 genes (approximately 500 peaks total) derived a recruitment motif for SYT-SSX2 rich in C and T residues (Figure 3B, first column) and contained in one hundred thirty-two (132) peaks. This motif contains potential binding sites for a group of transcription factors belonging to the homeodomain, nuclear receptor, and Sp1 families (Figure 3B, third column) known to be involved in stem cell programming

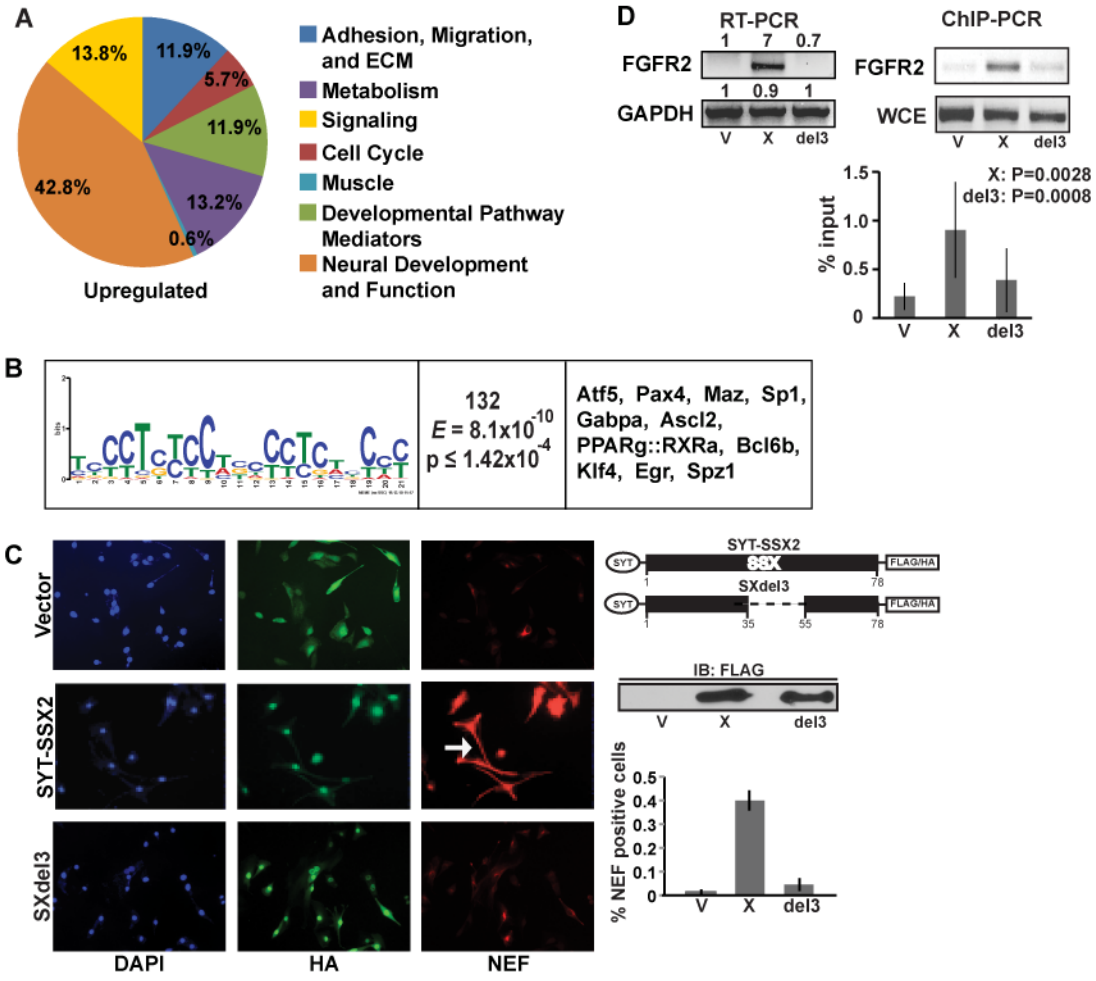

Figure 3. Activation of a neural program by SYT-SSX2.
A) Functional categorization of significantly upregulated genes that also have SYT-SSX2 complex binding sites between 0 and 10kb upstream of their TSS. The functions of 159 genes were annotated and are represented in the pie chart. B) Motif analysis of SYT-SSX2 ChIPSeq peaks. First column: a putative SYT-SSX2 complex binding motif derived by MEME. Residue height is proportional to the probability of its presence at a given position. Second column: number of peaks containing the motif. The E score and P value denote the statistical validity of the consensus sequence. Third column: transcription factors that may bind to the given motif. C) Neurofilament (NEF) formation in SYT-SSX2- and SXdel3-myoblasts. HA-Flag-vector- (top row), HA-Flag-SYT-SSX2- (middle row), and HA-Flag-SXdel3 cells were stained for HA (green) and NEF (red) and visualized by fluorescence microscopy. DAPI (blue) is nuclear stain. Arrow highlights a cell with a long projection. Images were taken at 20x magnification. Diagram shows the deleted segment of SSX2 in SXdel3. A Flag immunoblot shows expression levels in V (vector), X (SYT-SSX2), and del3 (SXdel3) cellular lysates. Histogram represents the average ratio of NEF-positive cells to HA-positive cells, in V control, X, and del3 cells (n=3). Error bars denote standard deviation. F) FGFR2 RT-PCR in myoblasts expressing vector control (V), SYT-SSX2 (X), or SXdel3 (del3). Numbers represent ratios of expression levels in X and del3 over V cells. Signal intensities were measured by the Fluorchem 8900 densitometer with the AlphaEase FC program. Lower panel: chromatin immunoprecipitation (ChIP) of SYT-SSX2 and SXdel3 at the peak located upstream of the Fgfr2 gene, using the anti-Flag antibody, in V control, X, and del3 myoblasts. Whole cell extract DNA (WCE) served as positive control. Histogram represents average of SYT-SSX2, SXdel3, and control vector binding to the Fgfr2 peak, measured as percent input. Results from 4 ChIP-PCR experiments were used for the analysis. Error bars are standard deviations. X:P denotes significance of X values relative to V. Del3:P denotes significance of SXdel3 values relative to X.

and differentiation. The extensive association of SYT-SSX2 with neural genes led us to question if these myoblasts exhibited a matching phenotype. In a background of 80% to 90% infection efficiency, 40% of SYT-SSX2-myoblasts expressed neurofilament (NEF, Figure 3C, middle row, right panel and histogram), while control cells showed minimal (< 2%) neurofilament staining (Figure 3C, top row, right panel). The empty vector produces a short HA-Flag-peptide that allows the visualization of positively infected control cells (Figure 3C, top row, middle panel). Moreover, oncogene-expressing cells exhibited long projections (Figure 3C, arrow), similar to a phenotype we observed in SYT-SSX2-expressing fibroblasts (Barco et al., 2007) and consistent with the neurogenic features noted in synovial sarcoma cells (Ishibe et al., 2008). Overall, stimulation of a pro-neural program appears to be a pronounced feature of SYT-SSX2.

Mediators of differentiation including the Wnt, Hedgehog, and FGF pathways formed an additional 11.9% (19 genes) of the 200 genes occupied by SYT-SSX2 (Figure 3A; Appendix B Table B2, asterisks). In particular, we noticed the presence of FGF mediators throughout our analyses. By microarray, a number of FGF pathway members were upregulated (Appendix B Table B2), and increased expression of FGF receptors *Fgfr2* and *Fgfr3* was confirmed by RT-PCR (Figure 2A). Importantly, the same *FGFR2 and FGFR3* were also upregulated in human synovial sarcomas (Appendix B Table B1; Nielsen et al., 2002). ChIPSeq analysis indicated that the *Fgfr2* gene is directly targeted by SYT-SSX2, and further ChIP experiments confirmed the presence of SYT-SSX2

at the peak located 4.3 kb upstream of the *Fgfr2* gene (Figure 3D, ChIP-PCR panel). Notably, the *Fgfr2* peak contains a sequence matching the SYT-SSX2 recruiting motif (Figure 3B). Thus, the FGF receptor appears to be a direct target of the oncogene.

SYT-SSX2 associates with Polycomb complexes, modulators of chromatin and lineage determination. To determine whether the ability of SYT-SSX2 to target chromatin is required for the observed effects, we tested SXdel3, a SYT-SSX2 mutant with a twenty-residue deletion in its SSX-targeting module (Figure 3C, diagram). SXdel3 is unable to co-localize with Polycomb and antagonize its Bmi1 component in U2OS cells (Barco et al., 2009). When assayed in C2C12 cells, SXdel3 failed to induce neurofilament formation (Figure 3C, bottom row, right panel), indicating an inactive neural program. Furthermore, we observed that the ability of SXdel3 to upregulate *FGFR2* expression (Figure 3D, RT-PCR panel), or bind upstream of the gene (Figure 3D, ChIP-PCR panel and histogram), was markedly diminished. To summarize, these studies demonstrate that SYT-SSX2 activates a pro-neural program and blocks normal myogenesis. Its ability to bind chromatin is required for its transcriptional and phenotypic effects.

SYT-SSX2 causes aberrant differentiation in human mesenchymal stem cells

Myoblast reprogramming by SYT-SSX2 prompted us to question whether dictating lineage commitment in undifferentiated precursors is an intrinsic feature of the oncogene. As synovial sarcoma is thought to arise in a mesenchymal stem

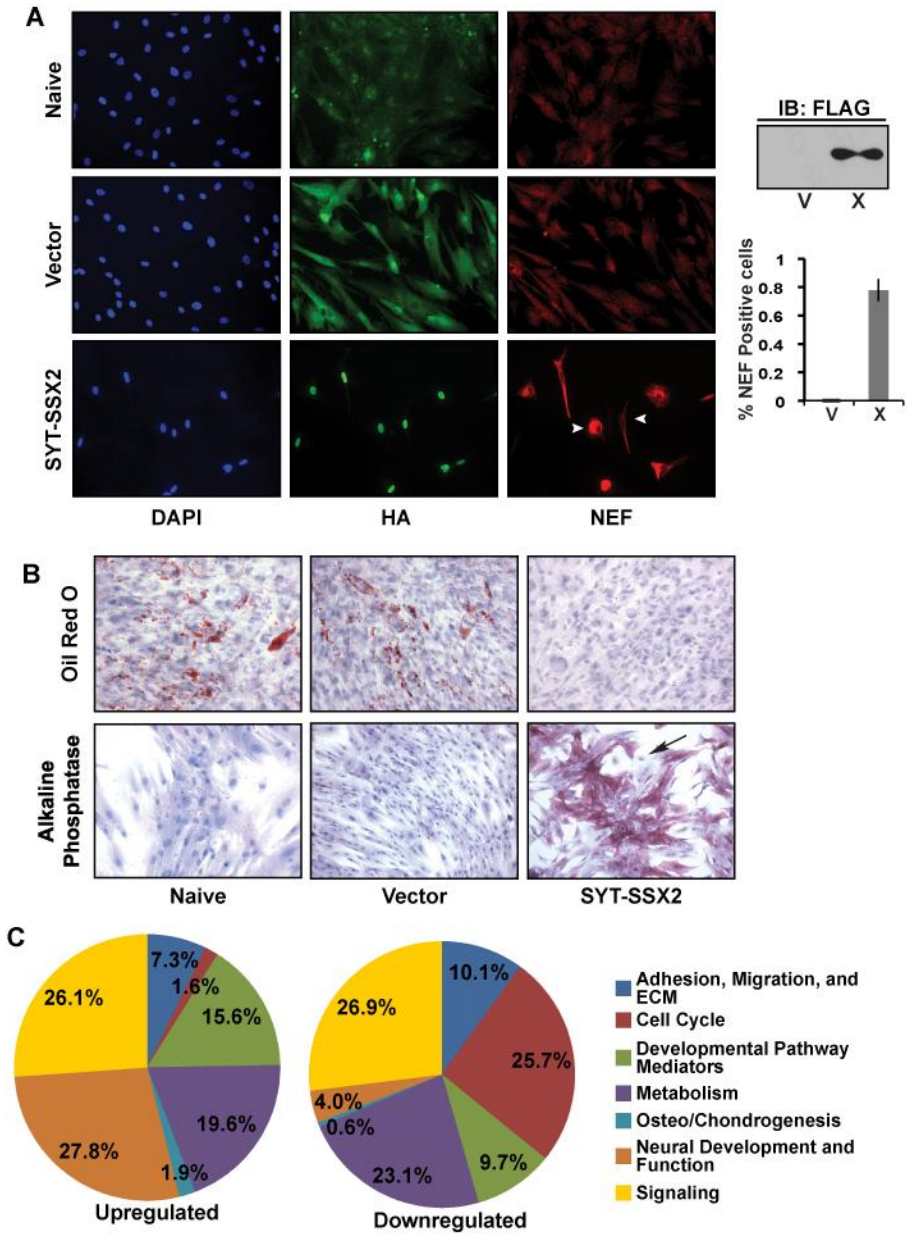

Figure 4. SYT-SSX2 deregulates differentiation in mesenchymal stem cells.
A) Neurofilament expression in SYT-SSX2-hMSCs. Naïve, vector control (V), and SYT-SSX2 (X)-expressing hMSCs were stained for HA (green) and NEF (red). Images were taken at 20x magnification. Arrowheads indicate heterogenous expression of NEF. Flag immunoblot shows SYT-SSX2 expression in X-cells. Histogram represents the average ratio of neurofilament-positive cells to HA-positive V and X cells (n=3). Error bars represent standard deviation. B) SYT-SSX2 effects on hMSC differentiation. Brightfield microscopy of naïve, vector-, and SYT-SSX2-expressing cells stained with Oil Red O after adipogenic stimulation (top row) or for alkaline phosphatase expression (bottom row) without osteogenic stimulation. Images were taken at 20x magnification. Arrow highlights heterogeneous expression of alkaline phosphatase. C) Functional categorization of significantly (2.0-fold change) regulated genes in SYT-SSX2-hMSCs. The functions of 735 upregulated (left chart) and 506 downregulated (right chart) genes were documented, and these genes are represented in the pie charts.

cell (Naka et al., 2010; Mackall et al., 2004), we questioned whether SYT-SSX2 expression could elicit similar effects in multipotent, human bone marrow-derived mesenchymal stem cells (hMSCs; Colter et al., 2001; Sekiya et al., 2002; Appendix B Figure B3). Searching for a neural phenotype in SYT-SSX2-hMSCs, we observed a robust and heterogeneous NEF expression in a significant population (Figure 4A, bottom row, right panel and arrowheads). Neither naïve nor vector-hMSCs produced neurofilaments (Figure 4A, top and middle rows, right panels).

We next asked whether SYT-SSX2 influenced the ability of hMSCs to differentiate into their normal lineages. We discovered that oncogene expression caused a marked inhibition of adipogenesis, while naïve and vector-expressing cells differentiated normally (Figure 4B, top row). In contrast, SYT-SSX2 expression accelerated osteogenesis as evidenced by an intense alkaline phosphatase staining 48 hours post-infection without added osteogenic factors (Figure 4B, bottom row, right panel). As expected, in the absence of inducing factors, naïve and vector-expressing hMSCs showed minimal alkaline phosphatase staining, (Figure 4B, bottom row, left and middle panels). Alkaline phosphatase positivity was heterogeneous (Figure 4B, arrow), indicating that the early osteogenesis was activated at varying degrees across the cell population. Inhibition of adipogenesis and acceleration of osteogenesis by SYT-SSX2 were observed in two additional hMSCs lines, one human (Appendix B Figure B4), and one murine (Alfaro et al., 2008; data not shown). Altogether, these data suggest

that SYT-SSX2 induces a neural and/or osteogenic program(s) in hMSCs, while inhibiting their adipogenic differentiation.

Table 3. Selected list of genes involved in neural development and function upregulated by SYT-SSX2 in human mesenchymal stem cells.
Asterisks (*) denote upregulated genes in hMSCs that are also occupied and upregulated by SYT-SSX2 in C2C12 myoblasts.

Symbol	Gene Description	Symbol	Gene Description
Development and Differentiation			
ENC1	ectodermal-neural cortex	EYA4	eyes absent homolog
FGF11	fibroblast growth factor 11	GBX2	brain homeobox 2
L1CAM*	cell adhesion molecule	NEUROD1	neurogenic differentiation
NEUROG3	neurogenin 3	PROX1*	prospero homeobox 1
Patterning and Axon Guidance			
CRMP1*	collapsin response mediator	DPYSL5*	dihydropyrimidinase-like 5
EFNA4	ephrin-A4	EFNB1*	ephrin-B1
EPHA3	EPH receptor A3	EPHB1*	EPH receptor B1
GLDN	gliomedin	NRP2	neuropilin 2
ROBO1	roundabout	SEMA3D	semaphorin
SLIT1	slit homolog 1	UNC5A*	netrin receptor
Neurotransmitter Signaling and Metabolism			
ABAT*	aminotransferase	ADRA1D	adrenergic, receptor
CHRNA4*	cholinergic receptor	DRD2	dopamine receptor D2
GABRE	GABA receptor, epsilon	GATM	glutamate decarboxylase
GRIK3*	glutamate receptor	GRM4*	glutamate receptor metabotropic
SLC18A3*	acetylcholine transporter		
Neuropeptide, Lipid, and Hormone Signaling			
CRHR1*	neuropeptide receptor	GAL*	galanin
GPR50*	G protein-coupled receptor 50	NPY	neuropeptide Y
NTSR1*	neurotensin receptor 1	PCSK1	convertase subtilisin/kexin
PNOC	pronociceptin	SST*	somatostatin
Adhesion, Growth, and Survival			
AREG	amphiregulin	BAI2*	brain angiogenesis inhibitor 2
GFRA2	GDNF receptor	GPC4	glypican 4
NCAM1	neural cell adhesion molecule 1	NGFR*	nerve growth factor receptor
PCDH10	protocadherin 10	TPPP3	tubulin polymerization

A full characterization of the gene expression profiles initiated by SYT-SSX2 in hMSCs identified approximately 750 significantly upregulated and more than 500 significantly downregulated genes when compared to vector-transduced hMSCs. Functional categorization of the upregulated genes revealed nearly one

Table 4. Selected list of developmental pathway mediators upregulated by SYT-SSX2 in human mesenchymal stem cells.
Asterisks (*) denote upregulated genes in hMSCs that are also occupied and upregulated by SYT-SSX2 in C2C12 myoblasts.

Symbol	Gene Description	Symbol	Gene Description
WNT			
AXIN2*	conductin, axil	SFRP1	secreted frizzled-related protein
DACT1	antagonist of b-catenin	TLE1	transducin-like enhancer protein
FZD3	frizzled homolog	TLE2	transducin-like enhancer protein
FRZB	frizzled-related protein	TLE3	transducin-like enhancer protein
KREMEN1	kringle containing protein	WNT4	WNT ligand 4
LEF1	lymphoid enhancer-binding factor	WNT7B	WNT ligand 7B
PRICKLE1	prickle homolog	WNT11	WNT ligand 11
RSPO1	R-spondin homolog		
NOTCH			
DLL1	delta-like	JAG1	jagged 1
DTX1	deltex homolog	JAG2	jagged 2
DTX4	deltex 4 homolog	LFNG	lunatic fringe
HES1	hairy and enhancer of split	NOTCH1	notch homolog
HEY2	HES-related with YRPW motif	SIX1	SIX homeobox
TGFb/BMP			
BAMBI	BMP and activin inhibitor	FAM46C	family with sequence similarity 46
BMP3	BMP ligand 3	FSTL4	follistatin-like
BMP4	BMP ligand 4	GDF6	growth differentiation factor
BMP7	BMP ligand 7	SOST	sclerosteosis
BMPER	BMP binding endothelial regulator	TGFB2	transforming growth factor, beta
SHH			
PTCH1	patched homolog 1	PTCHD2	patched domain 2
PTCHD1	patched domain 1	SHH*	sonic hedgehog homolog
FGF			
FGFBP2	FGF binding protein 2	FGFR2*	fibroblast growth factor receptor 2

third (27.8%) participate in neural differentiation and signaling (Figure 4C and Table 3). Notably, several of these genes were also shown to be occupied and upregulated by SYT-SSX2 in myoblasts (Table 3, asterisks). This implies that SYT-SSX2 targets the same genes and promotes neural programs regardless of cell type. By contrast, promoters of osteoblast differentiation (*BMP2*, *BMP6*, *FGFR3*, and *OSR2*) represented 1.9% of the upregulated genes (Figure 4C and

Appendix B Table B5). Taken together, these data suggest that SYT-SSX2 indeed activates programs of neural and osteogenic differentiation in hMSCs.

Stem cell controllers such as Wnt, Notch, TGFβ/BMP, Shh, and FGF (Figure 4C and Table 4) constituted 16% of the upregulated genes. 3 of these genes, *AXIN2*, *SHH*, and *FGFR2*, were also upregulated and occupied by SYT-SSX2 in myoblasts (Table 4, asterisks).

Notably, the C2C12 and the hMSC microarrays overlapped with 248 differentially expressed genes, 85 (34%) of which belonged to the neurogenic program, and 54 (~22%) were developmental mediators and transcription factors (Appendix B Table B6).

The role of FGFR2 in SYT-SSX2 differentiation effects

Throughout our analyses *Fgfr2* held our interest as it was noticeably upregulated not only in hMSCs and myoblasts but also in human synovial sarcoma tumors (Nielsen et al., 2002). Moreover, our ChIPSeq analysis revealed *Fgfr2* as a direct target of SYT-SSX2. Importantly, FGFR2 is a major inducer of both osteogenesis and neurogenesis during development (Huang et al., 2007; Villegas et al., 2010) and could be contributing, in part, to the shift in lineage commitment seen in human MSCs. FGFR2 was, therefore, our prime candidate for an upstream signaling pathway whose activation would explain induction of the neural cascade by SYT-SSX2. To assess the contribution of FGFR2 to the visible effects of SYT-SSX2, we decided to analyze the consequences of its inhibition in the stem cells. Neurofilament formation and cell growth were both

used as read-outs to measure the dependence of SYT-SSX2-hMSCs on FGFR2. We started by inhibiting FGFR activity with PD173074, a small molecule with high selectivity for the FGFR kinase (Pardo et al., 2009). A two-day treatment with PD173074 led to a marked diminution of NEF signal in SYT-SSX2-hMSCs (Figure 5A, left histogram), reflecting the dependence of the neural marker on active FGFR. More specifically, infection of SYT-SSX2-hMSCs with two FGFR2-specific shRNA vectors (833 and 703, Figure 5A, right panel) exhibited significant growth retardation when compared to a non-targeting vector (2910; Figure 5A, right histogram, dark grey bars). Apart from growth inhibition, FGFR2 depletion caused a specific attenuation of the NEF signal in the SYT-SSX2-hMSCs (more pronounced in 703; Figure 5A, right histogram, light grey bars). Importantly, the 2910, 833 and 703 vectors did not affect the growth of vector-control hMSCs. These findings suggest that FGFR2 signaling is required for the proper growth of SYT-SSX2-mesenchymal stem cells and the expression of neural differentiation markers.

We then repeated these analyses in the human SYO-1 synovial sarcoma cells that carry the *SYT-SSX2* translocation (Kawai et al., 2004). We observed that approximately 15% of the SYO-1 cell population contained NEF, and PD173074 caused a graded disappearance of NEF-positive SYO-1 cells and an incremental inhibition of their growth (Figure 5B, left and middle panels). As in the SYT-SSX2-hMSCs, FGFR2 depletion with the 833 and 703 shRNAs also led to a marked decrease in the number of NEF-positive SYO-1 cells as well as a slight reduction in their growth (Figure 5B, right panel). We next asked whether

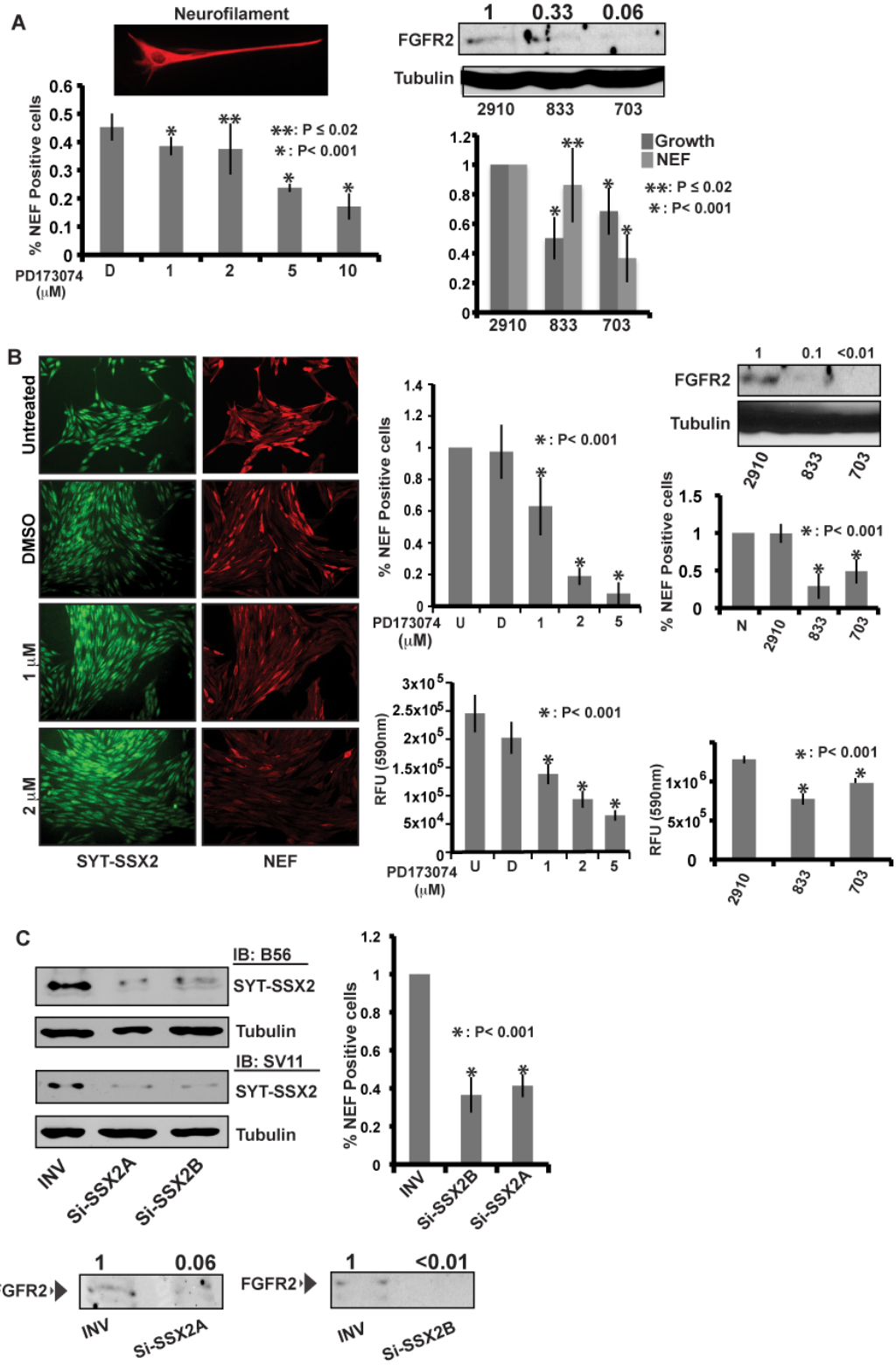
A
Neurofilament
% NEF Positive cells
PD173074 (μM)
D
1
2
5
10
**: P ≤ 0.02
*: P< 0.001
FGFR2
Tubulin
1
0.33
0.06
2910
833
703
Growth
NEF
B
Untreated
DMSO
1 μM
2 μM
SYT-SSX2
NEF
U
<0.01
0.1
N
RFU (590nm)
C
IB: B56
SYT-SSX2
Tubulin
IB: SV11
INV
Si-SSX2A
Si-SSX2B

Figure 5. Contribution of FGFR2 to SYT-SSX2 differentiation effects and to cell growth *A)* Loss of neurite extensions and NEF signal intensity after inhibition of FGF signaling in SYT-SSX2 (HA-positive) hMSCs. Top left image depicts a reference NEF (red)-positive SYT-SSX2-hMSC. Left histogram represents the average ratio of NEF-positive to HA-positive cells 2 days post-treatment with PD173074 at the indicated concentrations (n=4; approximately 1000 cells were included for each concentration). D is vehicle DMSO. Error bars denote standard deviation. P values reflect significance of the experimental values compared to vehicle (D). Middle panel: immunoblot of FGFR2 levels in SYT-SSX2-hMSCs infected with the indicated FGFR2-shRNAs. 2910 is non-targeting vector and tubulin is loading control. Numbers indicate ratio of FGFR2 signal in the cells expressing targeting shRNAs relative to non-targeting vector (value 1). Right histogram: dark grey bars are average of 833 and 703 cell number over 2910 (value 1). The 2910, 833 and 703 originated from the same SYT-SSX2-hMSCs pool (n=3). Light grey bars are the average ratio of NEF-positive 833 and 703 cells over 2910 NEF-positive (value 1) cells. Error bars indicate standard deviation. P values indicate significance of the experimental values with the targeting shRNAs compared to non-targeting vector (2910). *(B)* Decreased NEF expression and growth of synovial sarcoma SYO-1 cells after inhibition of FGF signaling. Left image panel depicts NEF signal (red) with increasing concentrations of PD173074 in SYO-1 cells. Nuclear SYT-SSX2 (green) was visualized with the anti-SSX2 B56 antibody. DMSO was the vehicle control. Images were taken at 20X magnification. Middle upper histogram: average ratio of NEF-positive cells exposed to DMSO (D) or PD173074 to untreated (U; value 1) SYO-1 cells (n=2; over 1000 cells were included in each category). Error bars indicate standard deviation. P value reflects significance of the experimental values compared to vehicle (D). Middle lower histogram shows growth inhibition of SYO-1 cells with increasing concentrations of PD173074 (n=2). Cell growth was estimated using the SRB colorimetric assay. Error bars represent standard deviation. P value reflects significance of the experimental values compared to vehicle (D). Immunoblot shows FGFR2 levels in shRNA-treated SYO-1 cells. Tubulin is loading control. Numbers indicate ratio of FGFR2 signal in targeting shRNA cells relative to non-targeting vector (2910). Upper right histogram: effect of 2910, 833 and 703 FGFR2-shRNAs on NEF expression in SYO-1 cells, relative to NEF-positive naïve (N; value 1) cells. Error bars represent standard deviation (n=3; approximately 1000 cells were included for each category). P value indicates significance of the experimental values with the targeting shRNAs compared to non-targeting vector (2910). Lower right histogram demonstrates the effect of the 3 FGFR2-shRNAs on SYO-1 growth using the SRB assay (n=2). Error bars represent standard deviation. P value indicates significance of the experimental values with the targeting shRNAs compared to non-targeting vector (2910). *(C)* Effect of SYT-SSX2 siRNA in SYO-1 cells. Left immunoblot: SYT-SSX2 levels in INV control and 2 SSX2-targeting RNAs (Si-SSX2A and Si-SSX2B) in SYO-1 lysates detected with antibodies B56 (anti-SSX2) and SV11 (anti-SYT). Tubulin is loading control. Middle immunoblot: FGFR2 levels in the same lysates. Numbers indicate ratio of FGFR2 signal with the targeting Si-SSX2 SiRNAs over control RNA (INV). Histogram: effect of SYT-SSX2 siRNA on NEF formation in SYO-1 cells. Numbers indicate the average ratio of NEF-positive Si-SSX2A and Si-SSX2B cells to NEF-positive INV control cells (value 1). Error bars denote standard deviation (n=3; over 1000 cells were counted for each category). P value indicates significance of the experimental values with the targeting Si-SSX2 SiRNAs compared to control RNA (INV). Measurements of FGFR2 depletion by the targeting shRNAs, or by the SYT-SSX2 SiRNAs were performed using the Fluorchem 8900 densitometer, and analyzed with the AlphaEase FC software.

these events in SYO-1 cells are dependent on SYT-SSX2 expression. We found that depletion of SYT-SSX2 in SYO-1 cells with specific siRNAs (Figure 5C, left panel) was accompanied by a concomitant decrease in FGFR2 levels (Figure 5C, lower panels) and a marked decrease in the relative number of NEF-positive cells (Figure 5C, histogram). We refrained from measuring the effect of SYT-SSX2 depletion on SYO-1 growth, as the inherent cell toxicity of RNAi assays would interfere with its accuracy.

In summary, these studies suggest that SYT-SSX2 recruitment to the *Fgfr2* gene results in the activation of FGF signaling, thereby driving the neural phenotype in hMSCs and affecting their growth. This mechanism appears to be occurring in the human synovial sarcoma cells as well.

Conclusions

The data presented here indicate that the synovial sarcoma oncogene SYT-SSX2 reprograms mesenchymal stem/progenitor cells by activating a pro-neural gene network while disrupting normal differentiation. This is most likely due to the recruitment of SYT-SSX2 to an extensive array of neural genes, resulting in their activation. This corroborates previous reports in which a neural phenotype was observed in SYT-SSX-expressing SS cell lines (Ishibe et al., 2008). Furthermore, knockdown of SYT-SSX in SS cells led to loss of neuronal features (the present study and Naka et al., 2010).

The upregulation of several mediators representing the central pathways known to modulate stem cell behavior is another striking result. It uncovers a propensity of SYT-SSX2 for regulating developmental pathways. This may reflect an ability of SYT-SSX2 to create an imbalance in the microenvironment of the cancer cell *in vivo,* furthering malignancy. We have previously reported that SYT-SSX2 mediates nuclear translocation and activation of β-catenin (Pretto et al., 2006). Consistent with this finding is the upregulation of Wnt ligands in our microarray analyses. The crosstalk among Wnt, TGFβ/BMP, FGF, Hedgehog, and Notch, and their impact on tumor cell behavior, are the focus of future studies.

Our high-throughput analyses identify FGFR2 as a critical signaling node in the behavior of SYT-SSX2-expressing cells. Its enhanced signaling by SYT-SSX2 may explain the accelerated osteoblastogenesis as well as the dominance

of the pro-neural gene profile. With MAPK/ERK and PI3K activation, FGFR2 signaling promotes neurogenesis and skeletogenesis through crosstalk with Wnt, Hedgehog, Notch, and BMP signals (Ever and Gaiano, 2005; Chadashvili and Peterson, 2006; Maric et al., 2007; Zhao et al., 2008; Miraoui and Marie, 2010). Furthermore, the benefit of FGF pathway attenuation to inhibit SS cell growth was previously reported (Ishibe et al., 2008) and corroborated by our studies. Chemical inhibition of FGFR2 signaling and its depletion with shRNA causes loss of neurofilament expression and decreased cell growth in both the SYT-SSX2 hMSCs and the SS SYO-1 tumor cells. Significantly, upregulation of FGF ligands in the myoblast and hMSC microarrays suggests that SYT-SSX2 establishes an autocrine FGF signaling loop. If this is the case, identification of FGFR2 as the mediator of these signals designates it as a candidate for potential SS tumor reversal. Increased FGFR2 activity is already linked to advanced malignant phenotypes in endometrial, uterine, ovarian, breast, lung and gastric cancers. Strategies designed to target FGFR2 in these cancers (Katoh, 2008; Katoh and Katoh, 2009) are ongoing.

The deregulation of differentiation in our model systems can also be explained by these findings. FGFR2-induced osteoblast maturation (Miraoui and Marie, 2010) inhibits adipogenesis in mesenchymal stem cells (Muruganandan et al., 2009). Similarly, the stimulation of a neural program by SYT-SSX2 may abrogate myogenesis. In C2C12 cells, the two outcomes are mutually exclusive (Watanabe et al., 2004). Alternatively, direct silencing of myogenic genes can also contribute to this phenotype. The ChIPSeq analysis revealed a putative

SYT-SSX2 binding site upstream of the downregulated MyoD gene. Additional studies are underway to test this possibility and identify potential recruitment factors associated with transcriptional silencing by SYT-SSX2.

In summary, our studies in mesenchymal stem and progenitor cells uncover a function of SYT-SSX2 in differentiation programming, and our genome-wide analyses provide a glimpse into the early events of tumor initiation by the oncogene. Overall, we believe that the deregulation of differentiation is a manifestation of the ability of SYT-SSX2 to target lineage-specific programs. FGFR2 was identified as a cardinal player in SYT-SSX2-associated phenotypes, but it is likely that additional pathway mediators also contribute to SYT-SSX2-induced characteristics. Future investigation of other targets identified through this method will lead to a better understanding of the interplay among these pathways and SS pathology. This combination analysis also provides a powerful tool in the discovery of novel therapeutic targets and will be advantageous in understanding the biology of other oncogenic proteins directly affecting transcriptional programs.

CHAPTER IV

EPIGENETIC RECRUITMENT AND REGULATION OF SYT-SSX2 ACTIVITY

Introduction

Dynamic regulation of chromatin structure allows for DNA-dependent processes to be controlled in an epigenetic fashion, or in other words, independently of the DNA sequence. Work in recent years has made it increasingly clear that gene expression not only depends on the presence of sequence-specific transcription factors but also on the structure of the chromatin fiber. Moreover, certain post-translational modifications of the core histone proteins are known to be associated with specific chromatin states. For example, heterochromatin is characterized by the presence of trimethylated histone H3 at lysine 9 or 27 (H3K9me3, H3K27me3) and ubiquitylated histone H2A at lysine 119 (H2AUb) (Bannister and Kouzarides, 2011; Trojer and Reinberg, 2007). In general, histone acetylation is associated with euchromatin and reflects transcriptional activation (Bannister and Kouzarides, 2011). Gene activity is also closely correlated with trimethylation of histone H3 on lysine 4 (H3K4me3) and ubiquitylation of histone H2B on lysine 123 (H2BUb) (Bannister and Kouzarides, 2011; Weake and Workman, 2008). Whether these modifications elicit functional changes themselves or whether they are part of a larger mechanism regulating chromatin stability that, in turn, controls DNA-dependent processes is a matter of

debate (Henikoff and Shilatifard, 2011). In either case, knowing the complement of epigenetic markers at a given locus provides valuable information regarding its functional status.

Indeed, recent evidence suggests that co-regulated gene subsets are characterized by common histone modification signatures. New computational methods are now considering histone modifications to predict cell-type specific transcription factor binding sites more accurately (Wang, 2011; McLeay et al., 2011). In addition, it has been shown that genes participating in similar functional pathways that also display identical expression patterns are marked by the same complement of histone modifications in yeast and mouse myoblasts (Natsume-Kitatani et al., 2011; Asp et al., 2011). Therefore, the combination of markers may serve as a signature for transcriptional regulators denoting the coordinated expression of these genes.

Development is one process during which many genes are coordinately regulated within specific cell-types. This is directed by sequence-specific transcription factors. For example, MyoD and REST/NRSF are master regulators of the myogenic and neurogenic programs, respectively, and these transcription factors control the expression of genes important in the differentiation and function of their respective lineages (Weintraub et al., 1989; Schoenherr and Anderson, 1995). Tissue-specific expression of individual genes may also be regulated by enhancers, non-coding DNA elements to which multiple transcription factors may bind. These are diverse regulatory elements that function independently of distance and orientation relative to their target genes

but have some distinguishing characteristics like DNase I hypersensitivity, p300 binding, and common histone modifications such as mono- and dimethylated histone H3 at lysine 4 and acetylated histone H3 at lysines 9, 14, 18, or 27 (Ong and Corces, 2011).

In the previous chapter, we described the activation of a neural program accompanied by the inhibition of the myogenic program in C2C12 myoblasts. This was due to the specific targeting of neural genes by the SYT-SSX2 fusion protein. Because the translocation product is known to associate with epigenetic regulators and that the subsets of genes in euchromatic versus heterchromatic regions is cell-type specific, we wanted to determine if there was a signature set of epigenetic markers that was associated with SYT-SSX2 recruitment. Furthermore, we wanted to ascertain whether a specific set of markers could predict transcriptional activation or repression mediated by the mutant protein.

Results

SYT-SSX2 binding is heterogeneous and strongly correlates with histone H3 lysine 27 trimethylation

In the previous chapter, we described a genomewide ChIPSeq experiment performed in C2C12 myoblasts expressing the oncogene SYT-SSX2. This analysis led to the identification of nearly 53,000 regions (or peaks) bound by the SYT-SSX2 complex. In order to generate a global picture of SYT-SSX2 binding sites throughout the genome, we performed a sliding window analysis in which each chromosome was subdivided into 500kb bins, and the number of SYT-SSX2 peaks in each bin was tabulated.

SYT-SSX2 displays heterogeneous binding among the chromosomes as a whole and along each chromosome individually (Figure 6A, Appendix B Figure B5). Nearly 20% of the binding sites (9,750) are located on the X chromosome, whereas chromosome 3 has 674 binding sites (1.3%) (Table 5). Interestingly, areas with high levels of binding are located at chromosome ends, notably on chromosomes 2, 4, 11, 15, and X (Figure 6A, Appendix B Figure B5). This trend is also seen to a lesser degree on chromosomes 7, 8, 12, and 16-19 (Appendix B Figure B5).

Binned binding sites appear to cluster loosely into 3 density categories: low, medium, and high. Low-density clusters are similar to the cluster centered around 5Mb on chromosome 2 and contain bins with <100 peaks (Figure 6A, arrowhead). Medium-density clusters contain 1-2 bins with 100-200 peaks

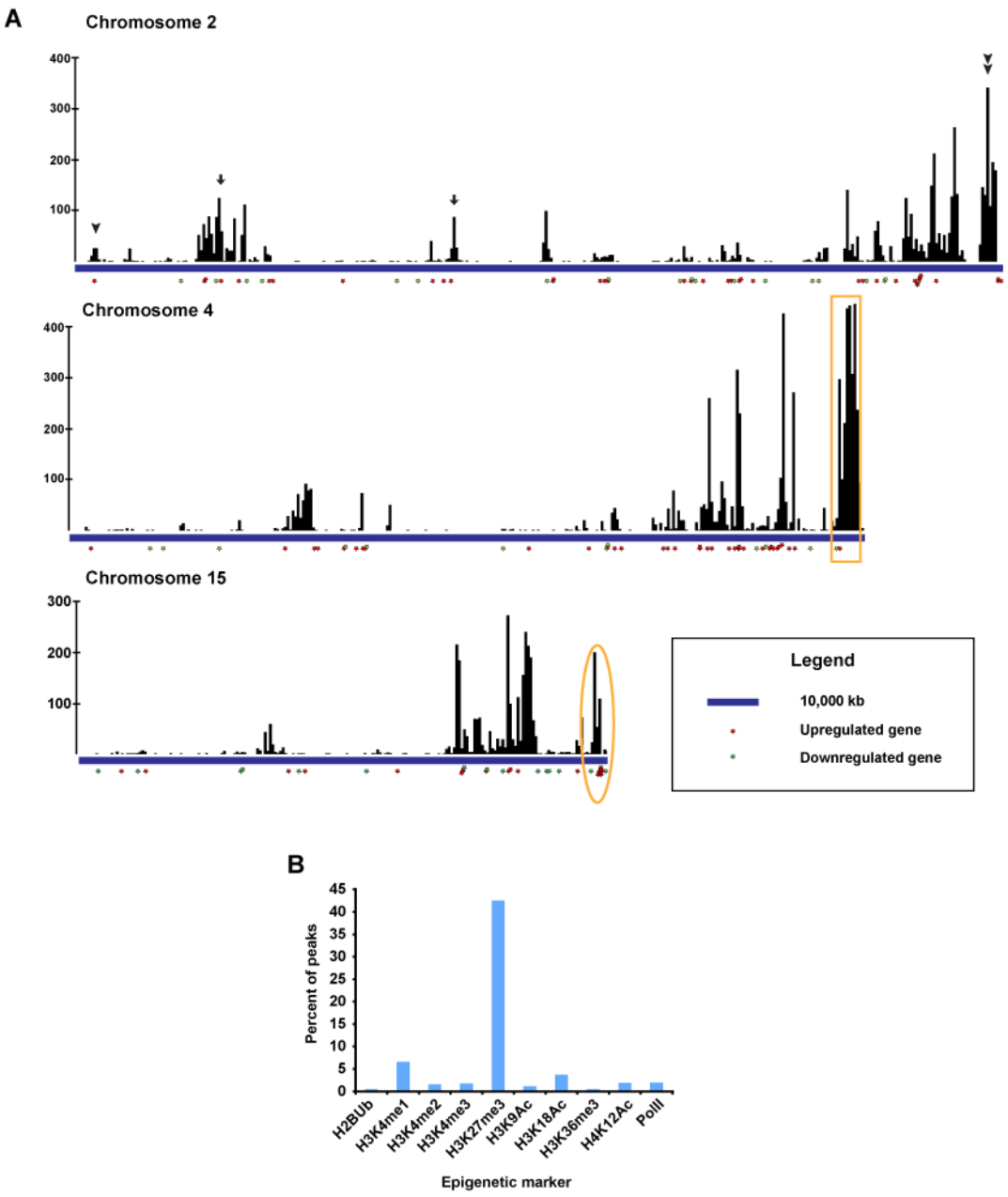

Figure 6. Distribution of SYT-SSX2 peaks with respect to chromosome and epigenetic markers.
A) Diagrams of chromosomes 2, 4, and 15. Chromosomes were subdivided into 500kb bins, and the number of SYT-SSX2 ChIPSeq peaks was tabulated for each bin. Black bars represent individual bins, and the height of each bar is proportional to the number of SYT-SSX2 peaks contained within that window. Scale bar shown represents a distance of 10 Mb. Red and green stars, respectively, depict the location of upregulated and downregulated genes determined by microarray analysis (described in Chapter 3) that could be annotated to SYT-SSX2 occupied regions. B) Overlap of SYT-SSX2 peaks with epigenetic markers. Published datasets that identified regions of enrichment for histone modifications and PolII binding (Asp et al., 2011) were compared with the locations of SYT-SSX2 peaks using the Galaxy analysis suite to determine sites of overlap. The bar graph shows the percent of SYT-SSX2 peaks that overlap with 10 epigenetic markers.

surrounded by other bins with less than 100 peaks like the clusters centered at 28Mb or 74Mb on chromosome 2 (Figure 6A, arrows). The cluster centered at 179Mb on chromosome 2 (Figure 6A, double arrowhead) is an example of a high-density cluster which contains bins with >200 peaks with nearby bins containing >100 peaks. These data indicate that SYT-SSX2 recruitment to target loci is non-random and displays a preference to specific chromosomal regions.

Table 5. Distribution of SYT-SSX2 peaks per chromosome.

Chromosome	Number of peaks	Percentage of peaks	Chromosome	Number of peaks	Percentage of peaks
1	1,651	3.1	11	3,712	7.0
2	5,311	10.0	12	2,573	4.9
3	674	1.3	13	1,145	2.2
4	6,309	11.9	14	1,493	2.8
5	4,146	7.8	15	3,202	6.0
6	1,913	3.6	16	798	1.5
7	1,846	3.5	17	1,842	3.5
8	2,759	5.2	18	836	1.6
9	1,466	2.8	19	801	1.5
10	765	1.4	X	9,750	18.4

Previous reports have shown that SYT-SSX2 interacts with proteins involved in transcriptional regulation by epigenetic mechanisms. Therefore, we wanted to determine if SYT-SSX2 binding might be associated with specific epigenetic markers. Previously published genome-wide datasets for histone modifications and RNA polymerase II binding sites (PolII) (Asp et al., 2011) in C2C12 myoblasts were compared with our SYT-SSX2 dataset allowing us to determine the nature of the epigenetic landscape to which SYT-SSX2 was recruited. Positions of histone modification enrichment and protein binding are reported as chromosomal positions, thus areas where the datasets intersect can

be determined computationally. For our study, we looked for regions that overlap ≥ 1 nucleotide since SYT-SSX2 interacts with large protein complexes, and a 1-base overlap suggests close proximity to a given modification. By this method, we found quite strikingly that 22,537 SYT-SSX2-occupied regions (42.5%) overlapped with H3K27me3 (Table 6 and Figure 6B, left panel), a modification associated with Polycomb repressive complexes. This represents approximately 13% of the total H3K27me3-enriched regions (Table 7) indicating that SYT-SSX2 is targeted to a subset of Polycomb-regulated genes. Overlap with other histone modifications and PolII was not as extensive (Figure 6B, left panel, Tables 6 and 7). The next highest amount of overlap was seen with H3K4me1 (3,498 peaks, 6.6%) followed by H3K18Ac (1,961 peaks, 3.7%). This accounts for 1.3% and 0.99% of the total number of regions marked by H3K4me1 and H3K18Ac, respectively (Table 7), indicating that SYT-SSX2 is associated with only a small subset of locations labeled by either of these modifications. It has been suggested that these marks identify enhancer elements (Ong and Corces, 2011) highlighting another possible mechanism by which SYT-SSX2 may affect gene expression.

Table 6. Number of SYT-SSX2 peaks that overlap epigenetic markers.
The number and percent of peaks are relative to the total number of SYT-SSX2 peaks (52,992).

Modification	Number of peaks	Percent of peaks	Modification	Number of peaks	Percent of peaks
H3K4me1	3498	6.6	H3K9Ac	595	1.12
H3K4me2	816	1.54	H3K18Ac	1961	3.70
H3K4me3	905	1.71	H3K36me3	238	0.45
H3K27me3	22,537	42.5	H4K12Ac	995	1.88
PolII	1034	1.95	H2BUb	245	0.46

Table 7. Overlap of epigenetic markers with SYT-SSX2.
The number and percent of peaks are relative to the total number of peaks for a given modification.

Modification	Number of peaks	Percent of peaks	Modification	Number of peaks	Percent of peaks
H3K4me1	4,118	1.28	H3K9Ac	727	1.12
H3K4me2	955	1.32	H3K18Ac	2,210	0.99
H3K4me3	1,118	1.48	H3K36me3	275	0.17
H3K27me3	27,608	13.1	H4K12Ac	1,155	1.16
PolII	1,054	2.25	H2BUb	263	0.14

The prominence of SYT-SSX2 occupying regions that were previously determined to be enriched in H3K27me3 led to the question of where these areas were located relative to known genes. It has been shown that PcG complexes can mediate both short- and long-range control of gene expression (Sparmann and van Lohuizen, 2006; Mateos-Langerak and Cavalli, 2008), thus we determined the location of the overlapping regions between SYT-SSX2 and H3K27me3 relative to known genes. 3,692 genes could be annotated to SYT-SSX2/H3K27me3 intersecting areas, and of these, 45.6% of the peaks were located within the gene itself (Table 8). Nearly 900 genes had overlapping sites from 0-5kb upstream of the TSS, and together with the genes marked by SYT-SSX2/H3K27me3 regions within the coding sequence, they account for 50% of the total SYT-SSX2-Polycomb labeled genes (Table 8). These data strongly indicate that SYT-SSX2 interacts with Polycomb complexes that function at short-range. Altogether, these data illustrate that SYT-SSX2 may be preferentially targeted to specific genomic locations through interaction with Polycomb complexes and/or their associated histone modifications. This is consistent with previous studies in which SYT-SSX2 was able to associate with Polycomb proteins (Barco et al., 2009; Lubieniecka et al., 2008). Moreover, SYT-

SSX2 may function through the modulation of Polycomb activity via short-range interactions.

Table 8. Distribution of SYT-SSX2 peaks overlapping with H3K27me3 with respect to gene TSS.
Regions of SYT-SSX2 binding intersecting with regions of H3K27me3 (≥ 1 nucleotide) were annotated to the closest TSS. 3,692 genes were found to be associated with SYT-SSX2/H3K27me3 in this manner. Percent of genes refers to the number of genes with an SYT-SSX2/H3K27me3 overlapping region at a given distance over 3,692.

Distance	Number of genes	Percent of genes
In gene	1682	45.6
0-5 kb	872	23.6
In-5 kb	1874	50.8
0-20 kb	1672	45.3
20-50 kb	1524	41.3
>50 kb	1917	51.9

Differential binding patterns are associated with transcriptional activity

SYT-SSX2 can elicit changes in gene expression in target cells through direct association with transcriptional regulators, thus we wanted to correlate SYT-SSX2 occupancy with gene expression. In the previous chapter, we described the binding of SYT-SSX2 peaks with respect to gene transcription start sites and found that approximately 10% of the peaks fell within 10kb upstream of TSS whereas the majority of peaks are located at distances greater than 50kb (Table 1). Through gene expression profiling we were able to associate approximately 200 upregulated and 50 downregulated genes with SYT-SSX2 occupancy within a 10kb window. By including differentially regulated genes with binding sites at any distance upstream of the TSS or within the gene body, we identified a total of 460 upregulated and 280 downregulated genes associated with SYT-SSX2 peaks. These genes were mapped to their relative chromosomal location to determine if there was an association between the number of SYT-

SSX2 peaks and gene activity. As a general trend, negatively regulated genes are associated with low-density clusters (Figure 6A) while high-density clusters most often correspond to positively regulated genes (Figure 6A). Interestingly, there does not appear to be a correlation between the degree of SYT-SSX2 binding and the number of genes that are either up- or downregulated. On chromosome 4, a high-density cluster is centered around 153Mb, however only 2 genes (1 upregulated and 1 downregulated) are associated with this area (Figure 6A, box). Conversely, on chromosome 15, a region dense with activated genes centered at 102Mb most closely corresponds to a low-medium density cluster (Figure 6A, oval). Taken together, these data indicate that SYT-SSX2 binding correlates with alterations in gene activity; however, not all binding sites are associated with changes in gene expression suggesting that SYT-SSX2 may have additional functions in the nucleus.

We narrowed our focus to study differentially regulated genes locally in order to determine if gene activation versus repression could be distinguished by SYT-SSX2 binding patterns. Interestingly, the distribution of SYT-SSX2 binding sites upstream of the TSS was markedly different depending on whether a gene was positively or negatively regulated by oncogene expression. Overall, more than half of the upregulated genes bound by SYT-SSX2 (53.9%) have at least 1 peak within a window from 0-20kb upstream of the TSS. This number decreases with increasing distance (Figure 7, top panel). In contrast, 21.4% of the genes that are downregulated and bound by SYT-SSX2 have peaks within a 0-20kb window upstream of the TSS. This percentage increases with increasing

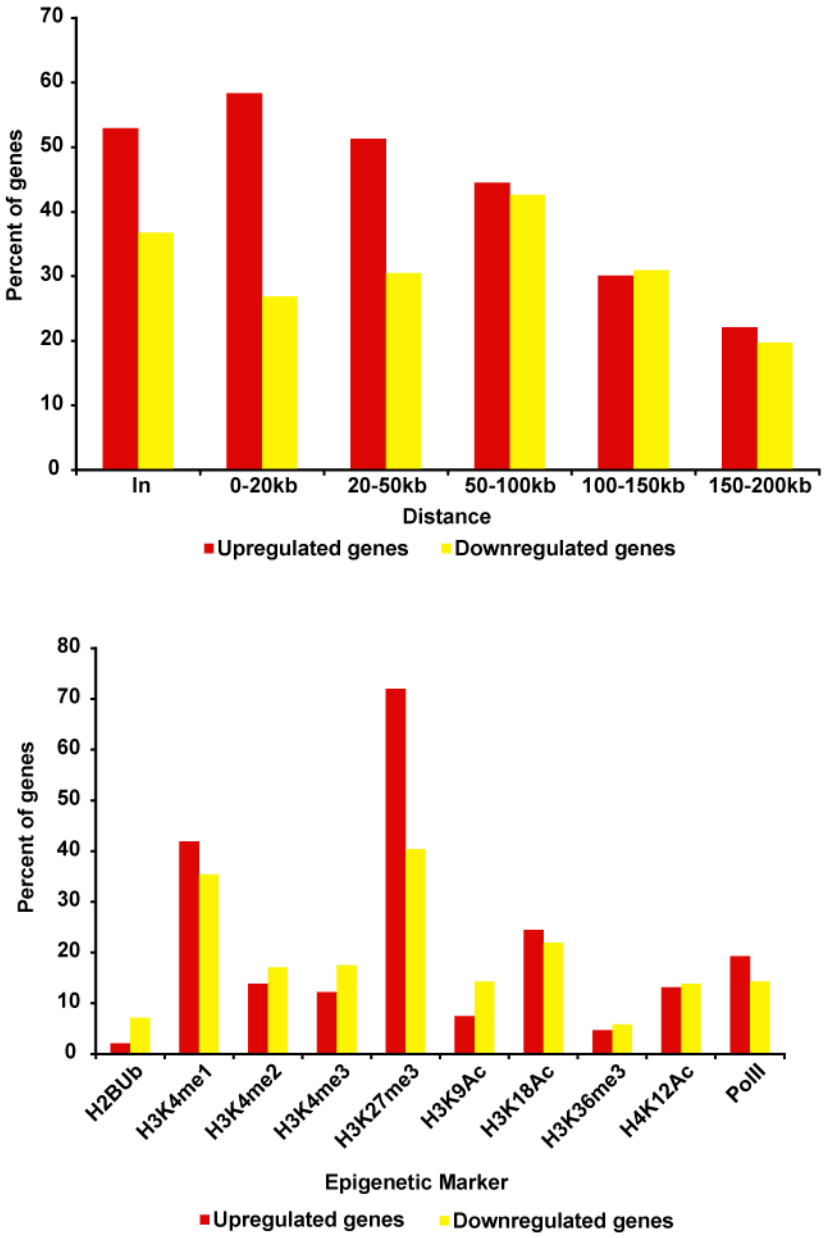

Figure 7. Differential pattern of binding between upregulated and downregulated genes targeted by SYT-SSX2. 425 upregulated and 223 downregulated genes were bound by SYT-SSX2 ranging from within the gene body up to 200kb upstream of the TSS. Top panel shows the percentage of genes that are occupied by SYT-SSX2 within given distance windows. Bottom panel depicts a bar graph showing the percentage of genes for which the associated SYT-SSX2 occupied regions overlap with the given epigenetic markers. Red bars represent upregulated genes, and yellow bars signify downregulated genes.

distance, peaks from 50-100kb then decreases at distances between 100-150kb and 150-200kb (Figure 7, top panel). These data suggest that SYT-SSX2-associated transcriptional activation is correlated with binding at close range whereas transcriptional repression associates with binding at farther distances.

Binding patterns associated with differentially regulated genes

Recently, it has been shown that genes within specific functional categories can be distinguished by the pattern of histone modifications surrounding them. This suggests that genes within a particular pathway have a specific epigenetic signature that allows them to be differentially recognized by activating and/or repressing factors. In this way, the cell can co-regulate the expression of genes involved in a given process (Asp et al., 2011; Natsume-Kitatani et al., 2011). We have hypothesized that SYT-SSX2 targets genes through an epigenetic mechanism. To further delineate the SYT-SSX2 binding pattern, overlap of SYT-SSX2 peaks with histone modifications at differentially regulated genes was determined. Seventy-two percent (72%) of the upregulated genes and 43.6% of the downregulated genes bound by SYT-SSX2 have associated peaks that overlap with H3K27me3 (Figure 7, bottom panel) corroborating previous reports that the fusion protein is targeted to Polycomb-regulated genes. Surprisingly, 43.6% of the upregulated genes and 33.6% of the downregulated genes have SYT-SSX2 peaks that overlap with H3K4me1. This is significant considering that the overlap with H3K4me1 occurs with only 6.6% of the total SYT-SSX2 peaks overall. Since this modification labels enhancer

elements (Ong and Corces, 2011), the association of SYT-SSX2 with these sites as well as Polycomb target sites suggests that SYT-SSX2 may affect transcription by modulating both enhancer and Polycomb function.

Next we wanted to discover if the overlap of SYT-SSX2 binding exhibited any patterns that would allow us to distinguish differentially regulated genes. As a first step, we tabulated the number SYT-SSX2 peaks for each gene within a particular expression category (positively or negatively regulated) that overlapped with histone modifications, PolII binding, and DNA methylation in 5kb windows up to 50kb upstream of TSS and within the gene. We limited our analyses to this distance because of the association of SYT-SSX2 with Polycomb-marked regions at close-range to gene TSS and because of the difficulty in definitively assigning functional significance to binding sites at farther distances. For this analysis we also only characterized genes that had SYT-SSX2 binding sites that overlapped with at least 1 epigenetic marker and identified 314 upregulated and 110 downregulated genes by this criterion. Of these upregulated genes, 50% had overlapping sites between the fusion protein and H3K27me3 (Table 9). This percentage decreases with increasing distance consistent with the trend described above with respect to all genes with SYT-SSX2/H3K27me3 intersecting regions. Also consistent with trends described above, the second most abundant overlap occurred between SYT-SSX2 and H3K4me1 within the gene body. Association between SYT-SSX2 and other histone modifications, particularly those related to transcriptional activation (but not elongation) was also seen within gene bodies, although to a much lesser extent than either

H3K27me3 or H3K4me1 (Table 9). In general, the number of genes in which SYT-SSX2 associated with these other modifications decreased with increasing distance, although there are a few exceptions.

Table 9. Distribution of SYT-SSX2-overlapping epigenetic markers with respect to upregulated genes.
Percentages are relative to the total number of upregulated genes with SYT-SSX2 peaks that overlap any epigenetic marker from 0-50kb upstream of the TSS and including the gene body (total = 314). Distances are measured in kilobases.

Marker	In	0-5	5-10	10-15	15-20	20-25	25-30	30-35	35-40	40-45	45-50
DNA me	9.55	4.46	0.32	0.96	0.32	0	0	0.64	0.32	0.64	0.64
H3K4me1	18.8	5.10	2.23	5.41	5.73	2.55	6.37	3.82	4.46	4.46	5.73
H3K4me2	8.28	5.10	0.32	1.27	0.64	0.64	0.96	0.32	0.96	0.96	0.64
H3K4me3	8.60	4.14	0.64	1.27	0.32	0.64	0.64	0.32	0.64	1.27	0.96
H3K27me3	50.0	31.2	29.3	25.7	23.9	24.5	23.6	21.3	21.3	22.0	19.4
H3K9Ac	5.10	0.64	0.32	0.64	0	0.32	0.96	0.32	0.64	1.91	0.64
H3K18Ac	9.24	2.23	1.91	2.23	2.55	2.55	2.55	2.23	3.82	4.78	3.50
H3K36me3	2.87	0	0	0.32	0.64	0.32	0.32	0.96	0	0.96	0.32
H4K12Ac	7.32	1.27	0.64	1.59	1.27	0.96	0.64	1.27	1.59	1.91	0.96
H2BUb	1.27	0	0	0.32	0.32	0.64	0.32	0.64	0	0.32	0
PolII	10.2	3.18	1.59	1.91	1.27	1.27	1.27	1.59	1.27	2.23	2.55

Table 10. Distribution of SYT-SSX2-overlapping epigenetic markers with respect to downregulated genes.
Percentages are relative to the total number of downregulated genes with SYT-SSX2 peaks that overlap any epigenetic marker from 0-50kb upstream of the TSS and including the gene body (total = 110). Distances are measured in kilobases.

Marker	In	0-5	5-10	10-15	15-20	20-25	25-30	30-35	35-40	40-45	45-50
DNA me	7.27	4.55	0.91	0.91	0	0.91	0.91	0	0	0.91	2.73
H3K4me1	23.6	8.18	9.09	8.18	5.45	3.64	8.18	5.45	3.64	8.18	1.82
H3K4me2	17.3	10.0	3.64	1.82	1.82	3.64	3.64	0	0	4.55	2.73
H3K4me3	17.3	10.9	2.73	3.64	1.82	4.55	2.73	0.91	0.91	3.64	6.64
H3K27me3	22.7	3.64	10.0	7.27	7.27	7.27	12.7	8.18	11.8	15.5	16.4
H3K9Ac	14.6	9.09	4.55	3.64	2.73	1.82	1.82	0	0	2.73	1.82
H3K18Ac	17.3	3.64	7.27	6.36	4.55	2.73	3.64	0	4.55	3.64	3.64
H3K36me3	8.18	0.91	1.82	1.82	0.91	2.73	0.91	0.91	1.82	0	0
H4K12Ac	12.7	9.09	3.64	7.27	1.82	3.64	1.82	0	0	3.64	2.73
H2BUb	7.27	0	1.82	0.91	0	1.82	0	0.91	1.82	0	0.91
PolII	18.2	10.0	3.64	0.91	4.55	2.73	1.82	2.73	0.91	2.73	4.55

Of the negatively regulated genes, the highest levels of overlap were also seen in the gene body and occurred with H3K4me1 and H3K27me3 (Table 10). For H3K4me1, the number of genes with intersection of this mark with SYT-SSX2 occupancy generally decreases with increasing distance upstream of the TSS; however, from 25-30kb and 40-45kb the number of genes with SYT-SSX2/H3K4me1 regions was increased relative to the surrounding windows (Table 10). For H3K27me3, a slightly different pattern is seen. The number of genes with SYT-SSX2/H3K27me3 sites decreases dramatically from 0-5kb but increases with increasing distance upstream of the TSS (Table 10).

With downregulated genes, SYT-SSX2 also appears to associate with modifications related to active transcription. Regions enriched in H3K4me2, H3K4me3, H3K9Ac, H3K18Ac, H4K12Ac, and PolII occupancy overlap with SYT-SSX2 binding sites in over 10% of the downregulated genes, and markers associated with transcriptional elongation (H3K36me3 and H2BUb) overlap with SYT-SSX2 sites in more than 5% of the downregulated genes (compared with less than 3% of the upregulated genes). In summary, SYT-SSX2 associates with epigenetic markers, particularly H3K27me3 and H3K4me1. Most of the upregulated genes in this analysis are marked by H3K27me3, and SYT-SSX2 appears to bind close to the TSS. In contrast, SYT-SSX2 occupies H3K4me1- or H3K27me3-enriched regions in a similar percentage of downregulated genes and also associates with more markers of transcriptional activation and elongation.

In order to determine higher order relationships among the histone modifications themselves and gene expression, and using the criterion that

genes were included if they contained a binding site for SYT-SSX2 that overlapped with at least 1 epigenetic marker, hierarchical clustering was performed on the differentially regulated genes. To do so, the degree of overlap between SYT-SSX2 and a given modification was calculated as a ratio of bases covered per 5kb bin upstream of the TSS or the ratio of bases covered in the gene body over the total number of bases in the coding sequence. This data generated a signature of modifications by distance for each gene and was used in hierarchical clustering analyses.

Analysis of the upregulated genes corroborated earlier results and identified H3K27me3 as the predominant modification associated with SYT-SSX2 binding and gene expression (Figure 8, top panel). The location and extent of H3K27me3 was variable across all genes, but there were 2 sub-clusters in which SYT-SSX2/H3K27me3 intersecting sites were located within the entire range of distances that we analyzed. The first of those sub-clusters is highlighted in Figure 8 (top panel). It has been reported previously that genes densely covered by H3K27me3 were involved in the differentiation and development of alternate lineage pathways, thus we wanted to determine the function of the genes within this sub-cluster. Based on our previous analysis (Chapter 3), we found that 50% of these genes are involved in neural development and function. To summarize, SYT-SSX2 occupies regions within and upstream of upregulated genes that are enriched in H3K27me3. Functionally, these genes can be subdivided based on the extent of SYT-SSX2/H3K27me3 intersection and are in line with our previous observation of the increased expression of neural characteristics and genes.

Similar hierarchical clustering was performed on the downregulated genes. This analysis led to the identification of 2 clusters of genes with differential signatures. The first is characterized by SYT-SSX2/H3K27me3 overlap from 0-10kb and 20-50kb upstream of gene TSS, whereas the second cluster is marked by the overlap of SYT-SSX2 with histone modifications related to transcriptional activation at close ranges (Figure 8, bottom panel). Interestingly, these two signatures appear to be mutually exclusive. SYT-SSX2/H3K27me3 overlaps are minimal or absent in the genes marked by close-range SYT-SSX2 intersection with activating modifications and vice versa (Figure 8, bottom panel). Additionally, unlike the upregulated genes, which were functionally related based on their clustering, the genes within these clusters were not clearly associated with a particular pathway or program. Together, these data suggest that SYT-SSX2-mediated downregulation of gene expression occurs through different mechanisms, one dependent on recruitment by Polycomb and the other independent of Polycomb.

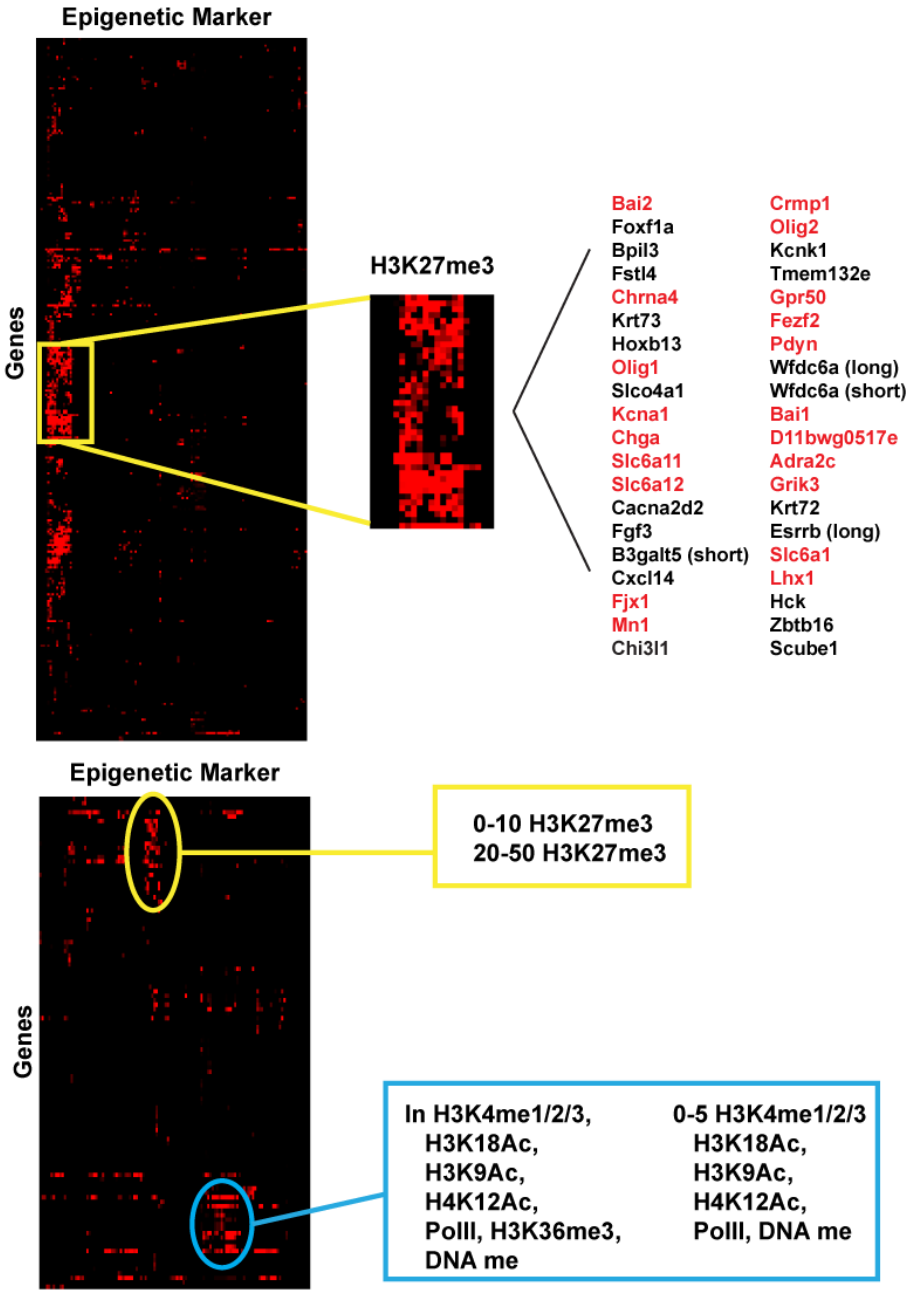

Figure 8. Hierarchical clustering of differentially regulated genes.
Signatures for each differentially regulated gene were derived from the extent of overlap between SYT-SSX2 peaks and the epigenetic markers within the gene body or in 5kb bins upstream of the TSS up to -50kb (defined as coverage ratio; each bin has a coverage ratio for each epigenetic marker). Signatures were used as the input for hierarchical clustering using Cluster 3.0. Heatmaps were generated using Java Treeview. Each row represents a gene, and each column represents an epigenetic marker for a given bin (for example H3K27me3 from 0-5kb or PolII in gene). Coverage ratios range from 0-1 with black squares representing bins with a ratio of 0 and red squares representing a ratio of 1. Top panel: Clustering of upregulated genes. Inset is enlarged portion of the heat map, and the epigenetic markers included in this region correspond to H3K27me3 at all distances and within the gene. Genes names are listed to the right. Highlighted in red are genes that are involved in neural development and function. Bottom panel: Clustering of downregulated genes. Yellow and blue ovals isolate 2 distinct clusters corresponding to genes with SYT-SSX2/H3K27me3 overlapping regions and SYT-SSX2 peaks overlapping with modifications associated with transcriptional activation, respectively. Listed to the right are the position and identity of the epigenetic marker(s) comprising a particular cluster.

Conclusions

Genome-wide analysis of SYT-SSX2 distribution and subsequent alterations in gene expression revealed that both its binding and functional consequences are non-random events. Heterogeneous binding of the fusion protein was found across all chromosomes in terms of the number of peaks per chromosome and density at specific loci on individual chromosomes. Comparison of these binding sites with epigenetic markers further supported the preference of SYT-SSX2 for regions bound by Polycomb complexes and established its association with a subset of Polycomb-regulated loci. In addition, a small subpopulation of the genes bound by SYT-SSX2 displayed alterations in expression. These genes were typified by certain epigenetic attributes: upregulated genes were characterized by the predominant association of SYT-SSX2 with regions enriched in H3K27me3, whereas downregulated genes could be subdivided into at least 2 categories distinguished by occupation of the fusion protein in regions displaying either H3K27me3 enrichment at short- and long-ranges or the presence of modifications associated with transcriptional activation within the gene body or near the TSS.

The data described here provide a foundation for uncovering the mechanism of SYT-SSX2 recruitment. The preeminent association of SYT-SSX2 with H3K27me3 supports previous reports of interaction with Polycomb complexes (Thaete et al., 1999; dos Santos et al., 2000; Barco et al., 2009) and indicates that the fusion protein does not simply target to regions of open

chromatin by default. Furthermore, because it occupies only a subset of Polycomb loci, the presence of additional targeting factors, genetic or epigenetic, is also likely. One possibility is PRC1. The H3K27me3 modification is catalyzed by PRC2, and it is known that PRC1 and PRC2 do not occupy completely identical sets of genes within a given cell type (Ku et al., 2008; Asp et al., 2011). Direct interaction of the fusion protein has only been seen with the PRC1 component Ring1b (Barco et al., 2009), thus it follows that SYT-SSX2 will not associate with all H3K27me3-labeled regions. Furthermore, PRC1 may also be recruited to chromatin independently of PRC2 (Kerppola, 2009). Recruitment of SYT-SSX2 by PRC1 could then explain at least some of the other binding sites that are not enriched for H3K27me3. Therefore, it would be interesting to determine the degree of overlap between SYT-SSX2 ChIPSeq and genome-wide binding patterns of PRC1 in C2C12 cells.

Our genome-wide analyses revealed that SYT-SSX2 is targeted to over 3,000 genes, yet alterations in expression are noted for, at most, 740 of these targets. This may be due to experimental errors from the high-throughput analyses in the forms of false-positive SYT-SSX2 peaks or false-negative changes in gene expression. Alternatively, it is not unprecedented that the number of binding sites for a particular factor is far greater than the number of genes that are differentially expressed when that factor is induced. MyoD was found to bind to the promoter region of 3,719 genes, yet only 384 of these genes were upregulated during myogenesis (Cao Y et al, 2010). Similarly, the PAX3-FKHR fusion associated with rhabdomyosarcoma bound to 1,072 genes,

however only 95 and 24 of these genes were found to be differentially regulated in PAX3-FKHR-bearing tumor cells and cell lines, respectively (Cao L et al., 2010). These data also suggest that additional signals may be required in order to produce functional outcomes after binding to target loci. In support of this notion, a recent report studying genome-wide binding of p53 indicated that differential gene expression upon treatment with etoposide versus actinomycin D was due to altered p53 phosphorylation rather than changes in binding sites (Smeenk et al., 2011). In the same way, alterations in gene expression by SYT-SSX2 may result from subsequent signaling events.

We were able to identify differential signatures for upregulated versus downregulated genes based on SYT-SSX2 binding site distance as well as the complement of epigenetic markers underlying SYT-SSX2-occupied regions. There is an apparent difference based on distance between positively- and negatively-regulated genes marked by H3K27me3. Most genes with increased expression have SYT-SSX2 binding sites within the gene body or near the TSS while greater numbers of genes with decreased expression are occupied at a distance. This dissimilarity may reflect alternate mechanisms of PRC-mediated silencing. For example, it has been reported that the structure of PRC1 may differ when it is proximal to the TSS versus when it is bound distally; functionally, this results in opposite consequences on gene expression after depletion of PRC1 components (Ren and Kerppola, 2011). Therefore, PRC1 dysfunction caused by SYT-SSX2 could result in opposite effects. Another explanation may involve the ability of SYT-SSX2 to interact with Brg1. In ES cells, Brg1 tunes expression of

Polycomb target genes resulting in either activation or enhanced silencing, and so may augment repression rather than antagonize it (Ho et al., 2011).

In addition, a second subcluster of downregulated genes was characterized by the presence of histone modifications associated with active transcription within the gene or proximal (0-5kb) to the TSS. Together with the fact that close-range binding by SYT-SSX2 at Polycomb-regulated genes results in gene activation, these data indicate that proximal binding by the fusion protein functions to antagonize the transcriptional status of target genes. Moreover, previous work has indicated that these are both consequences of aberrant Polycomb function since SYT-SSX2 has been shown both to antagonize and to initiate Polycomb silencing (Barco et al., 2009; Lubieniecka et al., 2008). In this way, SYT-SSX2 may act as a switch protein that generally opposes the gene expression profile of the cell.

The specificity for the upregulation of neural genes can be explained by a number of different mechanisms. The first involves the endogenous expression of certain factors that makes a particular outcome more likely in one cell versus a different type. It is hypothesized that expression is the result of the balance between Polycomb and Trithorax activity at a given gene, and some cell types may possess additional regulators that can affect gene expression once that balance has been perturbed (Schwartz and Pirotta, 2008; Schwartz et al., 2010). Interestingly, aberrant expression of E-cadherin results from the co-expression of SYT-SSX with the either of the tissue-specific transcriptional repressors Snail or Slug suggesting interaction with repressor molecules directs gene activation by

the fusion (Saito et al., 2006). C2C12 cells may then express certain factors that could guide the expression of neural genes. One potential factor is the REST/NRSF transcriptional repressor that silences neural genes in alternate lineages. Inhibition of its activity leads to neurogenesis in C2C12 cells so misexpression of its target genes by SYT-SSX2 may result in the ectopic neural program seen in these cells (Watanabe et al., 2004).

An alternate mechanism may involve the activation of tissue-specific enhancer elements. In ES cells, enhancers that control the expression of inactive genes involved in differentiation of multiple lineages are labeled by H3K27me3 and H3K4me1. When these elements become active K27 becomes acetylated, a modification that can be catalyzed by p300 (Rada-Iglesias et al., 2010; Tie et al., 2009). Recruitment of SYT-SSX2 to these elements by interactions with Polycomb may lead to increased acetylation of K27 by p300 resulting in their activation and subsequent perturbations in the balance between silencing and expression.

These data allow us to propose a model of recruitment and regulation of target gene expression by SYT-SSX2. In the case of upregulated genes, the fusion protein is recruited by interactions with PRC1, and gene activity is determined by the presence of lineage-specific transcription factors or the activation of specific enhancer elements (Figure 9A). For downregulated genes, SYT-SSX2 may be recruited by PRC1 or PRC2 at a distance from target promoters (Figure 9B, top) or directly targeted to activated genes (Figure 9B, bottom). Recruitment may occur through interactions with the modified histones

themselves, the complexes that catalyze those modifications, or additional proteins like sequence-specific transcription factors. The presence of other factors is likely to be important in specifying target genes for repression.

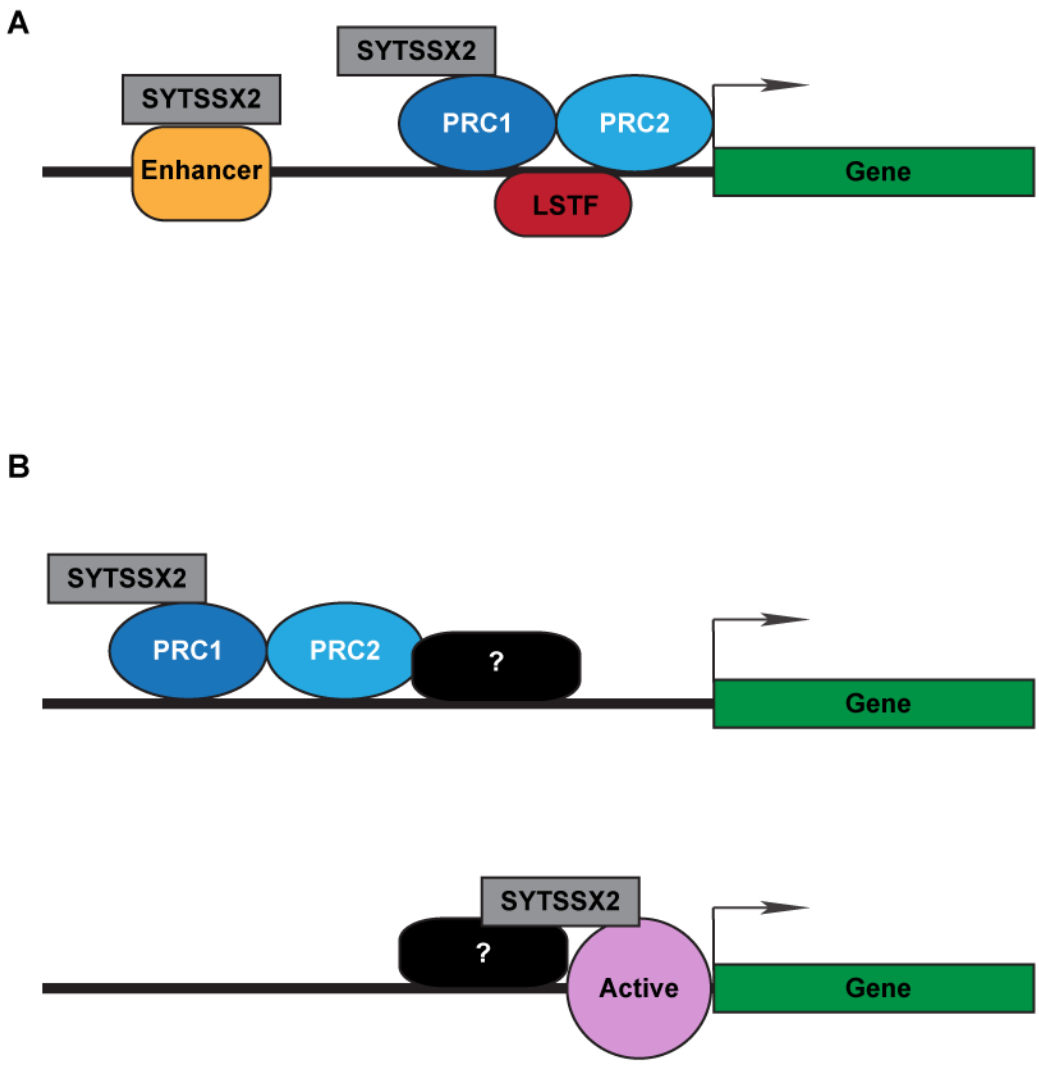

Figure 9. Models of SYT-SSX2 recruitment and activity.
A) Model of recruitment and activity at an upregulated gene. SYT-SSX2 is recruited primarily to silent genes involved in the specification of other lineages by interactions with Polycomb Repressive Complexes (PRC1, dark blue oval; PRC2, light blue oval). In the presence of certain lineage-specific transcription factors (LSTF, red oval) and/or by interaction with lineage-specific enhancers (Enhancer, orange rounded rectangle), SYT-SSX2 association with the gene results in transcriptional activation. B) Model of recruitment and activity at a downregulated gene. *Top)* SYT-SSX2 may be recruited by interactions with Polycomb Repressive Complexes at a distance from the gene TSS. Due to the presence of other regulators (?, black rounded rectangle), SYT-SSX2 carries out transcriptional silencing. *Bottom*) SYT-SSX2 may be directly recruited to the proximal regulatory region through association with activating histone modifications or other unidentified factors. These other factors also provide a signal to SYT-SSX2 such that it mediates repression.

CHAPTER V

DEREGULATION OF POLYCOMB COMPLEX ACTIVITY

Introduction

The Polycomb proteins are important regulators of gene expression in development as well as cancer, and much attention has focused on the mechanism through which these proteins regulate differentiation and contribute to tumorigenesis. One aspect of Polycomb function that has not been addressed extensively is how the activity of these proteins is regulated. PRC1 is considered to be the main controller of gene expression by Polycomb proteins, and the most detectable function that it performs is the ubiquitylation of histone H2A (Simon and Kingston, 2009). This is mediated by the Ring1b protein and facilitated by Bmi1, and accordingly, a few studies have concentrated on the regulation of these proteins.

Bmi1 protein levels are regulated by proteasomal degradation (Ben-Saadon et al., 2006), and its association with chromatin depends on phosphorylation which is modulated by cell cycle progression, mitogen stimulation, or induction of cellular stress (Voncken et al., 1999; Voncken et al., 2005). Like Bmi1, Ring1b undergoes phosphorylation. This is catalyzed by p38 MAPK and ERK1/2, and this modification is associated with changes in protein expression downstream of Ring1b (Rao et al., 2009). Ring1b activity is also

controlled by its auto-ubiquitylation as well as an association with Mel18, a Bmi1 homolog (Ben-Saadon et al., 2006; Elderkin et al., 2007).

Previous work in our lab revealed that SYT-SSX2 expression in human osteosarcoma cells (U2OS) causes loss of Bmi1 protein levels due to its increased degradation (Barco et al., 2009). This results in decreased association with its functional partner, Ring1b, and global loss of histone H2A ubiquitylation. These alterations are also associated with increased expression of putative Polycomb target genes (Barco et al., 2009). These data indicate that SYT-SSX2 functions, in part, by abrogating PRC1 activity resulting in the erroneous activation of Polycomb-silenced genes. Because the deregulation of Polycomb activity seems to be the heart of its function, we wanted to determine the molecular mechanism through which SYT-SSX2 mediates this effect.

Results

Bmi1 is phosphorylated in response to various stimuli

Our previous studies in U2OS cells indicate that enhanced degradation of Bmi1 is the mechanism through which SYT-SSX2 causes transcriptional deregulation of Polycomb target genes. To confirm this hypothesis, we determined Bmi1 protein levels in C2C12 cells after transduction with oncogene-containing expression vectors. In some experiments, we were able to detect a decrease in the amount of Bmi1 protein in SYT-SSX2-expressing cells compared to vector controls (data not shown); however, in the majority of experiments this decrease was not seen, and we noted a slight shift in the mobility of Bmi1 instead (Figure 10A). The slower migration of Bmi1 in the presence of SYT-SSX2 suggests that Bmi1 is post-translationally modified in C2C12 cells expressing the oncogene.

Firstly, because we could recapitulate the findings of our previous study, albeit with less reproducibility than the U2OS system, and secondly, because we also saw that SYT-SSX2 led to the accumulation of a slower migrating form of Bmi1 without a decrease in total protein levels, we hypothesized that the modified Bmi1 may be an intermediate in its degradation pathway. Differences between U2OS and C2C12 cells in terms of other regulators may account for the disparity between outcomes, nevertheless, we suspect that similar mechanisms are at work in both cell types. It has been reported that Bmi1 is subject to degradation by the ubiquitin-proteasome pathway (Ben-Saadon et al., 2006);

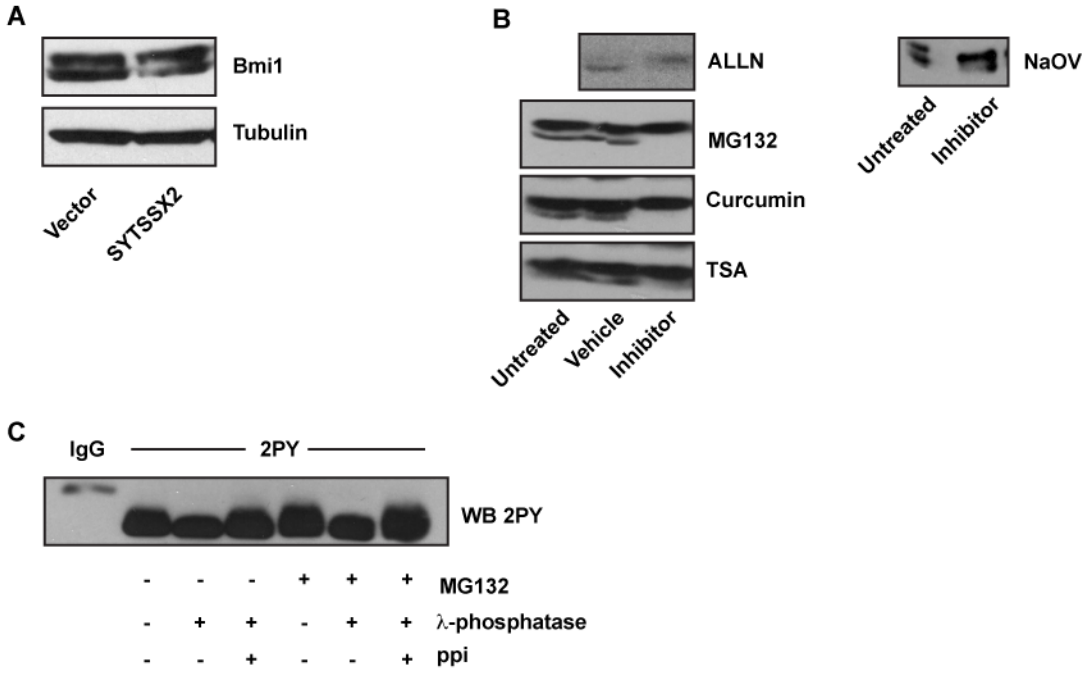

Figure 10. Bmi1 is phosphorylated in response to cellular stress.
A) SYT-SSX2 expression causes a shift in Bmi1 mobility. Cell lysates were harvested 48 hours post-infection with vector control and oncogene-expressing (SYTSSX2) virus. Top panel shows Western blotting for Bmi1. Bottom panel shows tubulin as a loading control. B) Chemical treatment results in altered mobility of Bmi1. C2C12 cells were treated with ALLN (6h, 40 μM), MG132 (overnight, 5 μM), curcumin (6h, 20 μM), TSA (4h, 50 μM), or NaOV (10 min, 300 μM). Bmi1 protein was detected by Western blot. C) Phosphorylation of Bmi by proteasome inhibition. 2PY-tagged Bmi1 was transduced into C2C12 cells by retroviral infection. 48 hours post-infection, cells were treated with MG132 (4h, 5 μM); 2PY-Bmi1 was immunoprecipitated then incubated in the presence of λ-phosphatase for 2 hours with or without phosphatase inhibitors (ppi). Bmi1 protein was detected by Western blotting for the 2PY epitope tag.

therefore, to determine if Bmi1 protein levels could be enhanced through proteasome inhibition, we treated C2C12 cells with ALLN or MG132. Interestingly, treatment with both inhibitors led to a decrease in Bmi1 mobility similar to what was seen in SYT-SSX2-expressing cells (Figure 10B).

The small shift in Bmi1 migration was indicative of the addition of a small modification, like phosphorylation, so in order to test whether Bmi1 was phosphorylated as a result of proteasome inhibition, we immunoprecipitated exogenously-expressed 2PY-tagged Bmi1 from C2C12 cells that were treated with MG132 then subjected the samples to a phosphatase assay. Incubation of the precipitated complexes from vehicle- and MG132-treated cells with λ-phosphatase led to a collapse in the 2PY-Bmi1 band compared to complexes with no λ-phosphatase (Figure 10C) indicating that Bmi1 was phosphorylated in both conditions. The inclusion of phosphatase inhibitors in the reaction mixture prevented the change in mobility further supporting this finding (Figure 10C). Treatment with MG132 led to a slight increase in the height of the 2PY-Bmi1 band suggesting either a higher amount of phosphorylated species or a higher degree of phosphorylation in these samples. Together these data indicate that 2PY-Bmi1 is phosphorylated under normal conditions. These modified species accumulate under conditions of proteasome inhibition and are an intermediate in the proteasomal degradation pathway.

In experiments where we observed SYT-SSX2-associated decrease in Bmi1 signal, proteasome inhibition failed to prevent this loss (data not shown), and instead resulted in the increased phosphorylation of Bmi1 as we have

described. Because SYT-SSX2 interacts with additional protein complexes involved in the epigenetic regulation of transcription, we wanted to determine whether the activity of other epigenetic modifiers was required for Bmi1 regulation. Treatment of C2C12 cells with either curcumin (p300 inhibitor) or trichostatin A (HDAC inhibitor) also led to a change in mobility of Bmi1 (Figure 10B). This indicates that alterations in the activity of epigenetic regulators that cooperate with or antagonize Polycomb repression result in modification of Bmi1. Interestingly, acute inhibition of tyrosine phosphatases also led to the accumulation of the lower mobility Bmi1 species (Figure 10B). Therefore, in general, it appears that cellular stress can cause the phosphorylation of Bmi1. This is in agreement with previous studies showing that Bmi1 becomes phosphorylated under stressed conditions like growth factor deprivation (Voncken et al., 2004). These data suggest that Bmi1 may act as a node through which various signaling networks may converge. More studies are required to understand the nature of Bmi1 regulation through phosphorylation as well as the functional consequences of this modification.

Antagonism of Polycomb repression by SYT-SSX2

In previous work, we show that SYT-SSX2-mediated antagonism of Polycomb repression requires the C-terminal end of SSX2 because of its targeting function (Barco et al., 2009). Reports by other groups indicate the importance of the N-terminus in transformation (Nagai et al., 2001); however the molecular basis for this requirement is unclear. To begin define the mechanistic

details of Polycomb antagonism by SYT-SSX2, we made N-terminal deletion mutants of the fusion lacking the first 20 (NΔ20) and 40 (NΔ40) amino acids of the SYT component and determined the expression of SYT-SSX2 target genes that we previously validated in C2C12 cells (Chapter 3, Figure 2). Deletion of the N-terminus of SYT-SSX2 led to a graded decrease in the expression of *Ngfr* such that the larger N-terminal deletion restored *Ngfr* transcript levels to basal. This is in contrast to *Dll1* and *Igf2* which are increased in cells expressing the NΔ20 mutant and either return to basal levels (Dll1) or a level nearly equivalent with full-length SYT-SSX2 (Igf2) (Figure 11A). These differential effects are rather confounding, so as a first step to understand the effect of N-terminal deletion on transcription, we decided to determine if these mutants retained their ability to bind to known SYT-SSX interactors. In preliminary studies, we tested the ability of SYT-SSX2 and its N-terminal mutants to associate with Brg1 by immunoprecipitation. SYT-SSX2 could co-precipitate Brg1, and this ability to bind Brg1 falls below basal levels in the NΔ20 mutant and is lost in the NΔ40 mutant (Figure 11C, top left panel). These data indicate that the ability to bind Brg1 may not be necessary for activation by SYT-SSX2 in all cases. Further experiments are required for the validation of these findings.

Our previous studies focused on the global regulation of Bmi1 and Polycomb by SYT-SSX2 (Barco et al., 2009), but the present data suggests that while global changes can be detected, the mechanism of how these changes occur are more likely to be discovered by studies of specific target genes. To understand how SYT-SSX2 antagonizes Polycomb complex activity locally, we

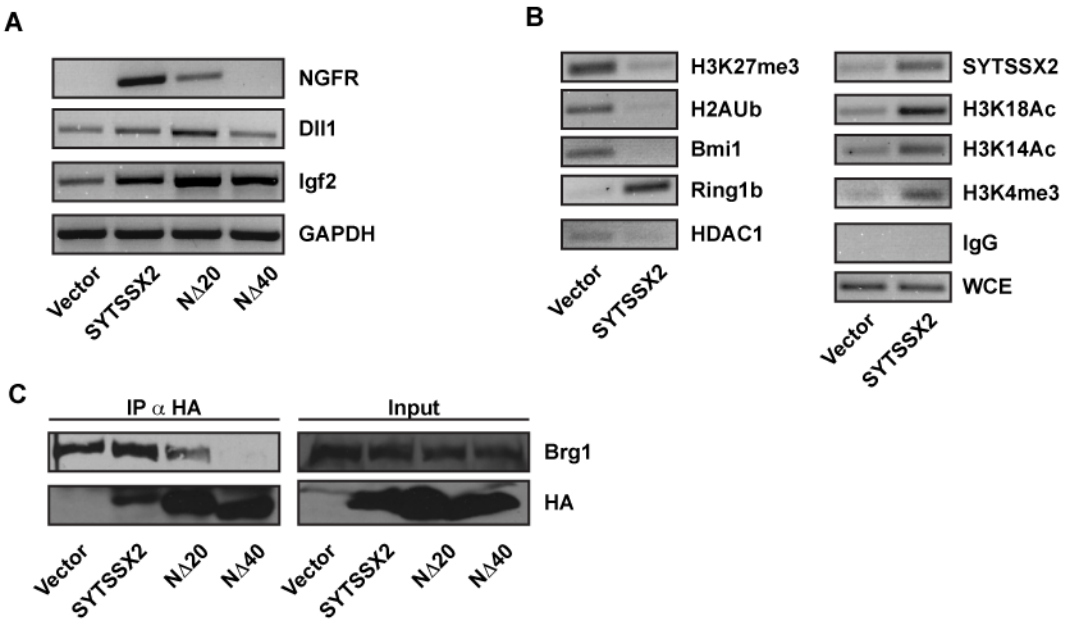

Figure 11. Activation of NGFR by SYT-SSX2.
A) Activation of target genes depends on the N-terminus of SYT-SSX2. Gene expression analysis of NGFR, Dll1, and Igf2 in C2C12 myoblasts expressing SYT-SSX2 or N-terminal deletion mutants of SYT-SSX2 lacking the first 20 (NΔ20) and 40 (NΔ40) amino acids. pOZ is the vector control sample. GAPDH is the loading control. B) ChIP analysis of the NGFR regulatory region. ChIP experiments were performed in either control (Vector) or SYT-SSX2 expressing cells with the antibodies indicated. IgG is a non-specific mouse antibody and serves as a negative control. WCE is the whole cell extract and is the positive control. C) Association of Brg1 with N-terminal mutants. Immunoprecipitation (IP) using HA antibody (12CA5) was performed with extracts from vector-, SYT-SSX2-, NΔ20-, and NΔ40-infected cells. Purified complexes and corresponding lysates were analyzed by Western blot for the presence of Brg1 and HA-tagged constructs.

decided to study the *Ngfr* gene. We were able to validate Polycomb-mediated silencing of *Ngfr* in C2C12 cells (Figure 11B). By chromatin immunprecipitation (ChIP) experiments, we detected the presence of Polycomb-associated histone modifications (H3K27me3 and H2AUb) and members of the PRC1 complex (Bmi1 and Ring1b) at the *Ngfr* promoter region in control cells (Figure 11B). When SYT-SSX2 was expressed, the levels of H3K27me3, H2AUb, and Bmi1 at the *Ngfr* gene were decreased indicating loss of Polycomb-mediated silencing. In addition, we observed lower association of HDAC1 with the *Ngfr* gene (Figure 11B). Conversely, ChIP experiments to detect markers of transcriptional activation (H3K18Ac, H3K14Ac, and H3K4me3) revealed an increase in these modifications in cells expressing SYT-SSX2. To validate that *Ngfr* is targeted by the oncogene, we were also able to demonstrate its presence by ChIP. Interestingly, the signal in the Ring1b ChIP increases in the presence of SYT-SSX2. This phenomenon was reproduced in multiple experiments; however, we have not been able to determine the mechanism by which this occurs. Altogether, we show that the *Ngfr* gene is directly targeted by the SYT-SSX2 oncoprotein and that its expression is associated with increased expression as well as alterations in the configuration of the promoter region. Repressive proteins and histone marks are lost, while activating marks are gained. Additional studies are required in order to understand the interplay of SYT-SSX2 and its associated proteins with the Polycomb complexes at this locus that result in gene expression.

Inhibition of Ring1b function by SYT-SSX2

In U2OS cells, loss of Bmi1 protein as a consequence of SYT-SSX2 expression results in decreased complex formation with Ring1b. This, in turn, was posited to be the cause of the global loss of histone H2A ubiquitylation since Bmi1 is known to enhance Ring1b E3-ligase activity (Barco et al., 2009; Cao et al., 2005). To understand the effects that SYT-SSX2 may have on Ring1b-Bmi1 activity, we performed *in vitro* ubiquitylation studies with recombinant Ring1b and Bmi1 purified from bacteria in the presence of immunoprecipitated SYT-SSX2. Ring1b has been reported to possess auto-ubiquitylation activity which is mitigated by the presence of Bmi1, and this could be seen in our assays (Figure 12, top panel, top arrow). In the presence of control IP, auto-ubiquitylation of Ring1b increased; however, when incubated with SYT-SSX2 IP, the amount of ubiquitylated Ring1b decreased relative to the control IP (Figure 12, top panel). Furthermore, the amount of total ubiquitylation was decreased in reactions containing SYT-SSX2 IP (Figure 12, bottom panel). This inhibition was especially decreased in reactions containing only Ring1b. Investigations to confirm this finding are required, but these data imply that SYT-SSX2 and/or its associated proteins could either inhibit Ring1b activity or recruit an enzyme with deubiquitylase activity. Either scenario would uncover a novel mechanism of SYT-SSX2 action.

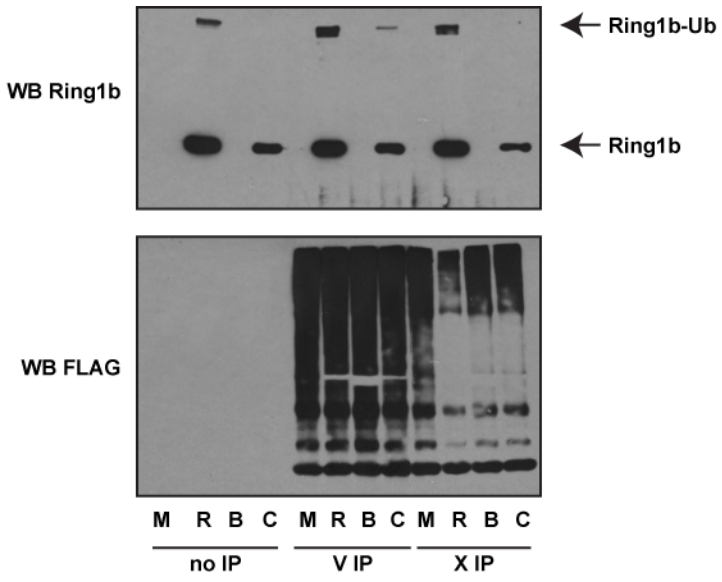

Figure 12. SYT-SSX2 inhibits ubiquitylation activity of Ring1b.
In vitro **ubiquitylation assays were performed using FLAG-tagged ubiquitin and bacterially purified Ring1b (R), Bmi1 (B), or Ring1b and Bmi1 in complex (C) as the E3-ubiquitin ligase. M labels samples in which no recombinant protein was added. These assays were carried out either in the absence (no IP) or presence of FLAG-immunoprecipitated protein complexes derived from vector- (V IP) or SYT-SSX2-expressing cells (X IP). Top panel shows Western blotting for Ring1b. Arrows mark the location of ubiquitylated Ring1b (upper) and the unmodified protein (lower). Bottom panel shows Western blotting for FLAG-tagged (ubiquitylated) species.**

Conclusions

The experiments described here provide a foundation for future studies to elucidate the molecular mechanism of SYT-SSX2 antagonism of Polycomb-mediated gene silencing. Bmi1 is phosphorylated in response to a number of different stimuli, including SYT-SSX2 expression. Phosphorylation of Bmi1 correlates with its dissociation from chromatin during the cell cycle (Voncken et al., 2004); therefore, this modification may explain how Bmi1 is lost from the *Ngfr* promoter. The fact that Bmi1 is phosphorylated after inhibition of HAT and HDAC activity suggests that changes in the epigenetic environment in general may also cause this event. Knock-down of Suz12 in C2C12 cells results in the re-distribution of Bmi1 such that the level of Bmi1 bound at genes where PRC1 is already resident increases without an overall change in protein level (Asp et al., 2011). Although it is hypothesized that this guards against the inappropriate expression of lineage-specific genes (Asp et al., 2011), the relocation of Bmi1 may be a more general mechanism that the cell (and perhaps a stem and progenitor cells in particular) uses to control the accessibility of certain subsets of genes when challenged with a given insult or signal. In consequence, signaling to Bmi1 may be one way that various pathways can regulate the expression of Polycomb target genes.

The initial studies we described here using the N-terminal SYT-SSX2 mutants and the profile of epigenetic markers at the *Ngfr* promoter provide a background for understanding the mechanism of SYT-SSX2 function. We show

that *Ngfr* is a Polycomb target in C2C12 cells and that its repression is reversed by SYT-SSX2. Our data also indicate that Brg1 binding may not be critical for *Ngfr* expression; however, its ability to associate with SYT-SSX2 correlates strongly with activation of this gene. Thus, Brg1 activity may be required for this process, but recruitment by other mechanisms, like histone acetylation, may compensate for the inability to associate with SYT-SSX2. Surprisingly, we also detected differences in expression among the genes we tested in their requirement for the N-terminal 20 amino acids of SYT-SSX2. This may reflect differences in the mechanism of regulation at these particular genes. From our ChIP and ChIPSeq data (Chapters 3 and 4), SYT-SSX2 binds in close proximity to the TSS of *Ngfr* but not *Dll1* or *Igf2*. This suggests that increased expression of these genes may be indirect or due to long-range interactions that are still poorly understood.

The change in histone modifications at the *Ngfr* promoter occurs as expected for a switch from the silenced to an active state. How SYT-SSX2 mediates these changes remains to be clarified. Histone acetylation is likely due to interaction of SYT-SSX2 with p300, and p300 activity may also directly inhibit H3K27me3 through acetylation of the same residue (Eid et al., 2000; Tie et al., 2009). Lysine 27 acetylation in *Drosophila* requires Trx activity suggesting that recruitment of MLL occurs prior to p300 catalytic function. Furthermore, removal of the H3K27me3 mark necessarily precedes acetylation and requires the activity of a demethylase like UTX or JMJD3 (Lee et al., 2007; Agger et al., 2007). Additional studies regarding the sequence of events that is orchestrated by SYT-

SSX2 at the *Ngfr* promoter and the identification of novel binding partners will contribute further insight into this mechanism.

Our preliminary data from *in vitro* ubiquitylation assays indicate the inhibition of Ring1b ligase activity or a deubiquitylation activity recruited by SYT-SSX2 and/or its associated proteins. Thus far we have focused our studies on the dynamics of Bmi1 as changes to this protein have been the most visible, and we hypothesize that the loss of Bmi1 from PRC1 leads to the derepression of Polycomb silencing. Indeed, our ChIP studies at the *Ngfr* gene indicate that Ring1b is retained at the promoter, so we conjecture that the loss of its partner protein caused the decrease in H2AUb making transcription permissible. In light of the present data, we must now consider the possibility that SYT-SSX2, either on its own or by the recruitment of other proteins, actively opposes Ring1b function in addition to any effects on Bmi1. A histone H2A deubiquitylase that opposes PRC1 has been identified in flies and is homologous to the mammalian BAP1 (Scheuermann et al., 2010). In addition, USP7 is able to deubiquitylate Ring1b and thus deactivate it (de Bie et al., 2010). It will be interesting to determine if SYT-SSX2 can interact with either of these proteins or others with similar functions.

In summary, the derepression of Polycomb target genes by SYT-SSX2 may take place through both passive and active mechanisms. Understanding how this is facilitated by the fusion protein may highlight possible avenues for therapeutic intervention as well as elucidate the regulation of Polycomb in normal conditions.

CHAPTER VI

DISCUSSION AND FUTURE DIRECTIONS

Cellular reprogramming by SYT-SSX2

Taken as a whole, the data presented in this study support cellular reprogramming as the mechanism by which SYT-SSX2 induces transformation. The remarkable number of neural and developmental genes shared by the myoblasts and the hMSCs showcases the dominant programming effect of SYT-SSX2. Imposing a lineage commitment on stem/progenitor cells appears to be a recurrent feature of sarcoma-associated translocations (Mackall et al., 2004). One prominent example is PAX3-FKHR, the rhabdomyosarcoma fusion product that drives NIH3T3 fibroblasts into a myogenic program (Khan et al., 1999). It is thought to induce tumorigenesis through stimulation of lineage commitment and simultaneous prevention of terminal differentiation (Charytonowicz et al., 2009). Whether SYT-SSX2 acts in a similar manner remains to be seen. Regardless, the dominant effect on cellular identity is postulated to be a part of oncogenesis initiation by sarcoma-associated translocations and a necessary step toward malignant transformation (Mackall et al., 2004).

These observations allow us to speculate on the cell-of-origin for this malignancy. The capacity of SS cells to be differentiated into mesenchymal and neural cell types (Naka et al, 2010; Ishibe et al, 2008) implies that the disease

originates in multipotent cells from either of these lineages. Our data indicate that the neural features are caused primarily by SYT-SSX2 itself, irrespective of cellular context, so the target cell may not necessarily be of neural origin. Expression of SYT-SSX2 in multiple lineages in mice recapitulates human synovial sarcoma in all cases, attesting to the dominant program established by the oncogene and its capacity to transform different cell types (Haldar et al., 2009). Additionally, expression of SYT-SSX2 in committed myogenic progenitor cells results in tumor formation in mice suggesting that the cell-of-origin could be a more differentiated entity. However, in this model, genomic plasticity was essential, as SYT-SSX2 was non-tumorigenic in differentiated muscle cells (Haldar et al., 2007).

Epigenetic mechanism of SYT-SSX2 targeting and function

A major mechanism of recruitment occurs through interactions with PRCs, but like other transcriptional regulators, binding of SYT-SSX2 does not completely correlate with changes in gene expression. Studies on cellular reprogramming as well as on alterations in chromatin structure during differentiation indicate that transcription factor binding and/or differential histone modification signatures pre-label genes that may undergo changes in expression when given the proper stimulus (Koche et al., 2010; Orford et al., 2008). Thus, genes that are bound but whose expression is unaltered may be “poised” for activation in response to certain signaling events. Indeed, the dependence of the

neural phenotype on FGF signaling supports such a scenario. In this model, binding by SYT-SSX2 alters the chromatin structure of neural genes into a poised state, and signaling downstream of FGFR2 induces the activation of these targets. This suggests that transcriptional activity is directed by extracellular signaling, and stimulation of other pathways will result in the generation of distinct phenotypes. Comprehension of the complete transformative program will consider these alternate fates.

Latent programs primed by SYT-SSX2 will also have important ramifications on disease progression and treatment response. The studies described here are concerned with the acute phase of transformation by the oncogene and document how targeting of the chimeric protein dictates early events. Genes that are involved in tumor maintenance during later stages of progression and/or metastasis could also be pre-marked by SYT-SSX2. It may then be possible to predict tumor behavior by knowing the identities of those genes and determining pathways that induce their activation.

Molecular mechanism of Polycomb derepression

Because of its interaction with multiple epigenetic regulatory complexes, SYT-SSX2 stands as the central node that organizes transcriptional deregulation. Transcription factors possess domains that allow them to interact with multiple downstream effectors and thus orchestrate transcription (Frietze and Farnham, 2011). This includes transactivation domains and other protein-protein interaction

modules with the capability to bind activators and repressors. Thus, one protein through the same domain can elicit distinct effects (Frietze and Farnham, 2011). The SNH domain of SYT may perform this function since it can interact with both p300 and mSin3a (Eid et al., 2000; Ito et al., 2004). Differential binding might be controlled by upstream extracellular cues like the FGF or other signaling pathways providing a direct link between the microenvironment and the control of Polycomb. In this way, SYT-SSX2 can execute multiple functions with diverse effects at a target gene.

Studying the molecular function of SYT-SSX2 will also illuminate the sequential recruitment of factors necessary to counteract Polycomb-mediated silencing. Understanding this process has considerable implications for normal cellular reprogramming (e.g. conversion of fibroblasts to induced pluripotent stem cells). Polycomb complexes are part of a larger epigenetic program that must be conformed to the structure of the target cell type in order for reprogramming to be complete (Gaspar-Maia et al., 2011). Our study on SYT-SSX2 suggests that targeted inhibition of PcG proteins in combination with specific signals can produce a distinct cell fate. In elaborating how SYT-SSX2 initiates and controls this process, and by identifying how genes within a specific program are targeted, it will become clearer how to change the epigenetic structure of one cell to that of an alternate lineage. Ultimately, this will improve the efficiency of cellular reprogramming.

Our data indicate that transformation by SYT-SSX2 occurs through improper reprogramming of the nucleus most likely via modulation of the

activities of epigenetic regulators with cooperation from signaling pathways. This has important implications in the treatment of synovial sarcoma. Although epigenetic reprogramming is a slow process, once complete, it is persistent. Therefore, even in the absence of the initiating signal (i.e. oncogene expression), this abnormal nuclear program remains intact (Abollo-Jiménez et al., 2010; Castellanos et al., 2010). Indeed, this is characteristic of normal Polycomb-mediated gene repression (Schuettengruber et al., 2007; Kerppola, 2009) suggesting that treatment of synovial sarcoma could become resistant to SYT-SSX-specific therapeutics and that the most effective therapies will instead target the aberrant program.

Future Directions

Molecular mechanism of SYT-SSX2 function

The extracellular signals that govern differentiation and development are well-characterized for many tissues, yet the manner in which these pathways regulate Polycomb function is incompletely understood. The data presented in this study indicate that SYT-SSX2 activity relies on extracellular signaling, specifically the FGF pathway. Contributions from other factors in the microenvironment are possible, and future efforts should delineate the relationship between signaling pathways and the control of transcription by the fusion protein. Although associated with a disease phenotype, the cycle of events directed by SYT-SSX2 with input from the FGF pathway likely reflect normal

mechanisms. Thus it will be informative for researchers who are interested in the transcriptional control of differentiation and development as well as those investigating possible therapeutic interventions for SS.

Three-dimensional structure of chromatin

Polycomb and SWI/SNF mediate higher-order chromatin configurations. Many binding sites in our ChIPSeq analysis occur in intergenic regions, so it will be fascinating to determine how SYT-SSX2 affects three-dimensional chromatin structure. Chromosome conformation capture experiments will build a more complete picture of SYT-SSX2 function. These studies will also demonstrate whether SYT-SSX2 modulates long-range transcriptional regulation. As a preliminary finding, our ChIPSeq analysis revealed the association of SYT-SSX2 within a region of the *H19-Igf2* locus between the 2 genes that drives expression of *Igf2* in mesodermal tissues (Drewell et al., 2002). As a whole, these investigations will yield valuable information concerning the mechanism by which chromatin architecture controls transcription.

Therapy and cellular reprogramming

The development of effective therapeutics in the treatment of SS will require a deep understanding of the tumorigenic program initiated by SYT-SSX2, and it will be necessary to establish how this predisposes the cell to respond to therapeutic interventions. Additional studies should focus on how the SYT-SSX2 program is maintained, whether it can be reversed, and the nature of changes in

gene expression and fusion protein targeting following various stimuli. Overall, these studies will advance our knowledge of how cellular identity is controlled and how the pathways that govern differentiation and plasticity may be exploited in cancer. This will lead to the generation of new therapeutics with increased ability to target the reprogrammed cells essential for tumor propagation.

APPENDIX A

SUPPLEMENTARY METHODS

In vitro phosphorylation

Bacterially purified Ring1b, Bmi1, or Ring1b-Bmi1 complex was incubated with 25 µL pOZ- or SYT-SSX2-expressing cell nuclear extract in kinase assay buffer (20 mM Tris pH 8.0, 150 mM NaCl, 2 mM DTT, 20 mM $MgCl_2$, 40 µM ATP [plus 5 µCi γ-^{32}P-ATP for hot kinase assay]) with protease and phosphatase inhibitors at 30˚C for 30 minutes. Reactions were stopped by the addition of 2x sample buffer.

In vitro acetylation

Acetylation assays were performed as previously described (Gu and Roeder, 1997) with some modification. Bacterially purified Ring1b (2.5 µg), Bmi1 (2.5 µg), or Ring1b-Bmi1 complex (2.5 µg each monomer) were incubated in assay buffer (50 mM HEPES pH 7.9, 10% glycerol, 1 mM DTT, 1 mM PMSF, 10 mM sodium butyrate, 1 µL ^{14}C-acetyl CoA [60 mCi/mmol]) with 100 ng of recombinant human p300 catalytic domain (Enzo Life Sciences, Plymouth Meeting, PA) and 2 µg HeLa nucleosomes for 1 hour at 30˚C. Reactions were stopped by the addition of 2x sample buffer. Samples were separated using SDS-PAGE, gels were Coomassie stained, dried, and proteins were visualized by autoradiography.

APPENDIX B

SUPPLEMENTARY DATA

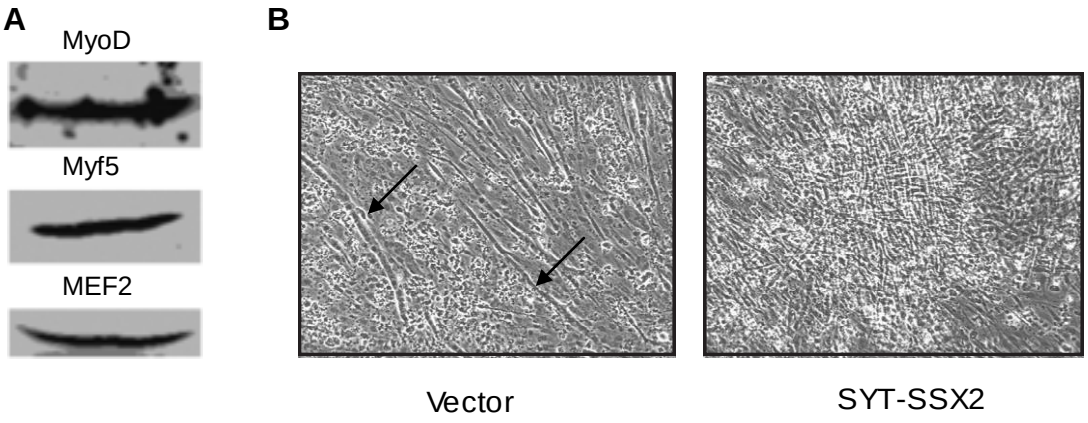

Appendix B Figure B1. SYT-SSX2 inhibits myogenesis in C2C12 myoblasts.
A) Myogenic profile of C2C12. Western blot shows expression of myogenic markers in the myoblasts lysates, detected by rabbit anti-MyoD, MEF2, and Myf5 (Santa Cruz). Differentiation of these C2C12 cells was restricted to the muscle lineage. B) Myogenic differentiation of C2C12 cells. Forty-eight hours post-infection, C2C12 cells expressing either vector control (left panel) or SYT-SSX2 (right panel) were stimulated with myogenic differentiation medium (DMEM supplemented with 5% horse serum) for 7 days. Brightfield images were captured at 10x magnification using a Zeiss Axiovert 200M inverted microscope. Arrows indicate multinucleated myotubes.

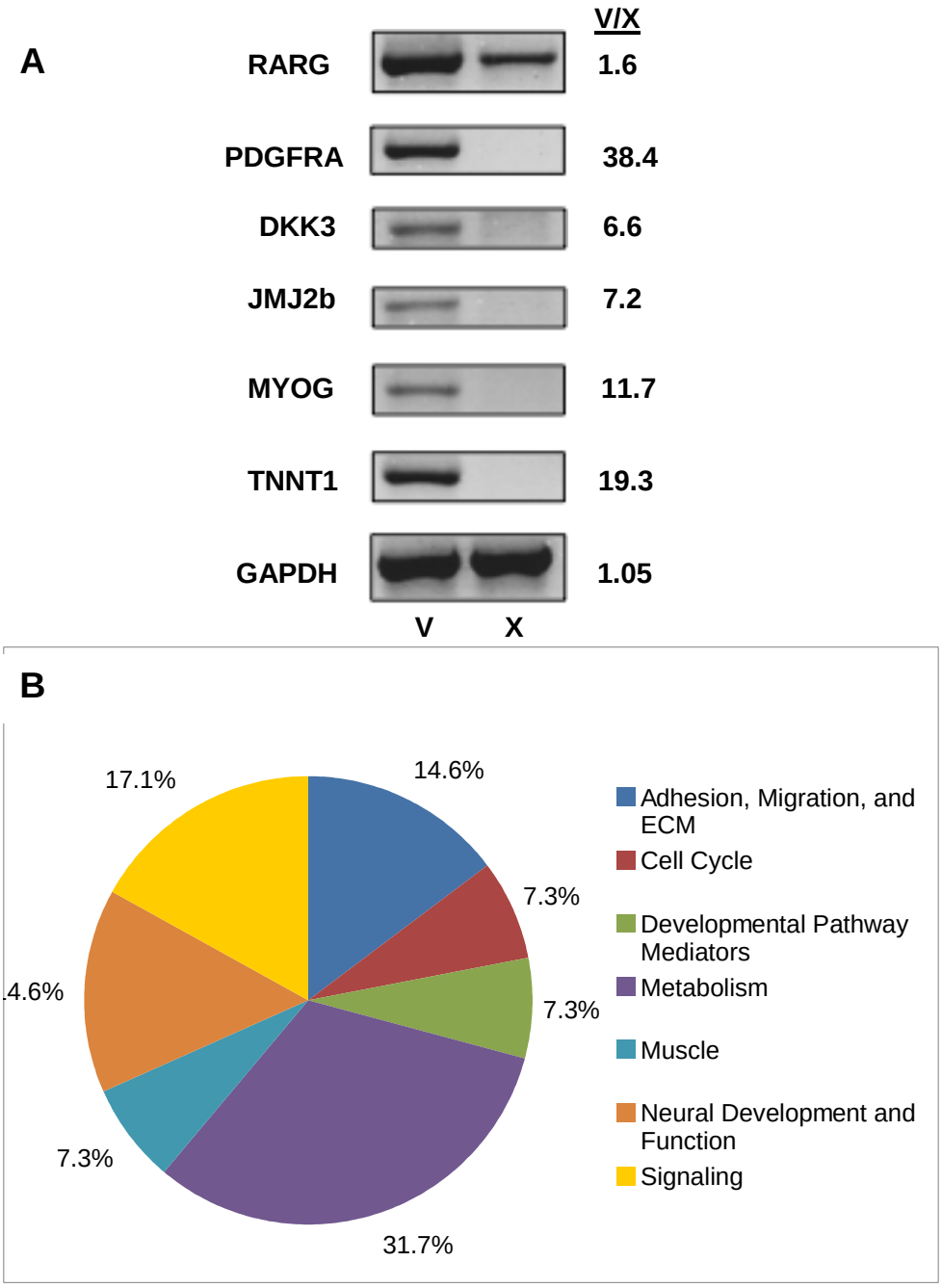

Appendix B Figure B2. Genes downregulated by SYT-SSX2 and their representation in the ChIPSeq analysis.
A) RT-PCR analysis confirmed decreased expression of 6 out of 9 genes selected from the C2C12 microarray. They represent mediators of diverse cellular pathways, ranging from nuclear receptors (*RARG*) and PDGF signaling (*PDGFRA*), to Wnt inhibition (*DKK3*), chromatin modification (*JMJ2b*), and muscle differentiation (*MYOG, TNNT1*). GAPDH served as cDNA input control. V/X represents the ratio of gene expression signal in vector control cells (V) over SYT-SSX2 (X) expressants. Signal intensities were measured with the Fluorchem 8900 densitometer and analyzed using the AlphaEase FC software.

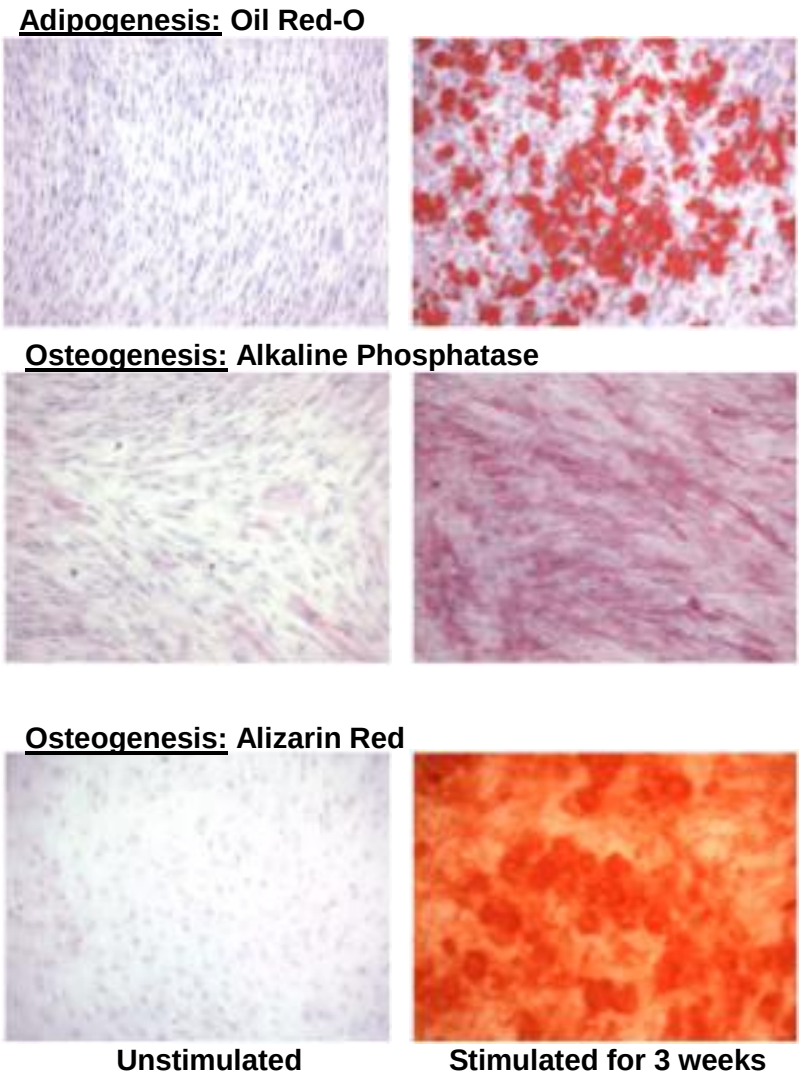

Appendix B Figure B3. Adipogenesis and osteogenesis in human hMSCs. Human bone marrow stem cells were acquired from Dr Prockop's laboratory and purified and tested for multipotentiality according to established protocols (Colter et al., 2001; Sekiya et al., 2002). Oil Red-O stains lipid droplets in differentiated adipocytes. Alkaline phosphatase is a marker for early osteoblast differentiation. Alizarin Red detects calcified deposits in late osteoblasts.

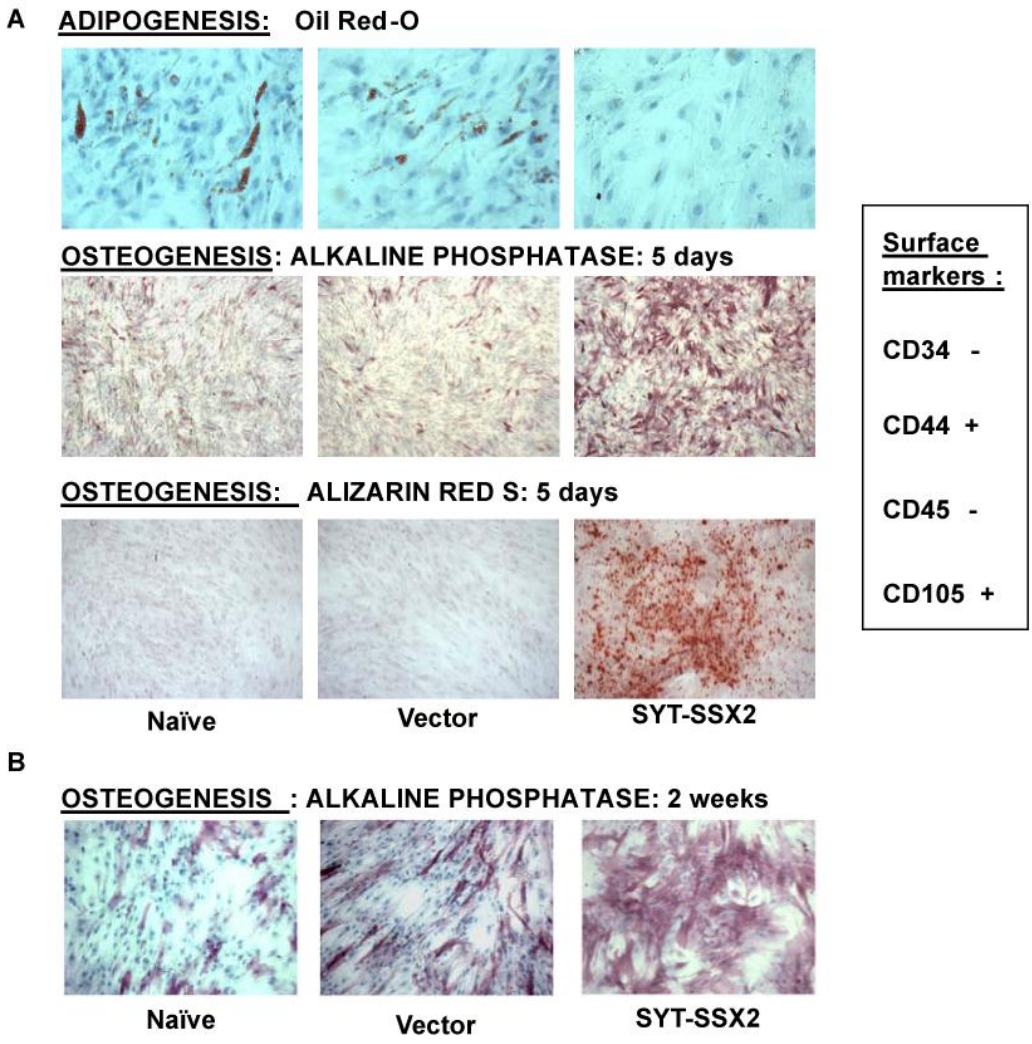

Appendix B Figure B4. Adipogenesis inhibition and osteogenesis acceleration in hMSCs by SYT-SSX2.
A) Effect of SYT-SSX2 on hMSCs differentiation. Human MSCs were isolated from normal bone marrow. Their multilineage potential was confirmed by their flow marker profile: 0.4% CD34, 99.6% CD44, 0.2% CD45 and 99.8% CD105 positives (M. Alfaro). These MSCs are capable of undergoing adipogenesis and osteogenesis. Inhibition of adipogenesis in SYT-SSX2 expressants was evidenced by the complete lack of fat deposition stained with Oil Red-O (Red globules in Vector control and Naïve MSCs). A striking acceleration of osteogenesis (Alkaline Phosphatase) and early calcium deposition (ALIZARIN RED) in SYT-SSX2-MSCs was visible as early as 5 days post-stimulation with differentiation medium. B) Osteogenic differentiation of naïve, Vector control, and SYT-SSX2 hMSCs after 2 weeks in differentiation media.

Appendix B Figure B5

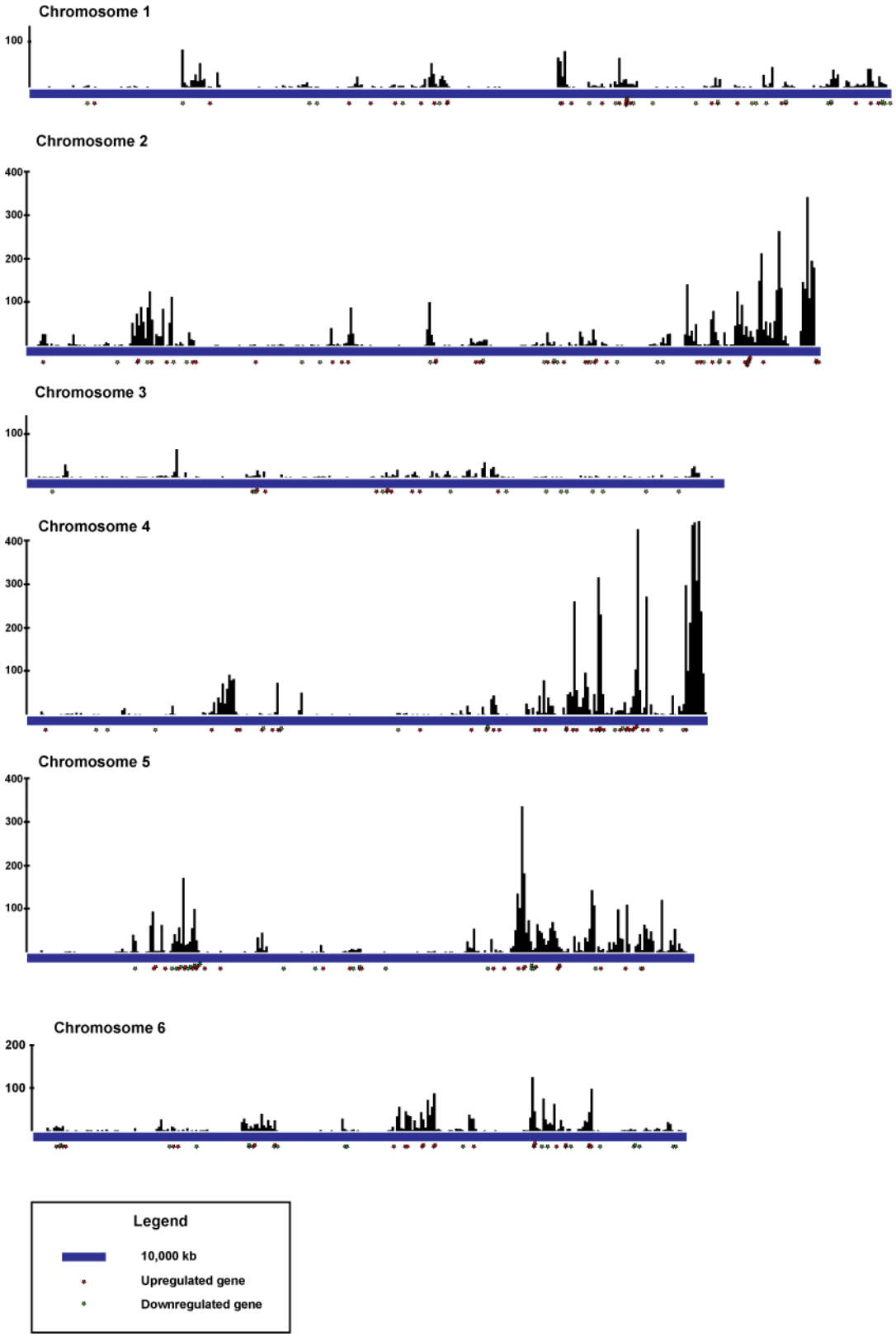

Appendix B Figure 5 cont'd

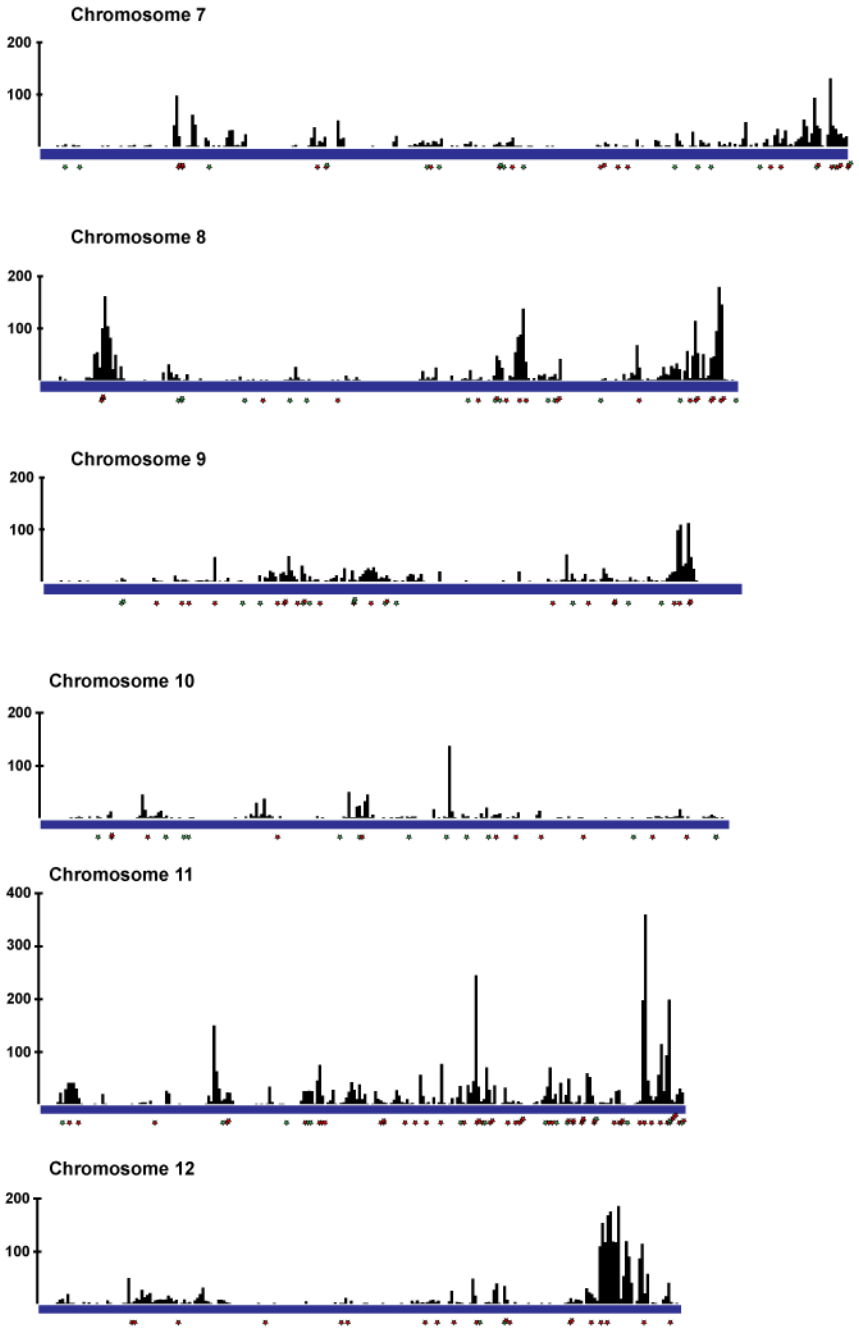

Appendix B FIgure B5 cont'd

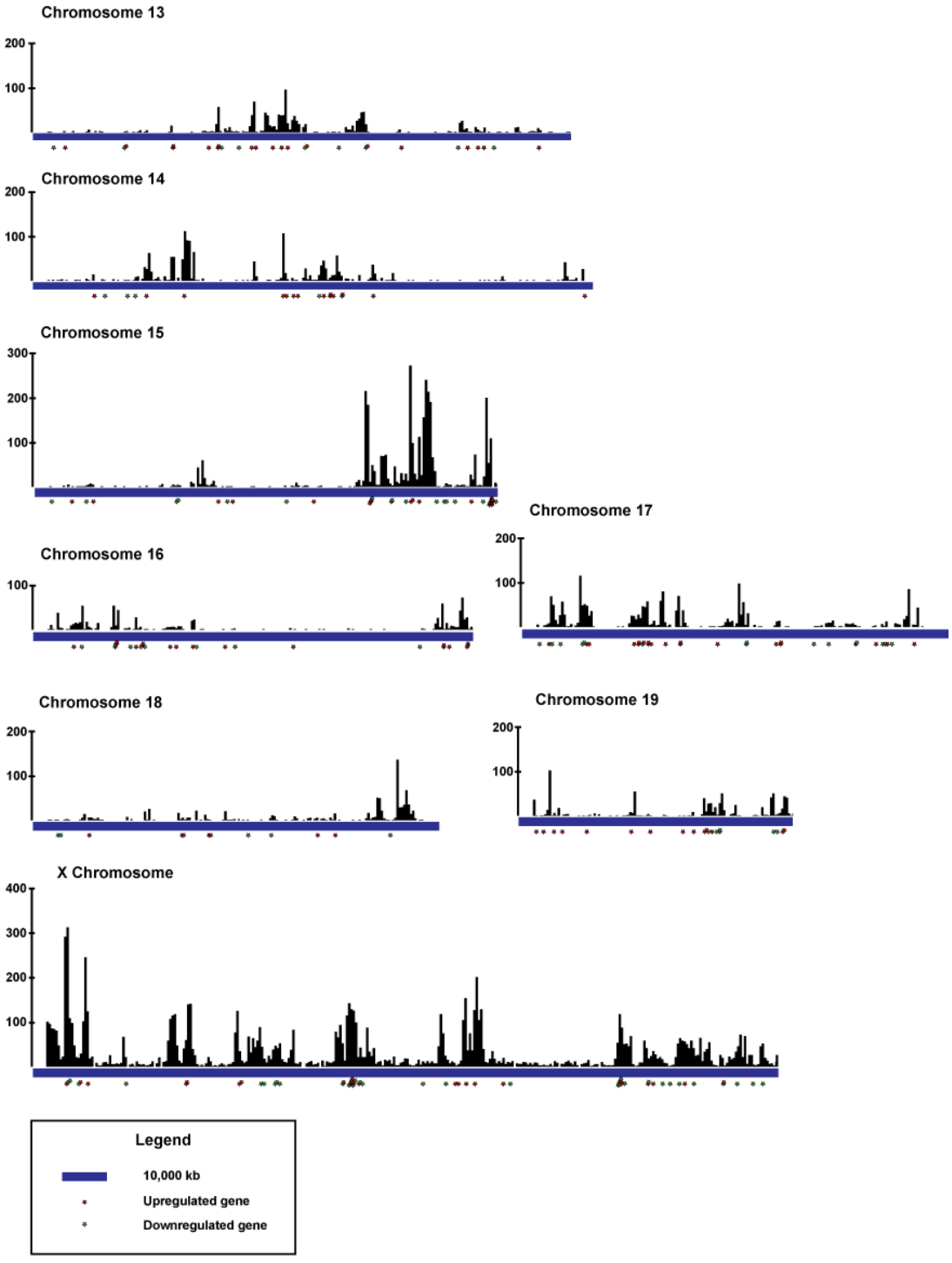

Appendix B Figure B5. Distribution of SYT-SSX2 binding sites and differentiatlly regulated genes per chromosome. A linear diagram of each mouse chromosome (1-19 and X) is presented. Black columns represent a 500kb bins. The height of each column is proportional to the number of peaks (y-axis) within a given bin. Scale bar denotes 10 Mb. Red and green stars mark the location of up- and downregulated genes, respectively.

Appendix B Table B1. Commonly upregulated genes between SYT-SSX2-expressing myoblasts and human synovial sarcoma tumors.

Developmental Pathway Mediators					
Gene Symbol	**Gene Name**	**Accession**	**Gene Symbol**	**Gene Name**	**Accession**
FGF18	fibroblast growth factor 18	NM_003862	FGFR2	fibroblast growth factor receptor 2	NM_000141
FGFR3	fibroblast growth factor receptor 3	NM_000142	GLI2	GLI-Kruppel family member GLI2	NM_005270
DLL1	delta-like 1	NM_005618	APCDD1	adenomatosis polyposis coli down-regulated 1	NM_153000
DACT1	dapper, antagonist of beta-catenin	NM_001079520	TLE4	transducin-like enhancer of split 4	NM_007005
MEST	mesoderm specific transcript homolog	NM_002402	PTH1R	parathyroid hormone 1 receptor	NM_000316
Developmental Transcription Factors					
CREB5	cAMP responsive element binding protein 5	NM_001011666	DLX5	distal-less homeobox 5	NM_005221
ETV4	ets variant gene 4	NM_001079675	FOXD1	forkhead box D1	NM_004472
HOXB5	homeobox B5	NM_002147	ID2	inhibitor of DNA binding 2	NM_002166
ID4	inhibitor of DNA binding 4	NM_001546	KLF4	Kruppel-like factor 4 (gut)	NM_004235
SOX9	SRY (sex determining region Y)-box 9	NM_000346	ZBTB10	zinc finger and BTB domain containing 10	NM_001105539
Signaling and Cell Cycle					
AKAP12	A kinase (PRKA) anchor protein (gravin) 12	NM_005100	CCND1	cyclin D1	NM_053056
CCND2	cyclin D2	NM_001759	CDKN1C	cyclin-dependent kinase inhibitor 1C (p57, Kip2)	NM_000076
IGF2	insulin-like growth factor 2	NM_000612	KCNA1	potassium voltage-gated channel, shaker-related subfamily, member 1	NM_000217
KCNK1	potassium channel, subfamily K, member 1	NM_002245	LGR5	leucine-rich repeat-containing G protein-coupled receptor 5	NM_003667
LRP8	low density lipoprotein receptor-related protein 8	NM_001018054	MYC	v-myc myelocytomato-sis viral oncogene homolog	NM_002467
PPP2R2C	protein phosphatase 2, regulatory subunit B, gamma isoform	NM_020416	PRKCZ	protein kinase C, zeta	NM_001033581
PTPN3	protein tyrosine phosphatase, non-receptor type 3	NM_001145368	PTPRN	protein tyrosine phosphatase, receptor type, N	NM_002846
TBKBP1	TBK1 binding protein 1	NM_014726	TOM1L1	target of myb1-like 1	NM_005486
Neural Development and Function					
CBLN1	cerebellin 1 precursor	NM_004352	CRHR1	corticotropin releasing hormone receptor 1	NM_001145146
CRMP1	collapsin response mediator protein 1	NM_001014809	DPYSL5	dihydropyrimidin-ase-like 5	NM_020134
ECEL1	endothelin converting enzyme-like 1	NM_004826	EPHA4	EPH receptor A4	NM_004438
EPHB1	EPH receptor B1	NM_004441	FAAH	fatty acid amide hydrolase	NM_001441
FJX1	four jointed box 1	NM_014344	GDAP1	ganglioside-induced differentiation-associated protein 1	NM_001040875
KIF1A	kinesin family member 1A	NM_004321	LRRN3	leucine rich repeat neuronal 3	NM_001099658
MAPT	microtubule-associated protein tau	NM_001123066	MN1	meningioma 1	NM_002430
NGFR	nerve growth factor receptor	NM_002507	NPTX1	neuronal pentraxin I	NM_002522
NRGN	neurogranin	NM_001126181	OLFM1	olfactomedin 1	NM_006334
OLIG2	oligodendrocyte lineage transcription factor 2	NM_005806	RDH10	retinol dehydrogenase 10 (all-trans)	NM_172037
RGS16	regulator of G-protein signalling 16	NM_002928	RTN4R	reticulon 4 receptor	NM_023004

Appendix B Table B1 cont'd

SLC6A1	solute carrier family 6, member 1	NM_003042	SLIT3	slit homolog 3	NM_003062
SULT4A1	sulfotransferase family 4A, member 1	NM_014351	TH	tyrosine hydroxylase	NM_000360
ZIC2	Zic family member 2	NM_007129			
Other					
CPXM2	carboxypeptidase X (M14 family), member 2	NM_198148	DUS4L	dihydrouridine synthase 4-like	NM_181581
ETV5	ets variant gene 5	NM_004454	FLRT3	fibronectin leucine rich transmembrane protein 3	NM_013281
HR	hairless homolog	NM_005144	HS3ST3A1	heparan sulfate (glucosamine) 3-O-sulfotransferase 3A1	NM_006042
HS3ST3B1	heparan sulfate (glucosamine) 3-O-sulfotransferase 3B1	NM_006041	KRT17	keratin 17	NM_000422
KRT19	keratin 19	NM_002276	MLLT4	myeloid/lymphoid or mixed-lineage leukemia; translocated to, 4	NM_001040000
NR4A1	nuclear receptor subfamily 4, group A, member 1	NM_002135	ODC1	ornithine decarboxylase 1	NM_002539
PDZD2	PDZ domain containing 2	NM_178140	PEG10	paternally expressed 10	NM_001040152
PVRL1	poliovirus receptor-related 1	NM_002855	RYBP	RING1 and YY1 binding protein	NM_012234
SIPA1L2	signal-induced proliferation-associated 1 like 2	NM_020808	SLC29A2	solute carrier family 29, member 2	NM_001532
TMEM100	transmembrane protein 100	NM_001099640	WDR43	WD repeat domain 43	NM_015131
WFDC2	WAP four-disulfide core domain 2	NM_006103			

Appendix B Table B2. Developmental pathway mediators and developmental transcription factors upregulated by SYT-SSX2 in myoblasts.

Asterisks (*) denote genes that are also bound by the SYT-SSX2 complex.

Developmental Pathways					
Gene Symbol	**Gene Name**	**Accession**	**Gene Symbol**	**Gene Name**	**Accession**
Wnt					
Apcdd1	adenomatosis polyposis coli down-regulated 1	NM_133237	Axin2*	Axin 2	NM_015732
Dact1	dapper homolog 1, antagonist of beta-catenin	NM_021532	Fzd3*	frizzled homolog 3	NM_021458
Tcf7	transcription factor 7, T-cell specific	NM_009331	Tle3	transducin-like enhancer of split 3	NM_001083927
Tle4	transducin-like enhancer of split 4	NM_011600	Wnt11	wingless-related MMTV integration site 11	NM_009519
Wnt4	wingless-related MMTV integration site 4	NM_009523	Wnt7a*	wingless-related MMTV integration site 7A	NM_009527
Wnt7b	wingless-related MMTV integration site 7B	NM_009528			
Notch					
Dll1	delta-like 1	NM_007865	Hes1	hairy and enhancer of split 1	NM_008235
Nrarp	Notch-regulated ankyrin repeat protein	NM_025980			
TGFβ/BMP					
Gdf6	growth differentiation factor 6	NM_013526	Nog	noggin	NM_008711
Tgfbr1	transforming growth factor, beta receptor I	NM_009370			

Appendix B Table B2 cont'd

Shh					
Gli2*	GLI-Kruppel family member Gli2	NM_001081125	Ptch1	patched homolog 1	NM_008957
Shh*	sonic hedgehog	NM_009170			
FGF					
Fgf18	fibroblast growth factor 18	NM_008005	Fgf3*	fibroblast growth factor 3	NM_008007
Fgf7	fibroblast growth factor 7	NM_008008	Fgf9	fibroblast growth factor 9	NM_013518
Fgfr2*	fibroblast growth factor receptor 2	NM_010207	Fgfr3	fibroblast growth factor receptor 3	NM_008010
Shisa2	shisa homolog 2	NM_145463			
Developmental Transcription Factors					
Gene Symbol	**Gene Name**	**Accession**	**Gene Symbol**	**Gene Name**	**Accession**
Dlx3	distal-less homeobox 3	NM_010055	Dlx5*	distal-less homeobox 5	NM_010056
Dmrta1	doubesex and mab-3 related transcription factor like family A1	NM_175647	Ehf	ets homologous factor	NM_007914
Esrrb	estrogen related receptor, beta	NM_011934	Foxc2	forkhead box C2	NM_013519
Foxf1a*	forkhead box F1a	NM_010426	Grhl3	grainyhead-like 3	NM_001013756
Hoxb13*	homeo box B13	NM_008267	Hoxb5	homeo box B5	NM_008268
Hoxb6	homeo box B6	NM_008269	Hoxb8	homeo box B8	NM_010461
Hoxb9	homeo box B9	NM_008270	Id2	inhibitor of DNA binding 2	NM_010496
Id4	inhibitor of DNA binding 4	NM_031166	Klf4	Kruppel-like factor 4 (gut)	NM_010637
Mafb*	v-maf musculoaponeurotic fibrosarcoma oncogene family, protein B	NM_010658	Msx1*	homeobox, msh-like 1	NM_010835
Nfil3	nuclear factor, interleukin 3, regulated	NM_017373	Nr4a3	nuclear receptor subfamily 4, group A, member 3	NM_015743
Pax9	paired box gene 9	NM_011041	Sox9	SRY-box containing gene 9	NM_011448
Spib*	Spi-B transcription factor	NM_019866	Tbx20	T-box 20	NM_194263
Zbtb16*	zinc finger and BTB domain 16	NM_001033324	Zfpm2	zinc finger protein, multitype 2	NM_011766

Appendix B Table B3. Genes involved in neural development and function upregulated by SYT-SSX2 in myoblasts.

Development and Differentiation					
Gene Symbol	**Gene Name**	**Accession**	**Gene Symbol**	**Gene Name**	**Accession**
Barx2	BarH-like homeobox	NM_013800	Bhlhb4	basic helix-loop-helix family, class B4	NM_080641
Bsnd	Bartter syndrome, infantile, with sensorineural deafness	NM_080458	Crim1	cysteine rich transmembrane BMP regulator 1	NM_015800
Dtx1	deltex 1 homolog	NM_008052	Fezf2	Fez family zinc finger 2	NM_080433
Foxd1	forkhead box D1	NM_008242	Gdap1	ganglioside-induced differentiation-associated-protein 1	NM_010267
L1cam	L1 cell adhesion molecule	NM_008478	Lhx1	LIM homeobox protein 1	NM_008498
Lhx2	LIM homeobox protein 2	NM_010710	Lhx5	LIM homeobox protein 5	NM_008499
Nog	noggin	NM_008711	Olig1	oligodendrocyte transcription factor 1	NM_016968
Olig2	oligodendrocyte transcription factor 2	NM_016967	Pou3f1	POU domain, class 3, transcription factor 1	NM_011141
Prox1	prospero-related homeobox 1	NM_008937	Ptpru	protein tyrosine phosphatase, receptor type, U	NM_001083119
Ret	ret proto-oncogene	NM_001080780	Rorb	RAR-related orphan receptor beta	NM_146095
Tcfap2a	transcription factor AP-2, alpha	NM_011547	Timm8a1	translocase of inner mitochondrial membrane 8 homolog a1	NM_013898

Appendix B Table B3 cont'd

Zcchc12	zinc finger, CCHC domain containing 12	NM_028325	Zic2	Zinc finger protein of the cerebellum 2	NM_009574
Patterning and Axon Guidance					
Crmp1	collapsin response mediator protein 1	NM_007765	Dpysl5	Dihydropyrimidin-ase-like 5	NM_023047
Efna3	ephrin A3	NM_010108	Efnb1	ephrin B1	NM_010110
Epha4	Eph receptor A4	NM_007936	Epha8	Eph receptor A8	NM_007939
Ephb1	Eph receptor B1	NM_173447	Gpr56	G protein-coupled receptor 56	NM_018882
Ntng2	netrin G2	NM_133501	Rtn4r	reticulon 4 receptor	NM_022982
Rtn4rl1	reticulon 4 receptor-like 1	NM_177708	Sema6b	semaphorin 6B	NM_013662
Sema7a	semaphorin 7A	NM_011352	Slit3	slit homolog 3	NM_011412
Srgap1	SLIT-ROBO Rho GTPase activating protein 1	NM_001081037	Tspan7	tetraspanin 7	NM_019634
Unc5a	unc-5 homolog A	NM_153131			
Neurotransmitter Signaling and Metabolism					
Abat	4-aminobutyrate aminotransferase	NM_172961	Adra2c	adrenergic receptor	NM_007418
Chrna4	cholinergic receptor	NM_015730	Grik3	glutamate receptor	NM_001081097
Grm4	glutamate receptor	NM_001013385	Kcnip3	Kv channel interacting protein 3, calsenilin	NM_019789
Nptx1	neuronal pentraxin 1	NM_008730	Slc18a3	solute carrier family 18, member 3	NM_021712
Slc6a1	solute carrier family 6, member 1	NM_178703	Slc6a11	solute carrier family 6, member 11	NM_172890
Slc6a12	solute carrier family 6, member 12	NM_133661	Slc6a13	solute carrier family 6, member 13	NM_144512
Syngr3	synaptogyrin 3	NM_011522	Th	tyrosine hydroxylase	NM_009377
Neuropeptide, Lipid, and Hormone Signaling					
Cck	cholecystokinin	NM_031161	Chga	chromogranin A	NM_007693
Crhr1	corticotropin releasing hormone receptor 1	NM_007762	Faah	fatty acid amide hydrolase	NM_010173
Gal	galanin	NM_010253	Gpr50	G protein-coupled receptor 50	NM_010340
Mgll	monoglyceride lipase	NM_011844	Npy	neuropeptide Y	NM_023456
Nrgn	neurogranin	NM_022029	Nts	neurotensin	NM_024435
Ntsr1	neurotensin receptor 1	NM_018766	Nxph4	neurexophilin 4	NM_183297
Pdyn	prodynorphin	NM_018863	Pnoc	prepronociceptin	NM_010932
Sst	somatostatin	NM_009215			
Adhesion, Growth, and Survival					
Amigo2	adhesion molecule with Ig like domain 2	NM_178114	Bai1	brain-specific angiogenesis inhibitor 1	NM_174991
Bai2	brain-specific angiogenesis inhibitor 2	NM_173071	Cadm1	cell adhesion molecule 1	NM_207676
Cdh22	cadherin 22	NM_174988	Cdh23	cadherin 23 (otocadherin)	NM_023370
Cntfr	ciliary neurotrophic factor receptor	NM_016673	Gap43	growth associated protein 43	NM_008083
Gdnf	glial cell derived neurotrophic factor	NM_010275	Gfra1	glial cell derived neurotrophic factor family receptor alpha 1	NM_010279
Gjb2	gap junction membrane channel protein beta 2	NM_008125	Gjb4	gap junction protein, beta 4	NM_008127
Ngf	nerve growth factor	NM_013609	Ngfr	nerve growth factor receptor	NM_033217
Nrcam	neuron-glia-CAM-related cell adhesion molecule	NM_176930			
Other					
Adcy5	adenylate cyclase 5	NM_001012765	Agrn	agrin	NM_021604
Arc	activity regulated cytoskeletal-associated protein	NM_018790	Asrgl1	asparaginase like 1	NM_025610
Brp16	brain protein 16	NM_021555	Cables1	CDK5 and Abl enzyme substrate 1	NM_022021

Appendix B Table B3 cont'd

Cacna1h	calcium channel, voltage-dependent, T type, alpha 1H subunit	NM_021415	Cacng5	calcium channel, voltage-dependent, gamma subunit 5	NM_080644
Camk2n1	calcium/calmodu-lin-dependent protein kinase II inhibitor 1	NM_025451	Camk4	calcium/calmodu-lin-dependent protein kinase IV	NM_009793
Cbln1	cerebellin 1 precursor protein	NM_019626	Cd40	CD40 antigen	NM_170701
Churc1	churchill domain containing 1	NM_206534	Ckb	creatine kinase, brain	NM_021273
Clu	clusterin	NM_013492	Cntn2	contactin 2	NM_177129
Cpeb1	cytoplasmic polyadenylation element binding protein 1	NM_007755	Cpne6	copine VI	NM_009947
Crlf1	cytokine receptor-like factor 1	NM_018827	D11Bwg0517e	DNA segment, Chr 11, Brigham & Women's Genetics 0517 expressed	NM_001039167
Dlgap4	discs, large homolog-associated protein 4	NM_146128	Dok7	docking protein 7	NM_172708
Ecel1	endothelin converting enzyme-like 1	NM_021306	Fjx1	four jointed box 1	NM_010218
Flrt1	fibronectin leucine rich transmembrane protein 1	NM_201411	Gatm	glycine amidinotransfer-ase (L-arginine:glycine amidinotransfer-ase)	NM_025961
Hpcal4	hippocalcin-like 4	NM_174998	Kcna1	potassium voltage-gated channel, shaker-related, subfamily, member 1	NM_010595
Kcnc4	potassium voltage gated channel, Shaw-related subfamily, member 4	NM_145922	Kcnj14	potassium inwardly-rectifying channel, subfamily J, member 14	NM_145963
Kcnma1	potassium large conductance calcium-activated channel, subfamily M, alpha member 1	NM_010610	Kcnn3	potassium intermediate/ small conduc-tance calcium-activated channel, subfamily N, member 3	NM_080466
Kif1a	kinesin family member 1A	NM_008440	Lgi1	leucine-rich repeat LGI family, member 1	NM_020278
Lrrc8d	leucine rich repeat containing 8D	NM_178701	Lrrn3	leucine rich repeat protein 3, neuronal	NM_010733
Mapt	microtubule-associated protein tau	NM_001038609	Mfsd2	major facilitator superfamily domain containing 2A	NM_029662
Mn1	meningioma 1	NM_001081235	Msi1	Musashi homolog 1	NM_008629
Mtap1b	microtubule-associated protein 1B	NM_008634	Myo7a	myosin VIIA	NM_008663
Ndrg1	N-myc downstream regulated gene 1	NM_008681	Nefh	neurofilament, heavy polypeptide	NM_010904
Nefm	neurofilament, medium polypeptide	NM_008691	Ninj1	ninjurin 1	NM_013610
Nos1ap	nitric oxide synthase 1 (neuronal) adaptor protein	NM_027528	Oc90	otoconin 90	NM_010953
Olfm1	olfactomedin 1	NM_019498	Olfr1029	olfactory receptor 1029	NM_001011852
Olfr171	olfactory receptor 171	NM_146958	Olfr172	olfactory receptor 172	NM_147001
Olfr767	olfactory receptor 767	NM_146318	Pcp4	Purkinje cell protein 4	NM_008791
Pde2a	phosphodiester-ase 2A, cGMP-stimulated	NM_001008548	Plxna4	plexin A4	NM_175750
Prph	peripherin	NM_013639	Prps1	phosphoribosyl pyrophosphate synthetase 1	NM_021463
Rcan1	regulator of calcineurin 1	NM_001081549	Rdh10	retinol dehydrogenase 10 (all-trans)	NM_133832
Reep6	receptor accessory protein 6	NM_139292	Rgnef	Rho-guanine nucleotide exchange factor	NM_012026
Rgs16	regulator of G-protein signaling 16	NM_011267	Rgs9	regulator of G-protein signaling 9	NM_011268

Appendix B Table B3 cont'd

Rnd1	Rho family GTPase 1	NM_172612	Rundc3a	RUN domain containing 3A	NM_016759
Serpina3n	serine (or cysteine) peptidase inhibitor, clade A, member 3N	NM_009252	Sez6l	seizure related 6 homolog like	NM_019982
Slc16a6	solute carrier family 16, member 6	NM_001029842	Slc17a7	solute carrier family 17, member 7	NM_182993
Slc1a1	solute carrier family 1, member 1	NM_009199	Spns2	spinster homolog 2	BC025823
Stra6	stimulated by retinoic acid gene 6	NM_009291	Syt12	synaptotagmin XII	NM_134164
Tac1	tachykinin 1	NM_009311	Tnfrsf21	tumor necrosis factor receptor superfamily, member 21	NM_178589
Tnr	tenascin R	NM_022312	Uchl1	ubiquitin carboxy-terminal hydrolase L1	NM_011670
Znrf2	zinc and ring finger 2	NM_199143			

Appendix B Table B4. Genes involved in muscle differentiation and function downregulated by SYT-SSX2 in myoblasts.

Gene Symbol	Gene Name	Accession	Gene Symbol	Gene Name	Accession
Acta1	actin, alpha 1, skeletal muscle	NM_009606	Acta2	actin, alpha 2, smooth muscle, aorta	NM_007392
Actc1	actin, alpha, cardiac	NM_009608	Actn3	actinin alpha 3	NM_013456
Atp2a1	ATPase, Ca++ transporting, cardiac muscle, fast twitch 1	NM_007504	Bgn	biglycan	NM_007542
Bves	blood vessel epicardial substance	NM_024285	Car3	carbonic anhydrase 3	NM_007606
Cdon	cell adhesion molecule-related/down-regulated by oncogenes	NM_021339	Chrna1	cholinergic receptor, nicotinic, alpha polypeptide 1 (muscle)	NM_007389
Chrnd	cholinergic receptor, nicotinic, delta polypeptide	NM_021600	Chrng	cholinergic receptor, nicotinic, gamma polypeptide	NM_009604
Col6a1	procollagen, type VI, alpha 1	NM_009933	Col6a2	procollagen, type VI, alpha 2	NM_146007
Col6a3	procollagen, type VI, alpha 3, mRNA	BC057903	Des	desmin	NM_010043
Dmpk	dystrophia myotonica-protein kinase	NM_032418	Dtna	dystrobrevin alpha	NM_207650
Ehd2	EH-domain containing 2	NM_153068	Eno3	enolase 3, beta muscle	NM_007933
Fbxo32	F-box protein 32	NM_026346	Fhl1	four and a half LIM domains 1	NM_001077361
Itga7	integrin alpha 7	NM_008398	Ldb3	LIM domain binding 3	NM_001039074
Mustn1	hypothetical protein (ORF1) clone Telethon(Italy_B41)_Strait 03708_FL626	AJ277212	Myf5	myogenic factor 5	NM_008656
Myl1	myosin, light polypeptide 1	NM_021285	Myl4	myosin, light polypeptide 4	NM_010858
Myl9	myosin, light polypeptide 9, regulatory	BC055439	Mylk	myosin, light polypeptide kinase	NM_139300
Mylpf	myosin light chain, phosphorylatable, fast skeletal muscle	NM_016754	Myod1	myogenic differentiation 1	NM_010866
Myog	myogenin	NM_031189	P2rx6	purinergic receptor P2X, ligand-gated ion channel, 6	NM_011028
Pdlim3	PDZ and LIM domain 3	NM_016798	Popdc3	popeye domain containing 3	NM_024286
Prrx1	paired related homeobox 1	NM_175686	Sgca	sarcoglycan, alpha (dystrophin-associated glycoprotein)	NM_009161

Appendix B Table B4 cont'd

Sgcb	sarcoglycan, beta (dystrophin-associated glycoprotein)	NM_011890	Sgcd	sarcoglycan, delta (dystrophin-associated glycoprotein)	NM_011891
Sgcg	sarcoglycan, gamma (dystrophin-associated glycoprotein)	ENSMUST00000077954	Six4	sine oculis-related homeobox 4 homolog (Drosophila)	NM_011382
Speg	SPEG complex locus	NM_007463	Sspn	sarcospan	NM_010656
Sync	syncoilin	NM_023485	Tnnc1	troponin C, cardiac/slow skeletal	NM_009393
Tnni1	troponin I, skeletal, slow 1	NM_021467	Tnnt1	troponin T1, skeletal, slow	NM_011618
Tnnt3	troponin T3, skeletal, fast	NM_011620	Ttn	titin	NM_011652
Unc93b1	unc-93 homolog B1 (C. elegans)	NM_019449	Boc	biregional cell adhesion molecule-related/down-regulated by oncogenes (Cdon) binding protein	NM_172506

Appendix B Table B5. Genes involved in bone formation upregulated by SYT-SSX2 in human mesenchymal stem cells.

Gene Symbol	Gene Name	Accession	Gene Symbol	Gene Name	Accession
ALPL	alkaline phosphatase	NM_000478	BMP2	bone morphogenetic protein 2	NM_001200
BMP6	bone morphogenetic protein 6	NM_001718	COMP	cartilage oligomeric matrix protein	NM_000095
CRTAC1	cartilage acidic protein	NM_018058	FGFR3	fibroblast growth factor receptor 3	NM_000142
HOXD1	homeobox D1	NM_024501	HOXD10	homeobox D10	NM_002148
IGSF10	immunoglobulin superfamily, member 10	NM_178822	LIFR	leukemia inhibitory factor receptor	NM_002310
MGP	matrix Gla protein	NM_000900	OSR2	odd-skipped related 2	NM_053001
ROR2	receptor tyrosine kinase – like 2	NM_004560	TNS4	tensin 4	NM_032865

Appendix B Table B6. Differentially regulated genes in C2C12 myoblasts and hMSCs expressing SYT-SSX2.
Underlined genes are downregulated in both C2C12 myoblasts and hMSCs expressing SYT-SSX2.

Gene Symbol	Gene Name	Accession	Gene Symbol	Gene Name	Accession
Adhesion, Migration, and ECM					
Arhgap20	Rho GTPase activating protein 20	NM_175535	Ceacam1	carcinoembryonic antigen-related cell adhesion molecule 1	NM_011926
Cldn1	claudin 1	NM_016674	Col4a1	collagen, type IV, alpha I	NM_009931
Crispld2	cysteine-rich secretory protein LCCL domain containing 2	NM_030209	Flrt3	fibronectin leucine rich transmembrane protein 3	NM_178382
Icam1	intercellular adhesion molecule 1	NM_010493	Iqgap2	IQ motif containing GTPase activating protein 2	NM_027711
Itga9	integrin alpha 9	NM_133721	Krt17	keratin 17	NM_010663
Krt6a	keratin 6a	NM_008476	Mmp10	matrix metallopeptidase 10	NM_019471
Rhou	ras homolog gene family, member U	NM_133955	Scube1	signal peptide, CUB domain, EGF-like 1	NM_022723
Tnxb	tenascin XB	NM_031176	Arhgap18	Rho GTPase activating protein 18	NM_176837
Ccbe1	collagen and calcium binding EGF domains 1	NM_178793	Ccdc80	coiled-coil domain containing 80	NM_026439
Dcn	decorin	NM_007833	Dlc1	deleted in liver cancer 1	NM_015802

Appendix B Table B6 cont'd

Fap	fibroblast activation protein	NM_007986	Hspb6	heat shock protein, alpha-crystallin-related, B6	NM_001012401
Itgb8	integrin beta 8	NM_177290	Loxl1	lysyl oxidase-like 1	NM_010729
Mfap5	microfibrillar associated protein 5	ENSMUST00000032210	Mmp19	matrix metallopeptidase 19	NM_021412
Nid1	nidogen 1	NM_010917	Pcdh18	protocadherin 18	NM_130448
Postn	periostin, osteoblast specific factor	NM_015784	Tenc1	tensin like C1 domain containing phosphatase	NM_153533
Developmental Pathway Mediators: Wnt					
Apcdd1	adenomatosis polyposis coli down-regulated 1	NM_133237	Axin2	Axin 2	NM_015732
Dact1	dapper homolog 1, antagonist of beta-catenin	NM_021532	Fzd3	frizzled homolog 3	NM_021458
Tle3	transducin-like enhancer of split 3	NM_001083927	Wnt11	wingless-related MMTV integration site 11	NM_009519
Wnt4	wingless-related MMTV integration site 4	NM_009523	Wnt7b	wingless-related MMTV integration site 7B	NM_009528
Fzd2	frizzled homolog 2	NM_020510			
Developmental Pathway Mediators: Notch					
Dll1	delta-like 1	NM_007865	Hes1	hairy and enhancer of split 1	NM_008235
Nrarp	Notch-regulated ankyrin repeat protein	NM_025980			
Developmental Pathway Mediators: TGFβ/BMP					
Gdf6	growth differentiation factor 6	NM_013526	Smad6	MAD homolog 6	NM_008542
Tgfbr2	transforming growth factor, beta receptor II	NM_009371			
Developmental Pathway Mediators: Shh					
Ptch1	patched homolog 1	NM_008957	Shh	sonic hedgehog	NM_009170
Developmental Pathway Mediators: FGF					
Fgf9	fibroblast growth factor 9	NM_013518	Fgfr2	fibroblast growth factor receptor 2	NM_010207
Fgfr3	fibroblast growth factor receptor 3	NM_008010	Shisa2	shisa homolog 2	NM_145463
Developmental Pathway Mediators: PDGF					
Pdgfc	platelet-derived growth factor, C	NM_019971	Pdgfra	platelet-derived growth factor receptor, alpha polypeptide	NM_011058
Developmental Pathway Mediators: Other					
Adssl1	adenylosuccinate synthetase like 1	NM_007421	Alpl	alkaline phosphatase	NM_007431
Calcr	calcitonin receptor	NM_007588	Flt4	FMS-like tyrosine kinase 4	NM_008029
Fstl4	follistatin-like 4	NM_177059	Igf2	insulin-like growth factor 2	NM_010514
Kcng1	potassium voltage-gated channel, subfamily G, member 1	NM_001081134	Kdr	kinase insert domain protein receptor	NM_010612
Laptm	lysosomal protein transmembrane 5	NM_010686	Sik1	salt inducible kinase 1	NM_010831
Angpt1	angiopoietin 1	NM_009640	Aspn	asporin	NM_025711
Emilin 1	elastin microfibril interfacer 1	NM_133918	Mylk	myosin, light polypeptide kinase	NM_139300
Popdc3	popeye domain containing 3	NM_024286	Sgcd	sarcoglycan, delta	NM_011891
Sync	syncoilin	NM_023485			
Developmental Transcription Factors					
Creb5	cAMP responsive element binding protein 5	NM_172728	Dlx3	distal-less homeobox 3	NM_010055
Etv4	ets variant 4	NM_008815	Grhl3	grainyhead-like 3	NM_001013756

Appendix B Table B6 cont'd

Hoxb6	homeo box B6	NM_008269	Hoxb9	homeo box B9	NM_008270
Lbh	limb bud and heart development	NM_029999	Mafb	v-maf musculoaponeurotic fibrosarcoma oncogene family, protein B	NM_010658
Nr4a3	nuclear receptor subfamily 4, group A, member 3	NM_015743	Tbx20	T-box 20	NM_194263
Bnc2	basonuclin 2	NM_172870			
Metabolism					
Ak4	adenylate kinase 4	NM_009647	Alox15	arachidonate 15-lipoxygenase	NM_009660
Atp1a3	ATPase, Na+/K+ transporting, alpha 3 polypeptide	NM_144921	Bcor	BCL6 interacting corepressor	NM_175045
Chd7	chromodomain helicase DNA binding protein 7	NM_001081417	Chi3l1	chitinase 3-like 1	NM_007695
Cnih2	cornichon homolog 2	NM_009920	Cyp26b1	cytochrome P450, family 26, subfamily b, polypeptide 1	NM_175475
Egr2	early growth response 2	NM_010118	Elovl7	ELOVL family member 7, elongation of long chain fatty acids	NM_029001
Fgg	fibrinogen gamma chain	NM_133862	Gfpt2	glutamine fructose-6-phosphate transaminase 2	NM_013529
Irf4	interferon regulatory factor 4	NM_013674	Mgat4a	mannoside acetylglucosaminyltransferase 4, isoenzyme A	NM_173870
Rnf125	ring finger protein 125	NM_026301	Slc38a3	solute carrier family 38, member 3	NM_023805
Strbp	spermatid perinuclear RNA binding protein	NM_009261	Anpep	alanyl (membrane) aminopeptidase	NM_008486
Dpyd	dihydropyrimidine dehydrogenase	NM_170778	Glrx	glutaredoxin	NM_053108
Mgst1	microsomal glutathione S-transferase 1	NM_019946	Mme	membrane metallo endopeptidase	NM_008604
Nqo1	NAD(P)H dehydrogenase, quinone 1	NM_008706	Nucb2	nucleobindin 2	NM_016773
Pdk4	pyruvate dehydrogenase kinase, isoenzyme 4	NM_013743	Ptgs1	prostaglandin-endoperoxide synthase 1	NM_008969
Ptgs2	prostaglandin-endoperoxide synthase 2	NM_011198	Slc44a1	solute carrier family 44, member 1	AK141895
Slc8a1	solute carrier family 8 (sodium/calcium exchanger), member 1	NM_011406	Sqrdl	sulfide quinone reductase-like	NM_021507
Ssbp2	single-stranded DNA binding protein 2	NM_024272			
Neural Development and Function: Development and Differentiation					
Dtx1	deltex 1 homolog	NM_008052	L1cam	L1 cell adhesion molecule	NM_008478
Lhx1	LIM homeobox protein 1	NM_008498	Lhx2	LIM homeobox protein 2	NM_010710
Lhx5	LIM homeobox protein 5	NM_008499	Nog	noggin	NM_008711
Prox1	prospero-related homeobox 1	NM_008937	Ptpru	protein tyrosine phosphatase, receptor type, U	NM_001083119
Ret	ret proto-oncogene	NM_001080780	Rorb	RAR-related orphan receptor beta	NM_146095
Zcchc12	zinc finger, CCHC domain containing 12	NM_028325	Gpr126	G protein-coupled receptor 126	NM_001002268

Appendix B Table B6 cont'd

Neural Development and Function: Patterning and Axon Guidance					
Crmp1	collapsin response mediator protein 1	NM_007765	Dpysl5	Dihydropyrimidin-ase-like 5	NM_023047
Efna3	ephrin A3	NM_010108	Efnb1	ephrin B1	NM_010110
Epha4	Eph receptor A4	NM_007936	Ephb1	Eph receptor B1	NM_173447
Gpr56	G protein-coupled receptor 56	NM_018882	Ntng2	netrin G2	NM_133501
Sema6b	semaphorin 6B	NM_013662	Slit3	slit homolog 3	NM_011412
Tspan7	tetraspanin 7	NM_019634	Unc5a	unc-5 homolog A	NM_153131
Sema3a	sema domain, immunoglobulin domain (Ig), short basic domain, secreted, (semaphorin) 3A	NM_009152			
Neural Development and Function: Neurotransmitter Signaling and Metabolism					
Abat	4-aminobutyrate aminotransferase	NM_172961	Chrna4	cholinergic receptor	NM_015730
Grik3	glutamate receptor	NM_001081097	Grm4	glutamate receptor	NM_001013385
Slc18a3	solute carrier family 18, member 3	NM_021712	Slc6a1	solute carrier family 6, member 1	NM_178703
Syngr3	synaptogyrin 3	NM_011522	Glrb	glycine receptor beta	NM_010298
Neural Development and Function: Neuropeptide, Lipid, and Hormone Signaling					
Chga	chromogranin A	NM_007693	Crhr1	corticotropin releasing hormone receptor 1	NM_007762
Gal	galanin	NM_010253	Gpr50	G protein-coupled receptor 50	NM_010340
Npy	neuropeptide Y	NM_023456	Nts	neurotensin	NM_024435
Ntsr1	neurotensin receptor 1	NM_018766	Nxph4	neurexophilin 4	NM_183297
Pnoc	prepronociceptin	NM_010932	Sst	somatostatin	NM_009215
Mrgprf	MAS-related GPR, member F	NM_145379			
Neural Development and Function: Adhesion, Growth, and Survival					
Bai1	brain-specific angiogenesis inhibitor 1	NM_174991	Bai2	brain-specific angiogenesis inhibitor 2	NM_173071
Cadm1	cell adhesion molecule 1	NM_207676	Cdh23	cadherin 23 (otocadherin)	NM_023370
Cntfr	ciliary neurotrophic factor receptor	NM_016673	Gfra1	glial cell derived neurotrophic factor family receptor alpha 1	NM_010279
Gjb2	gap junction membrane channel protein beta 2	NM_008125	Ngfr	nerve growth factor receptor	NM_033217
Nrcam	neuron-glia-CAM-related cell adhesion molecule	NM_176930	Drp2	dystrophin related protein 2	NM_010078
Neural Development and Function: Other					
Adcy5	adenylate cyclase 5	NM_001012765	Cacna1h	calcium channel, voltage-dependent, T type, alpha 1H subunit	NM_021415
Camk2n1	calcium/calmodu-lin-dependent protein kinase II inhibitor 1	NM_025451	Cbln1	cerebellin 1 precursor protein	NM_019626
Ckb	creatine kinase, brain	NM_021273	Clu	clusterin	NM_013492
Crlf1	cytokine receptor-like factor 1	NM_018827	Ecel1	endothelin converting enzyme-like 1	NM_021306
Flrt1	fibronectin leucine rich transmembrane protein 1	NM_201411	Gatm	glycine amidinotransfer-ase (L-arginine:glycine amidinotransfer-ase)	NM_025961
Hpcal4	hippocalcin-like 4	NM_174998	Kcnn3	potassium intermediate/ small conduc-tance calcium-activated channel, subfamily N, member 3	NM_080466

Appendix B Table B6 cont'd

Kif1a	kinesin family member 1A	NM_008440	Mapt	microtubule-associated protein tau	NM_001038609
Nefh	neurofilament, heavy polypeptide	NM_010904	Nefm	neurofilament, medium polypeptide	NM_008691
Olfm1	olfactomedin 1	NM_019498	Pde2a	phosphodiester-ase 2A, cGMP-stimulated	NM_001008548
Rdh10	retinol dehydrogenase 10 (all-trans)	NM_133832	Reep6	receptor accessory protein 6	NM_139292
Rgs16	regulator of G-protein signaling 16	NM_011267	Sez6l	seizure related 6 homolog like	NM_019982
Slc16a6	solute carrier family 16, member 6	NM_001029842	Slc17a7	solute carrier family 17, member 7	NM_182993
Spns2	spinster homolog 2	BC025823	Stra6	stimulated by retinoic acid gene 6	NM_009291
Tnfrsf21	tumor necrosis factor receptor superfamily, member 21	NM_178589	Plcb4	phospholipase C, beta 4	NM_013829
Srpx2	sushi-repeat-containing protein, X-linked 2	NM_026838	Tiam2	T-cell lymphoma invasion and metastasis 2	NM_011878
Signaling and Cell Cycle					
Atp2b2	ATPase, Ca++ transporting, plasma membrane 2	NM_001036684	C3	complement component 3	NM_009778
Cacna1g	calcium channel, voltage-dependent, T type, alpha 1G subunit	NM_009783	Cacna2d 2	calcium channel, voltage-dependent, alpha 2/delta subunit 2	NM_020263
Ccl2	chemokine (C-C motif) ligand 2	NM_011333	Ccl20	chemokine (C-C motif) ligand 20	NM_016960
Ccl7	chemokine (C-C motif) ligand 7	NM_013654	Ccnd2	cyclin D2	NM_009829
Cx3cl1	chemokine (C-X3-C motif) ligand 1	NM_009142	Cxcl1	chemokine (C-X-C motif) ligand 1	NM_008176
Cxcl14	chemokine (C-X-C motif) ligand 14	NM_019568	Cxcr4	chemokine (C-X-C motif) receptor 4	NM_009911
Cyfip2	cytoplasmic FMR1 interacting protein 2	NM_133769	Dapk1	death associated protein kinase 1	NM_029653
Errfi1	ERBB receptor feedback inhibitor 1	NM_133753	Gpr120	G-protein coupled receptor 120	NM_181748
Gucy1a3	guanylate cyclase 1, soluble, alpha 3	NM_021896	Lgr5	leucine rich repeat containing G protein coupled receptor 5	NM_010195
Lrp8	low density lipoprotein receptor-related protein 8, apolipoprotein e receptor	NM_053073	Lyn	Yamaguchi sarcoma viral (v-yes-1) oncogene homolog	NM_010747
Peg10	paternally expressed 10	NM_130877	Peli1	pellino 1	NM_023324
Ppp2r2c	protein phosphatase 2 (formerly 2A), regulatory subunit B (PR 52), gamma isoform	NM_172994	Prkch	protein kinase C, eta	NM_008856
Ptprn	protein tyrosine phosphatase, receptor type, N	NM_008985	Pyy	peptide YY	NM_145435
Rap1gap	Rap1 GTPase-activating protein	NM_001081155	Rgs5	regulator of G-protein signaling 5	ENSMUST00000 027997
Sgk1	serum/glucocorticoid regulated kinase 1	NM_011361	Slc9a3	solute carrier family 9 (sodium/hydrogen exchanger), member 3	NM_001081060
Slco4a1	solute carrier organic anion transporter family, member 4a1	NM_148933	Stxbp2	syntaxin binding protein 2	NM_011503
C1s	complement component 1, s subcomponent	NM_144938	Cfh	complement component factor h	NM_009888

Appendix B Table B6 cont'd

Copz2	coatomer protein complex, subunit zeta 2	NM_019877	Dab2	disabled homolog 2	NM_023118
Dock5	dedicator of cytokinesis 5	NM_177780	Gulp1	GULP, engulfment adaptor PTB domain containing 1	NM_027506
Npr3	natriuretic peptide receptor 3	NM_001039181	Psd3	pleckstrin and Sec7 domain containing 3	NM_177698
Rab27b	RAB27b, member RAS oncogene family	NM_001082553	Rgs4	regulator of G-protein signaling 4	NM_009062
Srpx	sushi-repeat-containing protein	NM_016911	Synj2	synaptojanin 2	NM_011523
Other					
Lonrf3	LON peptidase N-terminal domain and ring finger 3	NM_028894	Megf11	multiple EGF-like-domains 11	NM_172522
Sipa1l2	signal-induced proliferation-associated 1 like 2	NM_001081337	Slc35f2	solute carrier family 35, member F2	NM_028060
Tmcc3	transmembrane and coiled coil domains 3	NM_172051	Tmem132e	transmembrane protein 132E	NM_023438
Tmem63c	transmembrane protein 63c	NM_172583	Tspan18	tetraspanin 18	NM_183180
Dsel	dermatan sulfate epimerase-like	NM_001081316	Gramd1b	GRAM domain containing 1B	NM_172768
Lmo7	LIM domain only 7	NM_201529	Tmem119	transmembrane protein 119	ENSMUST00000067853

REFERENCES

Abollo-Jiménez F, Jimenez R, Cobaleda C. (2010). “Physiological cellular reprogramming and cancer.” *Semin Cancer Biol* **20:** 98-106.

Agger K, Cloos PAC, Christensen J, Pasini D, Rose S, Rappsilber J, Issaeva I, Canaani E, Salcini AE, Helin K. (2007). “UTX and JMJD3 are histone H3K27 demethylases involved in *HOX* gene regulation and development.” *Nature* **doi:** 10.1038/nature06145.

Alfaro MP, Pagni M, Vincent A, Atkinson J, Hill MF, Cates J, Davidson JM, Rottman J, Lee E, Young PP. (2008). “The Wnt modulator sFRP2 enhances mesenchymal stem cell engraftment, granulation tissue formation and myocardial repair.” *Proc Natl Acad Sci USA* **105**:18366-71.

Allander SV, Illei PB, Chen Y, Antonescu CR, Bittner M, Ladanyi M, Meltzer PS. (2002). “Expression profiling of synovial sarcoma by cDNA microarrays: association of ERBB2, IGFBP2, and ELF3 with epithelial differentiation.” *Am J Pathol* **161:** 1587-95.

Asp P, Blum R, Vethantham V, Parisi F, Micsinai M, Cheng J, Bowman C, Kluger Y, Dynlacht BD. (2011). “Genome-wide remodeling of the epigenetic landscape during myogenic differentiation.” *Proc Natl Acad Sci USA* **108**:E149-58.

Bailey TL and Elkan C. (1994). “Fitting a mixture model by expectation maximization to discover motifs in biopolymers.” *Proc Int Conf Intell Syst Mol Biol* **2:** 28-36.

Bannister AJ and Kouzarides T. (2011). “Regulation of chromatin by histone modifications.” *Cell Res* **21:** 381-95.

Barco R, Garcia CB, Eid JE. (2009). “The synovial sarcoma-associated SYTSSX2 oncogene antagonizes the Polycomb complex protein Bmi1.” *PLoS One* **4:** e5060. **doi:**10.1371/journal.pone.0005060.

Barco R, Hunt LB, Frump AL, Garcia CB, Benesh A, Caldwell RL, Eid JE. (2007). “The synovial sarcoma SYT-SSX2 oncogene remodels the cytoskeleton through activation of the ephrin pathway.” *Mol Biol Cell* **18:** 4003-12.

Blankenberg D, Von Kuster G, Coraor N, Ananda G, Lazarus R, Mangan M, Nekrutenko A, Taylor J. (2010). “Galaxy: a web-based genome analysis tool for experimentalists.” in *Curr Protoc Mol Biol*, ed Ausubel F (Wiley-Interscience, New York), Chapter 19: Unit 19.10.1-21.

Ben-Saadon R, Zaaroor D, Ziv T, Ciechanover A. (2008). “The Polycomb protein Ring1B generates self atypical mixed ubiquitin chains required for its in vitro histone H2A ligase activity.” *Mol Cell* **24:** 701-11.

Boyer LA, Lee TI, Cole MF, Johnstone SE, Levine SS, Zucker JP, Guenther MG, Kumar RM, Murray HL, Jenner RG, Gifford DK, Melton DA, Jaenisch R, Young RA. (2005). “Core transcriptional regulatory circuitry in human embryonic stem cells.” *Cell* **122:** 947-56.

Bozzi F, Ferrari A, Negri T, Conca E, L DR, Losa M, Casieri P, Orsenigo M, Lampis A, Meazza C, Casanova M, Pierotti MA, Tamborini E, Pilotti S. (2008). “Molecular characterization of synovial sarcoma in children and adolescents: evidence of Akt activation.” *Transl Oncol* **1:** 95-101.

Brett D, Whitehouse S, Antonson P, Shipley J, Cooper C, Goodwin G. (1997). “The SYT protein involved in the t(X;18) synovial sarcoma translocation is a transcriptional activator localized in nuclear bodies.” *Hum Mol Genet* **6:** 1559-64.

Brodin B, Haslam K, Yang K, Bartolazzi A, Xie Y, Starborg, M, Lundeberg J, Larsson O. (2001). “Cloning and characterization of spliced fusion transcript variants of synvial sarcoma: SYT/SSX4, SYT/SSX4v, and SYT/SSX2v. Possible regulatory role of the fusion gene product in wild type SYT expression.” *Gene* **268:** 173-82.

Brown MV, Burnett PE, Denning MF, Reynolds AB. (2009). “PDGF receptor activation induces p120-catenin phosphorylation at serine 879 via a PKCalpha-dependent pathway.” *Exp Cell Res* **315:** 39-49.

Cao L, Yu Y, Bilke S, Walker RL, Mayeenuddin LH, Azorsa DO, Yang F, Pineda M, Helman LJ, Meltzer PS. (2010). “Genome-wide identification of PAX3-FKHR binding sites in rhabdomyosarcoma reveals candidate target genes important for development and cancer.” *Cancer Res* **70:**6497-508.

Cao R, Tsukada Y, Zhang Y. (2005). “Role of Bmi1 and Ring1A in H2A ubiquitylation and Hox gene silencing.” *Mol Cell* **20:** 845-54.

Cao Y, Yao Z, Sarkar D, Lawrence M, Sanchez GJ, Parker MH, MacQuarrie KL, Davison J, Morgan MT, Ruzzo WL, Gentleman RC, Tapscott SJ. (2010). “Genome-wide MyoD binding in skeletal muscle cells: a potential for broad cellular reprogramming.” *Dev Cell* **18:**662-74.

Castellanos A, Vicente-Dueñas C, Campos-Sánchez E, Cruz JJ, García-Criado FJ, García-Cenador MB, Lazo PA, Pérez-Losada J, Sánchez-García I. (2010). “Cancer as a reprogramming-like disease: implications in tumor development and treatment.” *Semin Cancer Biol* **20**:93-7.

Chadashvili T and Peterson DA. (2006). “Cytoarchitecture of fibroblast growth factor receptor 2 (FGFR-2) immunoreactivity in astrocytes of neurogenic and non-neurogenic regions of the young adult and aged rat brain.” *J Comp Neurol* **498:** 1-15.

Charytonowicz E, Cordon-Cardo C, Matushansky I, Ziman M. (2009). “Alveolar rhabdomyosarcoma: is the cell of origin a mesenchymal stem cell?” *Cancer Lett* **279**:126-36.

Chen Y, Teng FYH, Tang BL. (2006). “Coaxing bone marrow stromal mesenchymal stem cells towards neuronal differentiation: progress and uncertainties.” *Cell Mol Life Sci* **63:** 1649-57.

Chittezhath M, Frump AL, Jourquin J, Lobdell N, Eid JE. (2008). “The proto-oncoprotein SYT (SS18) controls ATP release and regulates cyst formation by polarized MDCK cells.” *Exp Cell Res* **314:** 3551-62.

Cironi L, Prover P, Riggi N, Janiszewska M, Suva D, Suva M-L, Kindler V, Stamenkovic J. (2009). “Epigenetic features of human mesenchymal stem cells determine their permissiveness for induction of relevant transcriptional changes by SYT-SSX1.” *PLoS One* **4:** e7904. **doi:** 10.1371/journal.pone.0007904.

Clark J, Rocques PJ, Crew AJ, Gill S, Shipley J, Chan AM-L, Gusterson BA, Cooper CS. (1994). “Identification of novel genes, *SYT* and *SSX*, involved in the t(X;18)(p11.2;q11.2) translocation found in human synovial sarcoma.” *Nat Genet* **7:** 502-8.

Colter DC, Sekiya I, Prockop DJ. (2001). “Identification of a subpopulation of rapidly self-renewing and multipotential adult stem cells in colonies of human marrow stromal cells.” *Proc Natl Acad Sci USA* **98**:7841-5.

Crew AJ, Clark J, Fisher C, Gill S, Grimer R, Chand A, Shipley J, Gusterson BA, Cooper CS. (1995). “Fusion of *SYT* to two genes, *SSX1* and *SSX2* encoding proteins with homology to the Kruppel-associated box in human synovial sarcoma.” *EMBO J* **14:** 2333-40.

de Bie P, Zaaroor-Regev D, Ciechanover A. (2010). “Regulation of the Polycomb protein Ring1B ubiquitination by USP7.” *Biochem Biophys Res Commun* **400:** 389-95.

de Bruijn DR, Allander SV, van Dijk AHA, Willemse MP, Thijssen J, van Groningen JJM, Meltzer PS, Geurts van Kessel A. (2006a). “The synovial sarcoma-associated SS18-SSX2 fusion protein induces epigenetic gene (de)regulation.” *Cancer Res* **66:** 9474-82.

de Bruijn DR, Baats E, Zechner U, de Leeuw B, Balemans M, Olde Weghuis D, Hirning-Folz U, Geurts van Kessel A. (1996). “Isolation and characterization of the mouse homolog of *SYT*, a gene implicated in the development of human synovial sarcomas.” *Oncogene* **13:** 643-8.

de Bruijn DR, dos Santos NR, Kater-Baats E, Thijssen J, van den Berk L, Stap J, Balemans M, Schepens M, Merkx G, Geurts van Kessel A. (2002). “The cancer-related protein SSX2 interacts with the human homologue of a Ras-like GTPase interactor, RAB3IP, and a novel nuclear protein, SSX2IP.” *Genes Chromosomes Cancer* **34:** 285-98.

de Bruijn DR, dos Santos NR, Thijssen J, Balemans M, Debernardi S, Linder B, Young BD, Geurts van Kessel A. (2001). “The synovial sarcoma associated protein SYT interacts with the acute leukemia associated protein AF10.” *Oncogene* **20:** 3281-89.

de Bruijn DR, Peters WJM, Chuva de Sousa Lopes SM, van Dijk AHA, Willemse MP, Pfundt R, de Boer P, Geurts van Kessel A. (2006b). “Targeted disruption of the synovial sarcoma-associated *SS18* gene causes early embryonic lethality and affects *PPARBP* expression.” *Hum Mol Genet* **15:** 2936-44.

de Bruijn DR, van Dijk AHA, Willemse MP, Geurts van Kessel A. (2008). “The C terminus of the synovial sarcoma-associated SSX proteins interacts with the LIM homeobox protein LHX4.” *Oncogene* **27:** 653-62.

de Hoon MJL, Imoto S, Nolan J, Miyano S. (2004). “Open source clustering software.” *Bioinformatics* **20:** 1453-4.

dos Santos NR, de Bruijn DR, Balemans M, Janssen B, Gärtner F, Lopes JM, deLeeuw B, Geurts van Kessel A. (1999). “Nuclear localization of SYT, SSX, and the synovial sarcoma-associated SYT-SSX fusion proteins.” *Hum Mol Genet* **6:** 1549-58.

dos Santos NR, de Bruijn DR, Geurts van Kessel A. (2001). “Molecular mechanisms underlying human synovial sarcoma development.” *Genes Chromosomes Cancer* **30:** 1-14.

dos Santos NR, de Bruijn DR, Kater-Baats E, Otte AP, Geurts van Kessel A. (2000). “Delineation of the protein domains responsible for SYT, SSX, and SYT-SSX nuclear localization.” *Exp Cell Res* **256:** 192-202.

Drewell RA, Arney KL, Arima T, Barton SC, Brenton JD, Surani MA. (2002). “Novel conserved elements upstream of the H19 gene are transcribed and act as mesodermal enhancers.” *Development* **129:** 1205-13.

Edgar R, Domrachev M, Lash AE. (2002). “Gene Expression Omnibus: NCBI gene expression and hybridization array data repository.” *Nucleic Acids Res* **30:** 207-10.

Eid JE, Kung AL, Scully R, Livingston DM. (2000). “p300 interacts with the nuclear proto-oncoprotein SYT as part of the active control of cell adhesion.” *Cell* **102:** 839-48.

Elderkin S, Maertens GN, Endoh M, Mallery DL, Morrice N, Koseki H, Peters G, Brockdorff N, Hiom K. (2007). “A phosphorylated form of Mel-18 targets the Ring1B histone H2A ubiquitin ligase to chromatin.” *Mol Cell* **28:** 107-20.

Ever L and Gaiano N. (2005). “Radial 'glial' progenitors: neurogenesis and signaling.” *Curr Opin Neurobiol* **15:** 29-33.

Farnham PJ. (2009). “Insights from genomic profiling of transcription factors.” *Nat Rev Genet* **10**:605-16.

Feldman AT and Dapson RW. (1974). “Relative effectiveness of various solvents for Oil Red O.” *Med Lab Technol* **31:** 335-41.

Frietze S and Farnham PJ. (2011). “Transcription factor effector domains.” in *A Handbook of Transcription Factors, Subcell Biochem*, ed Hughes TR. (Springer) **52:** 261-77 **doi:** 10.1007/978-90-481-0_12.

Fujita PA, Rhead B, Zweig AS, Hinrichs AS, Karolchik D, Cline MS, Goldman M, Barber GP, Clawson H, Coelho A, Diekhans M, Dreszer TR, Giardine BM, Harte RA, Hillman-Jackson J, Hsu F, Kirkup V, Kuhn RM, Learned K, Li CH, Meyer LR, Pohl A, Raney BJ, Rosenbloom KR, Smith KE, Haussler D, Kent WJ. (2010). “The UCSC genome browser database: update 2011.” *Nucleic Acids Res* doi: 10.1093/nar/gkq963.

Fukukawa C, Nagayama S, Tsunoda T, Toguchida J, Nakamura Y, Katagiri T. (2009). “Activation of the non-canonical Dvl-Rac1-JNK pathway by Frizzled homologue 10 in human synovial sarcoma.” *Oncogene* **28:** 1110-20.

Gaspar-Maia A, Alajem A, Meshorer E, Ramalho-Santos M. (2011). “Open chromatin in pluripotency and reprogramming.” *Nature Rev Mol Cell Biol* **12:** 36-47.

Giardine B, Riemer C, Hardison RC, Burhans R, Elnitski L, Shah P, Zhang Y, Blankenberg D, Albert I, Taylor J, Miller W, Kent WJ, Nekrutenko A. (2005). "Galaxy: a platform for interactive large-scale genome analysis." *Genome Res* **15:**1451-5.

Goecks, J, Nekrutenko, A, Taylor, J and The Galaxy Team. (2010). “Galaxy: a comprehensive approach for supporting accessible, reproducible, and transparent computational research in the life sciences.” *Genome Biol* **11:**R86.

Gupta S, Stamatoyannopolous JA, Bailey T, Noble WS. (2007). “Quantifying similarity between motifs.” *Genome Biol* **8:** R24 **doi:**10.1186/gb-2007-8-2-r24.

Gurdon JB and Melton DA. (2008). “Nuclear reprogramming in cells.” *Science* **322**:1811-5.

Gu W and Roeder RG. (1997). “Activation of p53 sequence-specific DNA binding by acetylation of the p53 C-terminal domain.” *Cell* **90:** 595-606.

Güre AO, Wei IJ, Old LJ, Chen Y-T. (2002). “The *SSX* gene family: characterization of 9 complete genes.” *Int J Cancer* **101:** 448-53.

Haldar M, Hancock JD, Coffin CM, Lessnick SL, Capecchi MR. (2007). “A conditional mouse model of synovial sarcoma: insights into a myogenic origin.” *Cancer Cell* **11:** 375-88.

Haldar M, Hedberg ML, Hockin MF, Capecchi MR. (2009). “A CreER-based random induction strategy for modeling translocation-associated sarcomas in mice.” *Cancer Res* **69:** 3657-64.

Haldar M, Randall RL, Capecchi MR. (2008). “Synovial sarcoma: from genetics to genetic-based animal modeling.” *Clin Orthop Relat Res* **doi:** 10.1007/s11999-008-0340-2.

Henikoff S and Shilatifard A. (2011). “Histone modification: cause or cog?” *Trends Genet* **27:** 389-96.

Hernández-Muñoz I, Lund AH, van der Stoop P, Boutsma E, Muijrers I, Verhoeven E, Nusinow DA, Panning B, Marahrens Y, van Lohuizen M. (2005). “Stable X chromosome inactivation involves the PRC1 Polycomb complex and requires histone MACROH2A1 and the CULLIN3/SPOP ubiquitin E3 ligase.” *Proc Natl Acad Sci USA* **102:** 7635-40.

Ho L, Miller EL, Ronan JL, Ho WQ, Jothi R, Crabtree GR. (2011). “esBAF facilitates pluripotency for LIF/STAT3 signalling and by regulating polycomb function.” *Nature Cell Biol* **13** 903-13.

Huang W, Yang S, Shao J, Li YP. (2007). “Signaling and transcriptional regulation in osteoblast commitment and differentiation.” *Front Biosc***12:** 3068-92.

Hupkes M, van Someren EP, Middelkamp SH, Piek E, van Zoelen EJ, Dechering KJ. (2011). “DNA methylation restricts spontaneous multi-lineage differentiation of mesenchymal progenitor cells, but is stable during growth factor-induced terminal differentiation.” *Biochim Biophys Acta* **1813:** 839-49.

Ishibe T, Nakayama T, Aoyama T, Nakamura T, Toguchida J. (2008). “Neuronal differentiation of synovial sarcoma and its therapeutic application.” *Clin Orthop Relat Res* **466:** 2147-55.

Ishibe T, Nakayama T, Okamoto T, Aoyama T, Nishijo K, Shibata KR, Shima Y, Nagayama S, Katagiri T, Nakamura Y, Nakamura T, Toguchida J. (2005). “Disruption of fibroblast growth factor signal pathway inhibits the growth of synovial sarcomas: potential application of signal inhibitors to molecular target therapy.” *Clin Cancer Res* **11:** 2702-12.

Ishida M, Miyamoto M, Naitoh S, Tatsuda D, Hasegawa T, Nemoto T, Yokozeki H, Nishioka K, Matsukage A, hki M, Ohta T. (2007). “The SYT-SSX fusion protein down-regulates the cell proliferation regulator COM1 in t(X;18) synovial sarcoma.” *Mol Cell Biol* **27:** 1348-55.

Ishida M, Tanaka S, Ohki M, Ohta T. (2004). “Transcriptional co-activator activity of SYT is negatively regulated by BRM and Brg1.” *Genes Cells* **9:** 419-28.

Ito T, Ouchida M, Ito S, Jitsumori Y, Morimoto Y, Ozaki T, Kawai A, Inoue H, Shimizu K. (2004). “SYT, a partner of SYT-SSX oncoprotein in synovial sarcomas, interacts with mSin3A, a component of histone deacetylase complex.” *Lab Invest* **84:** 1484-90.

Iwasaki T, Koibuci N, Chin WW. (2005). “Synovial sarcoma translocation (SYT) encodes a nuclear receptor coactivator.” *Endocrinol* **146:** 3892-9.

Jones PA and Baylin SB. (2007). “The epigenomics of cancer.” *Cell* **128:** 683-92.

Kato H, Tjernberg A, Zhang W, Kruchinsky AN, An W, Takeuchi T, Ohtsuki Y, Sugano S, de Bruijn DR, Chait BT, Roeder RG. (2002). “SYT associates with human SNF/SWI complexes and the C-terminal region of its fusion partner SSX1 targets histones.” *J Biol Chem* **277:** 5498-5505.

Katoh M. (2008). “Cancer genomics and genetics of FGFR2.” *Int J Oncol* **33:** 233-237.

Katoh Y and Katoh M. (2009). “FGFR2-related pathogenesis and FGFR2-targeted therapeutics.” *Int J Mol Med* **23:** 307-11.

Kawai A, Naito N, Yoshida A, Morimoto Y, Ouchida M, Shimizu K, Beppu Y. (2004). “Establishment and characterization of a biphasic synovial sarcoma cell line, SYO-1.” *Cancer Lett* **204:** 105-13.

Kent WJ, Sugnet CW, Furey TS, Roskin KM, Pringle TH, Zahler AM, Haussler D. (2002). “The human genome browser at UCSC.” *Genome Res* **12:** 996-1006.

Kerppola TK. (2009). “Polycomb group complexes – many combinations, many functions.” *Trends Cell Biol* **19:** 692-704.

Khan J, Bittner ML, Saal LH, Teichmann U, Azorsa DO, Gooden GC, Pavan WJ, Trent JM, Meltzer PS. (1999). “cDNA microarrays detect activation of a myogenic transcription program by the PAX3-FKHR fusion oncogene.” *Proc Natl Acad Sci USA* **96:** 13264-9.

Kim J, Swee M, Parks WC. (2009). “Cytosolic SYT/SS18 isoforms are actin-associated proteins that function in matrix-specific adhesion.” *PLoS One* **4:** e6455. **doi:**10.1371/journal.pone.0006455.

Kimura T, Sakai M, Tabu K, Wang L, Tsunematsu R, Tsuda M, Sawa H, Nagashima K, Nishihara H, Hatakeyama S, Nakayama K, Ladanyi M, Tanaka S, Nakayama KI. (2009). “Human synovial saroma proto-oncogene Syt is essential for early embryonic development through the regulation of cell migration.” *Lab Invest* **89:** 645-56.

Koche RP, Smith ZD, Adli M, Gu H, Ku M, Gnirke A, Bernstein BE, Meissner A. (2010). “Reprogramming factor expression initiates widespread chromatin remodeling.” *Cell Stem Cell* **8:** 96-105.

Ku M, Koche RP, Rheinbay E, Mendenhall EM, Endoh M, Mikkelsen TS, Presser A, Nusbaum C, Xie X, Chi AS, Adli M, Kasif S, Ptaszek LM, Cowan CA, Lander ES, Koseki H, Bernstein BE. (2008). “Genomewide analysis of PRC1 and PRC2 occupancy identifies two classes of bivalent domains.” *PLoS Genet* **4:** e1000242 **doi:** 10.1371/journal.pgen.1000242.

Ladanyi M. (2001). “Fusions of the *SYT* and *SSX* genes in synovial sarcoma.” *Oncogene* **20:** 5755-62.

Langmead B, Trapnell C, Pop M, Salzberg SL. (2009). “Ultrafast and memory-efficient alignment of short DNA sequences to the human genome.” *Genome Biol* **10:** R25 **doi:**10.1186/gb-2009-10-3-r25.

Lee MG, Villa R, Troje P, Norman J, Yan K-P, Reinberg D, Di Croce L, Shiekhattar R. (2007). “Demethylation of H3K27 regulates Polycomb recruitment and H2A ubiquitination.” *Science* **doi:** 10.1126/science.1149042.

Lim FL, Soulez M, Koczan D, Thiesen H-J, Knight JC. (1998). “A KRAB-related domain and a novel transcription repression domain in proteins encoded by SSX genes that are disrupted in human sarcomas.” *Oncogene* **17:** 2013-8.

Lessard JA and Crabtree GR. (2010). “Chromatin regulatory mechanisms in pluripotency.” *Annu Rev Cell Dev Biol* **26:** 503-32.

Lobo NA, Shimono Y, Qian D, Clarke MF. (2007). “The biology of cancer stem cells.” *Annu Rev Cell Dev Biol* **23:** 675-99.

Lubieniecka JM, de Bruijn DR, Su L, van Dijk AHA, Subramanian S, van de Rijn M, Poulin N, Geurts van Kessel A, Nielsen TO. (2008). “Histone deacetylase inhibitors reverse SS18-SSX-mediated Polycomb silencing of tumor suppressor Early Growth Response 1 in synovial sarcoma.” *Cancer Res* **68:** 4303-10.

McLeay RC, Leat CJ, Bailey TJ. (2011). “Tissue-specific prediction of directly regulated genes.” *Bioinformatics* **27:** 2354-60.

Mackall CL, Meltzer PS, Helman LJ. (2004). “Focus on sarcomas.” *Cancer Cell* **2:** 175-8.

Maglott D, Ostell J, Pruitt KD, Tatusova T. (2006). “Entrez Gene: gene-centered information at NCBI.” *Nucleic Acids Res* **35 (suppl 1):** D26-31.

Machinis K, Pantel J, Netchine I, Léger J, Camand OJ, Sobrier ML, Dastoat-Le Moal F, Duquesnoy P, Abitbol M, Czernichow P, Amselem S. (2001). “Syndromic short stature in patients with a germline mutation in the LIM homeobox LXH4.” *Am J Hum Genet* **69:** 961-8.

Maric D, Fiorio Pla A, Chang YH, Barker JL. (2007). “Self-renewing and differentiating properties of cortical neural stem cells are selectively regulated by basic fibroblast growth factor (FGF) signaling via specific FGF receptors.” *J Neurosci* **27:** 1836-52.

Mateos-Langerak J and Cavalli G. (2008). “Polycomb group proteins and long-range gene regulation.” *Adv Genet* **61:** 45-66.

Miraoui H and Marie PJ. (2010). “Fibroblast growth factor receptor signaling crosstalk in skeletogenesis.” *Sci Signal* **3:** re9.

Morgulis A, Gertz EM, Schaffer AA, Agarwala R. (2006). “A fast and symmetric DUST implementation to mask low-complexity DNA sequences.” *J Comput Biol* **13:** 1028-40.

Muruganandan S, Roman AA, Sinal CJ. (2009). “Adipocyte differentiation of bone marrow-derived mesenchymal stem cells: crosstalk with the osteoblastogenic program.” *Cell Mol Life Sci* **66:** 236-53.

Nagai M, Tanaka S, Tsuda M, Endo S, Kato H, Sonobe H, Minai A, Hiraga H, Nishihara H, Sawa H, Nagashima K. (2001). “Analysis of transforming activity of human synovial sarcoma-associated chimeric protein SYT-SSX1 bound to chromatin remodeling factor hBRM/hSNF2α.” *Proc Natl Acad Sci USA* **98:** 3843-8.

Naka N, Takenaka S, Araki N, Miwa T, Hasimoto N, Yoshioka K, Joyama S, Hamada K-I, Tsukamoto Y, Tomita Y, Ueda T, Yoshikawa H, Itoh K. (2010). “Synovial sarcoma is a stem cell malignancy.” *Stem Cells* **28:** 1119-31.

Nakatani Y and Ogryzko V. (2003). “Immunoaffinity purification of mammalian protein complexes.” *Methods Enzymol* **370:** 430-44.

Natsume-Kitatani Y, Shiga M, Mamitsuka H. (2011). “Genome-wide integration on transcription factors, histone acetylation and gene expression reveals genes co-regulated by histone modification patterns.” *PLoS One* **6:** e22281. **doi:**10.1371/journal.pone.0022281.

Nielsen TO, West RB, Linn SC, Alter O, Knowling MA, O’Connell JX, et al. (2002). “Molecular characterisation of soft tissue tumours: a gene expression study.” *Lancet* **359:** 1301-7.

Odelberg SJ, Kohlhoff A, Keating MT. (2000). “Dedifferentiation of mammalian myotubes induced by msx1.” *Cell* **103:** 1099-109.

Ong C-T and Corces VG. (2011). “Enhancer function: new insights into the regulation of tissue-specific gene expression.” *Nat Rev Genet* **12:** 283-93.

Orford K, Kharchenko P, Lai W, Dao MC, Worhunsky DJ, Ferro A, Janzen V, Park PJ, Scadden DT. (2007). “Differential H3K4 methylation identifies developmentally posed hematopoietic genes.” *Dev Cell* **doi:** 10.1016/j.devcel.2008.04.002.

Pardo OE, Latigo J, Jeffery RE, Nye E, Poulsom R, Spencer-Dene B, Lemoine NR, Stamp GW, Aboagye EO, Seckl MJ. (2009). “The fibroblast growth factor receptor inhibitor PD173074 blocks small cell lung cancer growth *in vitro* and *in vivo*.” *Cancer Res* **69**:8645-51.

Perani M, Antonson P, Hamoudi R, Ingram CJE, Cooper CS, Garrett MD, Goodwin GH. (2005). “The proto-oncoprotein SYT interacts with SYT-interacting protein/Co-activator Activator (SIP/CoAA), an human nuclear receptor co-activator with similarity to EWS and TLS/FUS family of proteins.” *J Biol Chem* **280:** 42863-76.

Perani M, Ingram CJE, Cooper CS, Garrett MD, Goodwin GH. (2003). “Conserved SNH domain of the proto-oncoprotein SYT interacts with components of the human chromatin remodeling complexes, while the QPGY repeat domain forms homo-oligomers.” *Oncogene* **22:** 8156-67.

Pretto D, Barco R, Rivera J, Neel N, Gustavson MD, Eid JE. (2006). “The synovial sarcoma translocation protein SYT-SSX2 recruits β-catenin to the nucleus and associates with it in an active complex.” *Oncogene* **25:** 3661-9.

Pruitt KD, Tatusova T, Maglott DR. (2007). “NCBI Reference Sequence (RefSeq): a curated non-redundant database of genomes, transcripts and proteins.” *Nucleic Acids Res* **35(Database issue):** D61-5. **doi:** 10.1093/nar/gkl842.

Rada-Iglesias A, Bajpal R, Swigut T, Brugmann SA, Flynn RA, Wysocka J. (2010). “A unique chromatin signature uncovers early developmental enhancers in humans.” *Nature* **doi:**10.1038/nature09692.

Rao PS, Satelli A, Zhang S, Srivastava SK, Srivenugopal SK, Rao US. (2009). “RNF2 is the target for phosphorylation by the p38 MAPK and ERK signaling pathways.” *Proteomics* **9:** 1-12.

Ren X and Kerppola TK. (2011). “REST interacts with Cbx proteins and regulates Polycomb Repressive Complex 1 occupancy at RE1 elements.” *Mol Cell Biol* **31:** 2100-10.

Safran M, Dalah I, Alexander J, Rosen N, Iny Stein T, Shmoish M, Nativ N, Bahir I, Doniger T, Krug H, Sirota-Madi A, Olender T, Golan Y, Stelzer G, Harel A, Lancet D. (2010). “GeneCards Version 3:the human gene integrator.” *Database* **doi:**10.1093/database/baq020.

Saito T, Nagai M, Ladanyi M. (2006). “SYT-SSX1 and SYT-SSX2 interfere with repression of E-cadherin by Snail and Slug: a potential mechanism for aberrant mesenchymal to epithelial transition in human synovial sarcoma.” *Cancer Res* **66:** 6919-27.

Saldanha AJ. (2004). “Java Treeview – extensible visualization of microarray data.” *Bioinformatics* **20:** 3246-8.

Scheuermann JC, de Ayala Alonso AG, Oktaba K, Ly-Hartig N, McGinty RK, Fraterman S, Wilm M, Muir TW, Müller J. (2010). “Histone H2A deubiquitinase activity of the Polycomb repressive complex PR-DUB.” *Nature* **doi:** 10.1038/nature08966.

Schoenherr CJ and Anderson DJ. (1995). “The Neuron-Restrictive Silencer Factor (NRSF): a coordinate repressor of multiple neuron-specific genes.” *Science* **267:** 1360-3.

Schuettengruber B, Chourrout D, Vervoort M, Leblanc B, Cavalli G. (2007). “Genome regulation by Polycomb and Trithorax proteins.” *Cell* **128:** 735-45.

Schwartz YB, Kahn TG, Stenberg P, Ohno K, Bourgon R, Pirrotta V. (2010). “Alternative epigenetic chromatin states of Polycomb target genes.” *PLoS Genet* **6:** e1000805. **doi:** 10.1037/journal.pgen.1000805.

Schwartz YB and Pirotta V. (2008). “Polycomb complexes and epigenetic states.” *Curr Opin Cell Biol* **20:** 1-8.

Sekiya I, Larson BL, Smith JR, Pochampally R, Cui JG, Prockop DJ. (2002). “Expansion of human adult stem cells from bone marrow stroma: conditions that maximize the yields of early progenitors and evaluate their quality.” *Stem Cells* **20**:530-41.

Shakhova O and Sommer L. (2010). “Neural crest-derived stem cells.” in *Stembook*, eds Gage F and Watt F. (The Stem Cell Research Community) **doi/**10.3824/stembook1.51.1**,** http://www.stembook.org.

Simon JA and Kingston RE. (2009). “Mechanisms of Polycomb gene silencing: knowns and unknowns.” *Nat Rev Mol Cell Biol* **10:** 697-708.

Skytting B, Nilsson G, Brodin B, Xie Y, Lundeberg J, Uhlén M, Larsson O. (1999). “A novel fusion gene, SYT-SSX4, in synovial sarcoma.” *J Natl Cancer Institute* **91:** 974-5.

Smeenk L, van Heeringen SJ, Koeppel M, Gilbert B, Janssen-Megens E, Stunnenberg HG, Lohrum M. (2011). “Role of p53 serine 56 phosphorylation in p53 target gene regulation.” *PLoS One* **6:**e17574.

Smith HA and McNeel DG. (2010). “The SSX family of cancer-testis antigens as targets for tumor therapy.” *Clin Dev Immunol* **doi:** 10.1155/2010/150951.

Sparmann A and van Lohuizen M. (2006). “Polycomb silencers control cell fate, development and cancer.” *Nat Rev Cancer* **6:** 846-56.

Storlazzi CT, Mertens F, Mandahl N, Gisselsson D, Isaksson M, Gustafson P, Domanski HA, Panagopoulos I. (2003). “A novel fusion gene, *SS18L1/SSX1* in synovial sarcoma.” *Genes Chromosomes Cancer* **37:** 195-200

Sun Y, Gao D, Liu Y, Huang J, Lessnick S, Tanaka S. (2006). “IGF2 is critical for tumorigenesis by synovial sarcoma oncoprotein SYTSSX1.” *Oncogene* **25:** 1042-52.

Thaete C, Brett D, Monaghan P, Whitehouse S, Renie G, Rayner E, Cooper CS, Goodwin G. (1999). “Functional domains of the SYT and SYT-SSX synovial sarcoma translocation proteins and co-localization with the SNF protein BRM in the nucleus.” *Hum Mol Genet* **8:** 585-91.

Tie F, Banerjee R, Stratton CA, Prasad-Sinha J, Stepanik V, Zlobin A, Diaz MO, Scarcheri PC, Harte PJ. (2009). “CBP-mediated acetylation of histone H3 lysine 27 antagonizes *Drosophila* Polycomb silencing.” *Dev* **136:** 3131-41.

Törnkvist M, Natalishvili N, Xie Y, Girnita A, D’Arcy P, Brodin B, Axelson M, Girnita L. (2008). “Differential roles of *SS18-SSX* fusion gene and insulin-like growth factor-1 receptor in synovial sarcoma.” *Biochem Biophys Res Commun* **368:** 793-800.

Trojer P and Reinberg D. (2007). “Facultative heterochromatin: Is there a distinctive molecular signature?” *Mol Cell* **28:** 1-13.

Tsuda M, Watanabe T, Seki T, Kimura T, Sawa H, Minami A, Akagi T, Isobe K-I, Nagashima K, Tanaka S. (2005). “Induction of $p21^{WAF1/CIP1}$ by human synovial sarcoma-associated chimeric oncoprotein SYTSSX1.” *Oncogene* **24:** 7984-90.

Vichai V and Kirtikara K. (2006). “Sulforhodamine B colorimetric assay for cytotoxicity screening.” *Nat Protoc* **1:** 1112-1116.

Villegas SN, Canham, M, Brickman, JM. (2010). “FGF signaling as a mediator of lineage transitions – Evidence from embryonic stem cell differentiation.” *J Cell Biochem* **110:** 10-20.

Voncken JW, Niessen H, Neufeld B, Rennefahrt U, Dahlmans V, Kubben N, Holzer B, Ludwig S, Rapp UR. (2005). “MAPKAP kinase 3pK phosphorylates and regulates chromatin association of the Polycomb group protein Bmi1.” *J Biol Chem* **280:** 5178-87.

Voncken JW Schweizer D, Aagaard L, Sattler L, Jantsch MF, van Lohuizen M. (1999). “Chromatin-association of the Polycomb group protein BMI1 is cell-cycle regulated and correlates with its phosphorylation status.” *J Cell Sci* **112:** 4627-39.

Wang J. (2011). “Computational study of associations between histone modifications and protein-DNA binding in yeast genome by integrating diverse information.” *BMC Genomics* **12:** 172. **doi:** 10.1186/1471-2164-12-172.

Watanabe T, Tsuda M, Makino Y, Ichihara S, Sawa H, Minami A, Mochizuke N, NagashimaK, Tanaka S. (2006). “Adaptor molecule Crk is required for sustained phosphorylation of Grb2-associated binder 1 and hepatocyte growth factor-induced cell motility of human synovial sarcoma cell lines.” *Mol Cancer Res* **4:** 499-510.

Watanabe T, Tsuda M, Tanaka S, Ohba Y, Kawaguchi H, Majima T, Sawa H, Minami A. (2009). “Adaptor protein Crk induces Src-dependent activation of p38 MAPK in regulation of synovial sarcoma cell proliferation.” *Mol Cancer Res* **7:** 1582-92.

Watanabe Y, Kameoka S, Gopalakrishnan V, Aldape KD, Pan ZZ, Lang FF, Majumder S. (2004). “Conversion of myoblasts to physiologically active neuronal phenotype.” *Genes Dev* **18:** 889-900.

Weake VM and Workman JL. (2008). “Histone ubiquitination: triggering gene activity.” *Mol Cell* **29:** 653-63.

Weintraub H, Tapscott SJ, Davis RL, Thayer MJ, Adam MA, Lassar AB, Miller AD. (1989). “Activation of muscle-specific genes in pigment, nerve, fat, liver, and fibroblast cell lines by forced expression of MyoD.” *Proc Natl Acad Sci USA* **86:** 5434-8.

Xie Y, Skytting B, Nilsson G, Brodin B, Larsson O. (1999). “Expression of Insulin-like Growth Factor-1 Receptor in synovial sarcoma: association with an aggressive phenotype.” *Cancer Res* **59:** 3588-91.

Zhang Y, Liu T, Meyer CA, Eeckhoute J, Johnson DS, Bernstein BE, Nusbaum C, Myers RM, Brown M, Li W, Liu XS. (2008). “Model-based analysis of ChIP-Seq (MACS)” *Genome Biol* **9**: R137 **doi:**10.1186/gb-2008-9-9-r137.

Zhao C, Deng W, Gage FH. (2008). “Mechanisms and functional implications of adult neurogenesis.” *Cell* **132:** 645-60.